MODIFICATION OF POROUS MATERIALS TO IMPROVE THEIR GAS STORAGE AND CATALYTIC ACTIVITY

A Dissertation

by

SAYAN BANERJEE

Submitted to the Office of Graduate and Professional Studies of
Texas A&M University
in partial fulfillment of the requirements for the degree of

DOCTOR OF PHILOSOPHY

Chair of Committee,	Hong-Cai Zhou
Committee Members,	Sarbajit Banerjee
	David P Barondeau
	Hae-Kwon Jeong
Head of Department,	Simon North

May 2021

Major Subject: Chemistry

ABSTRACT

Over the past decade, researchers have shown an increased interest in the field of highly porous materials. This dissertation herein will mainly focus on design and post-synthetic modification of two types of porous materials, such as **M**etal-**O**rganic **F**rameworks (MOFs) and **P**orous **C**oordination **C**ages (PCCs) for optimizing guest-host interaction.

First, an overview of the discovery of these porous materials is provided. Their properties and application were discussed. I conclude by defining specific aims of the subsequent research.

One of the drawbacks faced by MOFs is the difficulty in synthesizing frameworks that have a large pore size yet maintain framework stability under harsh conditions. To fulfill this challenge, a simple methodology for the generation of ordered mesopores in an inherently microporous MOF through Soxhlet extraction is discussed. This innovative method demonstrates a simple and reproducible process that results in a material that possesses the benefits of mesoporous while borrowing the robustness of a micropore framework. While many mesoporous MOFs have demonstrated good methane uptake, the stability of those MOFs is an issue when unrefined natural gases are attempted to capture. Here, I also report a way to overcome this problem by choosing a stable MOF and applying a post-treatment method by doping long-chain hydrocarbon in the MOF. By applying this process, we observed hydrocarbon doping improves the methane uptake performance for the material.

Based on these results, I discuss the investigation of the *in-situ* functionalization with alkyl chains and even more polar and non-polar groups during the MOF synthesis by using Ligand-Fragment Co-Assembly that will provide the additional steric and electronic interactions necessary to enhance gas binding.

To continue with porous materials, I discuss about another class of porous material PCCs for first row transition metal nanoparticle encapsulation. Design of a series of PCC cages and efforts towards first-row transition metal encapsulation are explained in detail.

Finally, a synopsis of the research and opinions on future directions in this field are provided. Overall, my results lay the foundation for optimized post-synthetic modification techniques in porous materials for gas storage and catalysis.

DEDICATION

To my grandfather, grandmother, mother, father and Nairita. You have done so much to support me morally, emotionally and financially and always kept me motivated in difficult times. I will always keep trying to make you proud.

ACKNOWLEDGEMENTS

I want to express my sincere gratitude to my advisor Dr. Hong Cai Zhou, who offered me a fantastic opportunity to work in his research group. Before joining Texas A&M, I was trained primarily in organic chemistry and never had the opportunity to work with porous materials. It was, therefore, overwhelming when I joined the Zhou group working on gas storage in MOFs. But Dr. Zhou provided me with immense freedom to explore the new field. At the same time, his patience with my mistakes, productive feedback, and guidance helped me navigate effectively through this long journey and reach the finish line of my Ph.D.

I would like to thank my committee members, Professor Sarbajit Banerjee, Professor David Barondeau, and Professor Hae-Kwon Jeong, for their time, support, guidance, and expertise throughout the course of my research.

Within the Zhou group, I would like to recognize Dr. Zac Perry and Dr. Yu Fang for their mentorship, advice, and guidance in my research. I have learned many things related to porous materials science from them, and they helped to broaden my scientific outlook. I could not have grown so much without your assistance. I especially thank Zac for all the lunch trips and philosophical discussions. I miss brainstorming with him. I also would like to thank my lab mates (past and present) for all the help. I would especially like to thank Gregory Day, Elizabeth Joseph, Carol Li, Hannah Drake, Angelo Kirchon, Sean Xiao, Peiyu Cai, Liang Feng, Kunyu Wang, Christina Lollar, Wenmiao Chen, Mallory Smith,

and Aida Contreras-Remirez. I couldn't have asked for more wonderful friends, mentors, colleagues, and collaborators. I would also like to especially thank Carrie Frederiksen for holding our research group together and helping me throughout these five years.

I taught organic chemistry lab courses for several years. I am grateful to Dr. Amber Schaefer and all the organic chemistry staff to help many graduate students like me successfully juggle research and teaching balance. Dr. Schaefer also mentored me during my Academy for Future Faculty training. I learned a lot about classroom teaching from her. I am also grateful to the Texas A&M Chemistry graduate office staff, especially Sandy Horton and Valerie McLaughlin, for always helping me and countless international graduate students settle down in a new country and endless support in every grad school problem, however small it might be.

I will remain immensely indebted to all my seniors and friends from Bengal in College Station, especially Isita-di, Shyamalendu-da, and Rajat da, for all their selfless help and support during these five years. They hosted me the first night I arrived in this country, taught me how to drive a car, and probably helped me with every nonacademic problem. They are my surrogate family and made my life much more comfortable in this new country.

I want to acknowledge my parents Sangita Banerjee and Swapan Banerjee, and grandmother Krishna Goswami for their unconditional love and support, and encouragement. During these five year, they always rooted for me and supported me in my every choice, even across the globe. They always encouraged me to do my best, and I

wish I could visit them more. I am also thankful to my late grandfather Arun Kr Goswami who always trusted me and wanted me to pursue a Ph.D. I wish he was alive today to see me completing this long journey of education. Last but not least, I can't thank my best friend (and girlfriend) Nairita enough for being by my side throughout the graduate school marathon. Being a Ph.D. student herself, she understands grad school problems and always made sure to keep me happy and motivated with her love and support. It will be my honor to spend the rest of my life with her.

Many people supported me with kindness and care in my grad school journey and my professional growth, and I thank them all. We are indeed in a disturbing time right now as COVID-19 pandemic is spreading across the world like wildfire. I want to thank all the frontline workers who are risking their lives to keep us safe. We do not know how the world's system will be changed over the next few months, but I believe, just like the Ph.D., there will always be light at end of this dark tunnel.

CONTRIBUTORS AND FUNDING SOURCES

This work was supervised by a dissertation committee consisting of Professor Hong-Cai Zhou (Advisor), Professor Sarbajit Banerjee of the Department of Chemistry, Professor David Barondeau of the Department of Chemistry, and Professor Hae-Kwon Jeong of the Department of Chemical Engineering.

The work in chapter II was conducted with assistance from Elizabeth Joseph (Analysis of Soxhlet treated samples), Yu Fang (Initial Gas chromatography testing) and Jialuo Li (SEM analysis) The work described here was published in 2018.

The work in chapter IV was conducted with assistance from Jialuo Li (TEM analysis), Yu Fang (cage crystal structures solving and analysis) and Zhefeng Xiao (for assistance with catalytic activity studies with PCC-2a) The work described here was published in 2018.

All other work conducted for this dissertation was completed by the student independently.

Graduate study was supported in part by teaching assistantship from Texas A&M University and as a part of Center for Gas Separations, an Energy Frontiers Research Center funded by the U.S. Department of Energy, Office of Science, Basic Energy Sciences under award number DESC0001015. Gas storage studies were supported by Department of Energy Office of Fossil Energy, National Energy Technology Laboratory award number DE-FE0026472. The work described in chapter II and III was funded by

National Science Foundation Small Business Innovation Research (NSF-SBIR) under award number 1632486. Work described in chapter IV and additional support in terms of supplies, materials and salary was provided by Welch Foundation under grant number A0030. The contents of this dissertation are solely responsibility of the student and do not necessary represent the official views of the Department of Energy, National Science Foundation or the Welch Foundation.

NOMENCLATURE

3D	3-dimensional
ABTC	Azobenzenetetracarboxylic acid
BDC	Benzene Dicarboxylate
BET	Brunauer-Emmett-Teller
BJH	Barrett-Joyner Halenda
DFT	Density Functional Theory
DMF	*N,N*-Dimethylformamide
FID	Flame Ionization Detection
GC	Gas Chromatography
HPVA	High-Pressure Volumetric Analysis
IR	Infrared
IUPAC	International Union of Pure and Applied Chemistry
LFCA	Ligand Fragment Co-assembly
MOF	Metal-Organic Framework
PCN	Porous Coordination Network
PCC	Porous Coordination Cage
PSM	Post Synthetic Modification
PSMO	Post Synthetic Modification and Oxidation
PVP	Polyvinylpyrrolidone
PXRD	Powder X-Ray Diffraction

SBU	Secondary Building Unit
SEM	Scanning Electron Microscope
TEM	Transmission Electron Microscopy
TGA	Thermogravimetric Analysis

TABLE OF CONTENTS

Page

LIST OF FIGURES

Page

LIST OF TABLES

Page

CHAPTER I

INTRODUCTION TO POROUS MATERIALS: DESIGN, APPLICATIONS, AND SCOPE OF THIS RESEARCH*

Introduction to Porous Materials

Porous materials are substances that have intrinsic pore (void) volumes imbibed in their structures.[1] The study of these materials has been dated back ta as early as 1500 BCE in ancient Egypt, India, and Greece. These civilizations used porous charcoal in holistic applications such as medical uses, drinking water purification, and writing ink.[2] However, until the 18th century, it was unknown that these unique properties of the charcoal are actually resulting from its intrinsic pores. In 18th century Swedish chemist Carl Scheele first tested gas adsorptive properties of charcoal. Upon heating a vessel filled with charcoal attach to a bladder, he observed the bladder volume expanded much higher than that found in a typically sealed container.[3] With the cooling of the vessel, he observed the subsequent volume loss of the bladder is due to re-adsorption of the gases, and this process is highly reproducible. This study opened new avenues to adsorption science and porous materials exploration. During the industrial revolution in 18th and 19th-century

---

*Part of this chapter and Figures 2,3 and 4 are reprinted with permission from **Banerjee, S.**; Lollar, C. T.; Xiao, Z.; Fang, Y.; Zhou, H.-C., Biomedical Integration of Metal–Organic Frameworks. *Trends in Chemistry* **2020,** *2* (5), 467-479. Copyright Elsevier 2020

materials with intrinsic pore volume was widely used in water filtration[4], and eliminating dark color of sugars.[5] In the same time onward when newer avenues of structural characterizations were being explored other classes of naturally occurring porous materials such as Zeolites (Greek word *zeo* to boil and *lithos* to stone)[6], silicas[7], and humanmade materials such as cement and ceramics came into pictures. Substantial academic research with porous materials started heavily on 1950 onwards with the better structure elucidating tools[8] and better adsorption models. In the present scenario, a significant amount of scientific and industrial research focuses on design, structural characterizations, and applications of natural and synthetic occurring porous materials such as Zeolites, Mesoporous Silicas, **P**orous **P**olymer **N**etworks (PPNs), **M**etal-**O**rganic **F**rameworks (MOFs), **C**ovalent **O**rganic **F**rameworks (COFs), and **P**orous **C**oordination **C**ages (PCCs). In this chapter, I try to provide a brief introduction of primarily two classes of compounds described above which is metal organic framework and porous coordination cage as the subsequent chapters these materials are discussed in detail.

Brief History and Definition of Metal-Organic Frameworks

Metal-Organic Frameworks (MOFs) are a special class of coordination polymers where metal ions or clusters are bound to organic linker results in permanent porous structures.[9] MOFs generally have a high degree of crystallinity and formed by simple coordination chemistry makes it a relatively easy compound to tune the inherent structure and study its properties chemically. The structural features such as geometry, porosity, stability lie in MOF frameworks in its coordination bonds between metal and ligand systems, which is

being studied for centuries, mainly in the chemistry of inorganic dyes.[10] One of the very classic examples will be Prussian Blue (iron (III) hexacyanoferrate (II)). This dye was first synthesized artificially in the early 1700s. This material is not only a simple coordination salt with iron metal and cyanide ligands. Coordination capability of cyanide ligand in both ends makes this material as one of the earliest examples of extended framework material.[11] During the early days of modern chemistry, there was little understanding of metal-ligand interactions, and the approaches to make these coordination polymers were limited to only pigment formation. However, seminal research work on Coordination chemistry by Alfred Werner[12] opened new avenues on understanding metal-ligand interactions, geometry, and charge of ions. It introduced concepts of neutral coordination ligands[13], the inner and outer sphere of coordination environment, and even chirality of inorganic coordination molecules. These new pathways stimulated other breakthrough inventions in coordination chemistry such as trans effect theory[14, 15] in 1926, Pearson's Hard-Soft Acid Base theory[16] etc. These theories are still handy to determine the geometry and stability of modern-day Metal-Organic Frameworks.

In the mid-20th century, landmark discoveries such as ferrocene by Wilkinson[17] and the discovery of coordination polymers[18] by Bailar shaped the modern field of inorganic and organometallic chemistry. They paved a clear avenue for Metal-Organic chemistry. These initial coordination organometallic compounds are referred to as 1-dimensional (1-D) coordination polymers, which uses a simple extension of basic organometallic chemistry. From the 1980s, efforts were made to prepare such polymers crystalline and pioneering works of Robson[19] and Fujita.[20] These crystalline coordination polymers paved the way

for modern-day MOFs. This crystallinity arises due to self-assembly of these frameworks where metal and ligands can reversibly coordinate with each other based on their affinity and lability.[21] This self-assembly usually takes high temperatures to prepare an ordered structure and typically happens in solvothermal conditions. This approach is similar to the zeolite materials, where hydrothermal processes shape the topology of the structures. So, with this approach of zeolite synthesis and science of coordination chemistry in the latter half of the 1990s, actual Metal-Organic Frameworks were reported. These works were pioneered by two scientists from very different backgrounds: Omar Yaghi and Susumu Kitagawa. Omar Yaghi's experience in oxalate type organometallic chemistry[22, 23], and solvothermal approach helped him to get a significant breakthrough to generate crystalline porous structures MOF-5, a zinc-based metal-organic framework which can retain its porosity after solvent removal.[24] Although the stability MOF-5 is considered quite low in today's standard; however, it is still regarded as one of the very first examples of real MOF.

On the other hand, Kitagawa, who already had a background in coordination chemistry[25], explored to increase the dimension of the 1D polymers to 2D or 3D, which helped him to get permanently porous structures[26], which is by definition a Metal-Organic Framework. After these initial discovery, research related to permanent porous Metal-Organic Frameworks gradually increased in the academic community **(Fig 1)** with several aspects in mind such as expanding the pore sizes with isoreticular expansion with IRMOFs[27] , creating more robust structures with other high valent metals such as Fe (III)[28], Cr (III)[29], Zr (IV)[30] and alternate ligand variants with nitrogen based ligands were also explored such

as metal azolate frameworks (MAF)[31] and Zeolitic imidazolate framework (ZIF)[32]. And even these ligands were used in traditional MOFs[33] without disturbing its crystallinity as hierarchical structures.[34] This thesis also discusses some of the efforts on post synthetic modifications to create

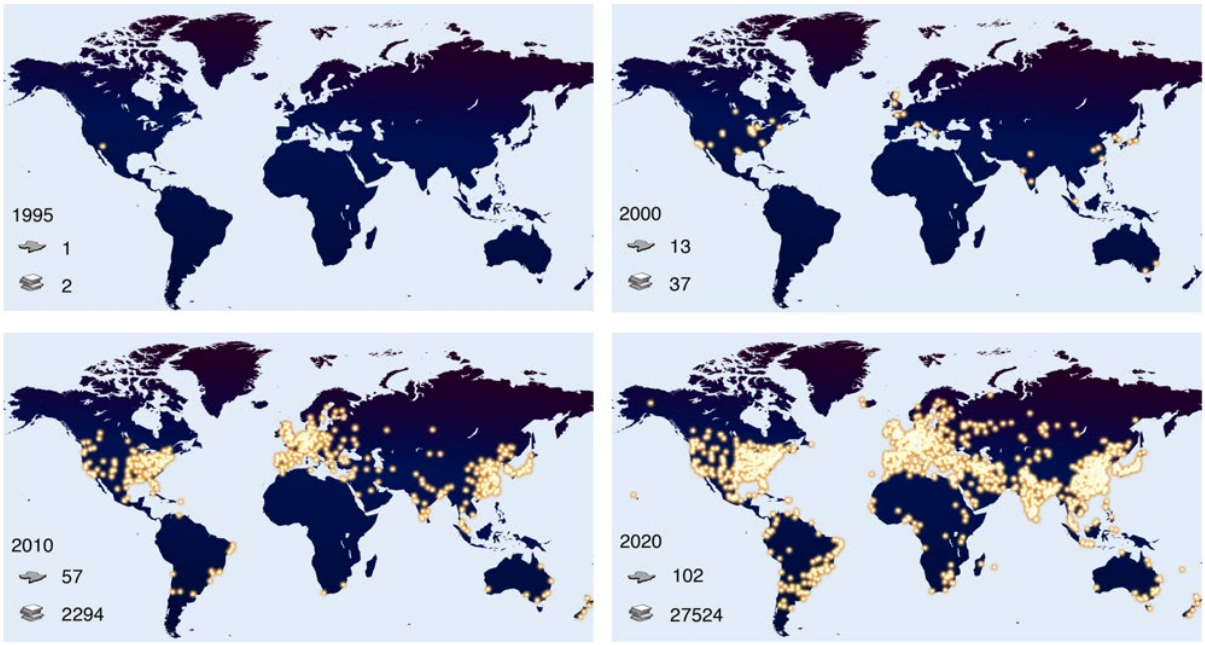

Figure 1. Pictorial description of porous material research growth increase from 1995-2020.Yellow dots represent institutions involved in porous materials research. Adapted with permission from 35

Mesopores in metal-organic frameworks. In terms of terminology, MOFs are named either using the formula units such as M-BTT (M stands for metal)[36] or structure descriptors such as PCN as **P**orous **C**oordination **N**etworks. They are also published as the location of their first discovery, such as HKUST as **H**ong **K**ong **U**niversity of **S**cience and **T**echnology, MIL as **M**aterial **I**nstitute of **L**avoisier and numbered sequentially or by structural similarity. IUPAC task force recommends on terms on publishing topology of coordination polymers but no clear recommendations were made to nomenclature of MOFs.[37]

Definition and Brief History of Porous Coordination Cages

Another class of porous material which also utilizes the same concepts of coordination chemistry (discussed in the previous section), structural fragments without the bridging between each unit, also developed the mid-1990s, which utilizes a broad range of molecules especially crown ethers[38] and cryptands.[39] However, two pioneers in this field Saalfrank[40] and Fujita[41, 42] in the late 1990s (almost the same time when the metal-organic frameworks were reported) developed these kinds of supramolecular self-assembled structures using discrete trinuclear magnesium and palladium clusters assembling in a tetrahedral fashion. This invention develops a new class of porous material called coordination cages which is widely studied today. Since the emergence of these pioneering work, many groups across the world have developed new and diverse structures of this kind of compounds including Stang[43], Cotton[44] , Mirkin[45] ,Yaghi[46], Kitagawa[47], Cook[48], and Zhou group as well.[49] These porous coordination cages share many of the same

structural characterizes and moiety as Metal-Organic Frameworks. However, they form discrete polyhedral structures, which leads to some inherent complications in solid-state chemistry.[50] Geometrically, MOFs, and Cages differs the ligand and metal connectivity. The first using divergent connectivity, which helps it to polymerize symmetrically. Cages, on the other hand, uses convergent geometry, such as when the symmetry of the node and ligand are combined, the resulting polymer meets itself and closes its structure. For this generally, a capping ligand is required to reduce the coordination sites of metal clusters to stop propagation.[51] In solution these cages have shown to encapsulate large range of guest molecules inside its pores which leads to its applicability in several sectors discussed in later sections. These cages suffer from a challenge to retain permanent porosity without guest molecules and they sometime collapse under solvent evacuation conditions.[52] This happens mainly of two factors: 1) the solvents and other molecules may play a major role in the packing forces leading to aggregation when removed, 2) the high temperature of the degas process sometime result in cage disorder or collapse as the metal ligand interactions are ruptured. Thus, in the vast library of all the cages reported only a few cages retain permanent micro porosity in the solid state. Some of these rare examples were reported by Stang group[53], Zhou Group[54-57] and very recently Bolch group.[50, 58] As there is no standard nomenclature for these Metal-Organic Cages, they are termed in several nomenclatures in literature such as **M**etal-**O**rganic **P**olyhedron (MOP), **M**etal-**O**rganic **C**ages (MOCs), Molecular Flasks[59], Porous **C**oordination **C**ages[60, 61] (PCCs) etc. by different research groups and numbering were assigned by sequential discovery or similar structures. This thesis will discuss a class of **P**orous **C**oordination **C**age (PCC) developed using same

coordination chemistry and convergent ligand approach for catalysis application in later chapters.

Applications of Porous Materials

One of the main reasons porous materials received attention over the years because they have a wide array of potential applications[62] such as gas storage/separation, drug delivery, imaging and sensing, and combinatorial therapy. We will briefly discuss these applications.

Gas Storage and Separation

Gas storage and separation are one of the most crucial aspects of modern-day industrial development, such as reducing greenhouse gases and clean energy applications. Metal-Organic Framework and Porous Coordination Cages, in some cases, are most discussed and used materials in this aspect. Judiciously designed pores of these materials, and high surface area helps to store and separate gases very effectively. For example, let's discuss one of the most energetically relevant gases, which is hydrogen. Hydrogen is designated as the fuel of the future as it can eliminate all the problems generated by using excessive fossil fuels.[63] However, the boiling point and crucial temperature of hydrogen are 20K and 38K, which makes it very difficult to store, and methods involving cryo preservations are very expensive.[64] Tuning metal clusters and ligand alignment both can help to increase the gas interaction with the adsorbent, which makes MOFs an excellent candidate for hydrogen storage. MOFs with uncoordinated metal sites or open metal sites (OMS) with high charged metal ions such as Al^{+3}, Fe^{+3} $Co^{+2,}$ etc. provide stronger interactions with

these gas molecules and help to "liquify" the gas molecules.[65] Not only open metal sites, but interpenetration can also help to achieve high hydrogen storage by dividing the larger pore voids into smaller chambers. Some of the well-established MOFs for hydrogen storage include MOF-5[66], MOF-177[67], SNU-4[68], Mn-BTT[69], PCN-6[70] PCN-250[71], and PCN-12[72]. Recently an Al-based MOF termed NU-1501 (NU stands for Northwestern University) developed by Farha and coworkers[73] using these principles is reported to have reached significantly closer to 2020 DOE target[74] by providing 46.2 g/L volumetric adsorption.

Apart from hydrogen, natural gas or methane is another essential energy source in the US energy market.[75] Methane can also be very effectively stored in Metal-Organic frameworks via several approaches. The first approach is typically enhancing electrostatic interactions between methane gas and MOF metal clusters. Some of the representative examples include Ni-MOF-74.[76, 77] Another approach that has been very useful to provide van der Waals attractions in MOF pores increasing interaction in secondary binding sites. Representative examples include but not limited to PCN-14[78], HKUST-1[79], PCN-250, NU-125[79], etc. where most methane adsorption sites in high pressure are found to be primarily located at window sites. And tuning the pore volume can help to increase the working capacity as well.[79] Al-soc-MOF-1 is a representative example of such a case. Recently Farha group reported a delicate balance by two MOFs NU-1501 Al and NU-1501 Fe. in these two aspects to report an excellent candidate for methane storage, which surpasses the 2020 DOE target of 263 *v/v* methane uptake.[73] Some porous coordination

cages have also been reported as very nice methane storage recently.[50, 80] This thesis will discuss more complex aspects of methane storage in MOFs in later chapters.

Another very well studied gas for storage and separation aspects is carbon dioxide. MOFs are primarily utilized as sorbents to achieve CO_2 separation, and this is based on the interaction of target gases with the frameworks. There are namely three types[81] of CO_2 capture, and separation techniques exist that can be achieved using MOFs i.e., 1) Post-combustion capture 2) Pre combustion capture 3) direct air capture. Post-combustion capture is generally aimed at separate the flue gas CO_2 from the significant product nitrogen in lower pressures.[82] Introducing alkylamine in the MOF frameworks has been very widely used in this method[83-85] in MOFs such as Mg_2(dobpdc).[86] On the other hand, Pre-combustion CO_2 capture requires separation H_2 and CO_2 in high pressures so that no CO_2 is burned in subsequent steps. The size difference of H_2 (kinetic diameter is 2.8 Å), and CO_2 (kinetic diameter 3.3 Å) plays an essential role using MOFs as size-selective separation membranes. Some representative examples include layered MOF, $Zn_2(bIm)_4$ (bIm=benzimidazolate) nanosheets membranes.[87] Lastly, Direct air capture refers to reducing the present concentration of CO_2 in airs.[88] This technology is very much useful to maintain low CO_2 levels in submarines or spacecraft where its critical to maintain a habitable environment. This capture needs to be done in shallow pressures making it a very challenging aspect. There has been ongoing research in this area with MOFs, and MOF derived membranes to solve this challenge.[89]

Guest Encapsulation and Release

Biologically relevant guest uptake, protection, and release are burgeoning domains of MOF applicability by virtue of their extraordinary surface areas and porosities, chemically tunable interiors, and adjustable stability and toxicity. In these cases, the MOFs themselves are not the biologically active species but are instead vehicles for such species. **Figure 2** presents information regarding the chemical effects exploited to produce these applications as well as uptake, activity comparisons, and release of MOF cargo from the papers discussed below. Fascinated by what advantages MOFs could afford towards sustained or site-selective delivery, the guest release has been the most popular of the three above mentioned MOFs-as-hosts applications. In particular, smart MOFs, a subcategory of MOFs responsive to external stimuli such as light, pH, temperature, pressure, or external fields, have been exploited to spatiotemporally regulate guest release.[90] Dong and coworkers published an elegant report on diffusion-driven guest release profiles of ibuprofen, rhodamine B, and doxorubicin in **multivariate MOF** hosts.[91]

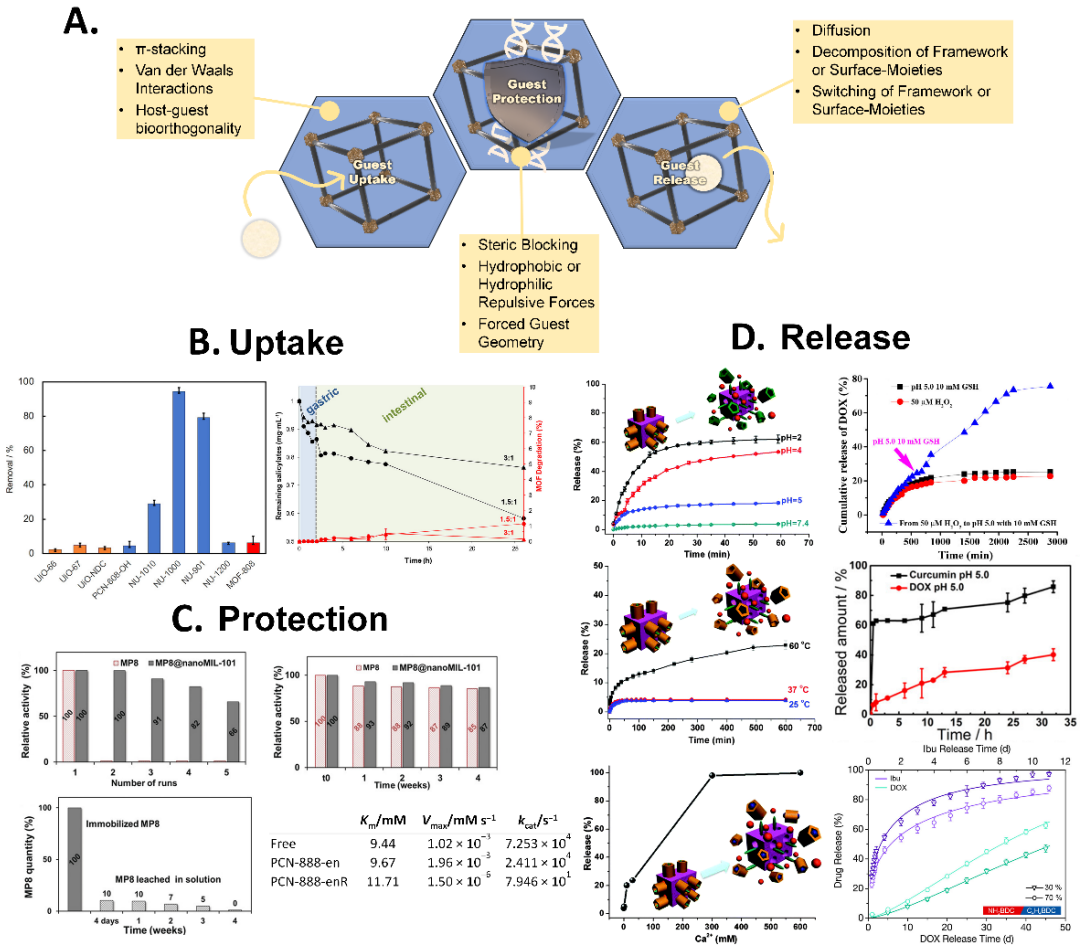

Figure 2. An overview of the key aspects and mechanism of porous materials in terms of guest uptake and release. The three main modes by which MOFs are used as hosts for biologically relevant cargo: guest uptake, guest protection, and guest release. Mechanisms by which these interactions are commonly accomplished are listed in respective yellow boxes.

Diffusion-driven drug release is promising due to its potential for prolonged, gradual release rather than burst release and its associated side-effects. While MIL-101(Fe) is typically composed of iron-oxo clusters and benzene dicarboxylate linkers, their group used normal benzene dicarboxylic acid as well as derivatives 2-aminobenzene-1,4-dicarboxylic acid and 1,4-naphthalenedicarboxylic acid in varying ratios to produce a continuum of MOFs. Disparities in the release rates of each type of cargo were observed depending on the linker percentages in the MOF. Using a host-guest interaction parameter, a guest-guest interaction parameter, and a time variable, they employed a mathematical model to predict the fraction of guest released. Although these studies were not performed in vivo, they are essential to pave the way for more clearly programmable MOF systems and to address the goldilocks issue of host-guest interactions: when host-guest interactions are too strong, the guest may struggle to release while interactions that are too weak may result in the guest being unable to efficiently load into the material. In contrast to diffusion-based release methods, decomposition-dependent release is another popular approach which requires either the dissociation of the framework or dissociation of some surface, pore-blocking layer to release cargo. In general, a MOF's stability is limited by the strength of the coordination bond between the linker and the metal cluster. Exposure to species that impede this bonding, such as acids which may protonate the linkers or hydroxide-producing species that occupy sites on the metal cluster, can result in weakening and eventual decomposition of the framework. Various factors ought to be considered to predict and understand MOF stability including the ligand pKa, the oxidation state of the metal, the coordination number and coordination sphere size of the

metal cluster, the Pearson hard/soft acid/base match between the binding species, and hydrophobicity/hydrophilicity of the MOF pore environment. A more in-depth discussion on MOF stability is available in various insightful reviews and book chapters.[92-94] ZIF-8 is a framework composed of Zn-oxide clusters and imidazolate linkers. Although this MOF is known to deteriorate in acidic conditions, this shortcoming can be exploited advantageously for drug delivery applications since the decomposition products of ZIF-8 are considered biologically innocuous. Recently, judiciously designed composite materials have been constructed, intelligently uniting the advantages of each component. For instance, Wang and coworkers constructed a microporous ZIF-8/mesoporous silica (MSN) hybrid nanocarrier cohered by polydopamine (PDA).[95] In this vehicle, steady decomposition of the ZIF-8 shell in the acidic conditions of cancerous cell cytoplasts first releases curcumin to inhibit P-glycoproteins. Following this, the now unblocked mesoporous cavities release their anticancer drug payload, doxorubicin (DOX). In another promising hybrid material-based avenue, ZIF-8 loaded with rhodamine B as a proof-of-concept cargo was coated onto a magnetically-controllable helical nanobot.[96] The 3D-printed, tractable microstructure was magnetically guided while the pH-induced decomposition of ZIF-8 released the model cargo. This decomposition approach to cargo delivery may feel familiar to those acquainted with drug delivery studies using other matrices, including polymers and silica nanoparticles.[97-99] Indeed, this methodology is widely applicable to MOF systems unstable to biologically relevant microenvironments such as reducing, glutathione concentrated, or acidic, oxidizing H_2O_2-rich locales. In contrast to the preceding systems, Miao and coworkers focused on minimizing premature

drug release and related side-effects with a dual-responsive system.[100] This system features a PDA outer layer to provide biocompatibility until the MIL-100 MOF interlayer encounters the H_2O_2-rich extracellular environment of a cancerous cell, at which point the MOF decomposes revealing the final DOX-incorporated polymethylacrylic acid layer which is then disintegrated in reducing endosomal conditions. This concept was first studied in vitro in buffered solution to simplify the quantification and comparison of drug release profiles under different conditions. They began with exposure of the drug-loaded system in buffered solutions to H_2O_2 at normal physiological concentrations (0.5 μM) as well as pathological concentrations (50 μM) for 48 hours followed by treatment with glutathione (GSH, reducing) at 10 μM (similar to the concentration in extracellular trafficking pathways) and 10 mM for 48 hours, at pH = 7.4 and pH = 5.0 at either room temperature or 37°C where the decreased pH and increased temperature resulted in an enhanced release of DOX. This examination was followed by cellular studies on PC-3 cells, tumor cells which express higher concentrations of H_2O_2, using confocal laser scanning microscopy to confirm intracellular release of the DOX molecules (particularly into the cell nuclei) without supplementary addition of H_2O_2 or GSH. Though complicated, each component of this matrix serves an elegantly designed purpose. The authors did not report such experiments but selection of other internal MOFs or polymer materials with varying degrees of stability or further customization through surface functionalization with biocompatible modules could conceivable lead to high cell viability or further protection of the interior material, prolonging the time before decomposition and release or enabling extended release of drug cargo that may result in less severe

medicated-related side-effects, discourage premature release, and reduce the need for re-administration. Finally, it is also being realized that larger cargo such as proteins for protein replacement therapy[101] and DNAzymes for gene therapy[102] can be incorporated into stimuli-responsive release systems. Rather than assuming decomposition of the host framework, necessitating nontoxic structural building units, Tan and coworkers have capitalized on the higher durability of Zr-carboxylate frameworks, explicitly UiO-66, to construct a drug delivery vehicle that relies on pH, temperature, or Ca^{2+} stimuli to dissociate CP5 rings blocking the release of internal guest molecules.[103] As methods of mesopore generation advance, it is expected that application of MOFs to larger scale cargo will advance in tandem. Although diffusion-, pH-, and dissociation-based release mechanisms have seen the most use, MOF-drug vehicles are also capable of light-[104, 105], pressure-[106], magnetic field-[107], environnemental hydrophobicity/hydrophilicity-[108], and complementary DNA-induced[109] Drug release mechanisms. Analogously, Silvestre-Albero's lab endeavored to apply more MOF variety in drug delivery applications and has helped to lay the groundwork with a methodical analysis of the loading, release, and cytotoxicity of four prevalent MOFs for intraocular therapeutics.[110] Enzymes require very specific environments to preserve their folded structures and functionality, rendering them vulnerable to minuscule variations in pH, temperature, or salinity. Their fragility situates them as excellent candidates for another branch of MOF applicability: guest protection. In contrast to guest delivery, the purpose of the MOF host is to provide a barrier between a fragile payload and denaturing conditions to retain activity without cargo liberation. As of late, MOFs loaded with enzymes have been employed for diverse applications such as the

activation of anticancer prodrugs [111] and degradation of toxic species in contaminated wastewater.[112]

Recently, MIL-101(Cr) was loaded with microperoxidase-8, resulting not only in preservation of the enzyme structure, but also enhancement of the oxidation rate of negatively charged methyl orange over positively charged methylene blue.[113] Zhou group has pursued the immobilization of two different enzymes, horseradish peroxidase and glucose oxidase, within a hierarchically porous MOF, PCN-888 in order to yield a tandem nanoreactor.[114] Stepwise enzyme insertion preferentially situates the larger enzyme within the larger pore and the smaller enzyme within the medium-sized pore, granting the smallest pore space available for the diffusion of substrates into and out of the MOF.

Finally, MOFs can internalize toxic species in biological environments, thereby mitigating damage to surrounding cells. In one example, Rojas and coworkers found MIL-127(Fe) to be exceptional at reducing intestinal salicylate absorption by a factor of 40, after which it is safely, fecally excreted, making it promising as an overdose treatment.[115] Additionally, nine Zr-based MOFs' with differing linker size, linker geometry, metal node connectivity, and overall topology were assessed in regards to their efficiency in uremic toxin removal.[116] It was found that NU-1000 is an efficient absorbent, almost entirely extracting *p*-cresyl sulfate from human serum albumin. This efficiency was attributed to the π-π interactions between the toxins and the pyrene-based ligands facilitated by carefully arranged with hydrophobic adsorption sites and nearby hydrogen bonding capacities.

Porous Materials in Biomedical Imaging and Sensing

Developments in biomedical imaging technologies assist in the diagnosis and detection of various diseases. In the past decade, MOFs have been widely used to produce detectable signals or enhance the contrast from targeted tissue, usually through modification of MOFs' metal nodes**. (Figure 3)** MRI, CT scan, and PET are some of the most widely used MOF-incorporated imaging techniques. Alternatively, incorporation of fluorophores in MOFs has also enabled optical imaging using upconversion in cells. We will discuss this in terms of four imaging and sensing technique. Such as Magnetic Resonance imaging, Xray CT scan, PDT and finally simply optical imaging. Magnetic resonance imaging employs radio wave-frequency radiation under the influence of an external, gradient magnetic field to detect relaxation signals from the copious amounts of hydrogen atoms present in biological systems. These signals provide precise anatomical structure maps and help detect diseases and other anomalies.

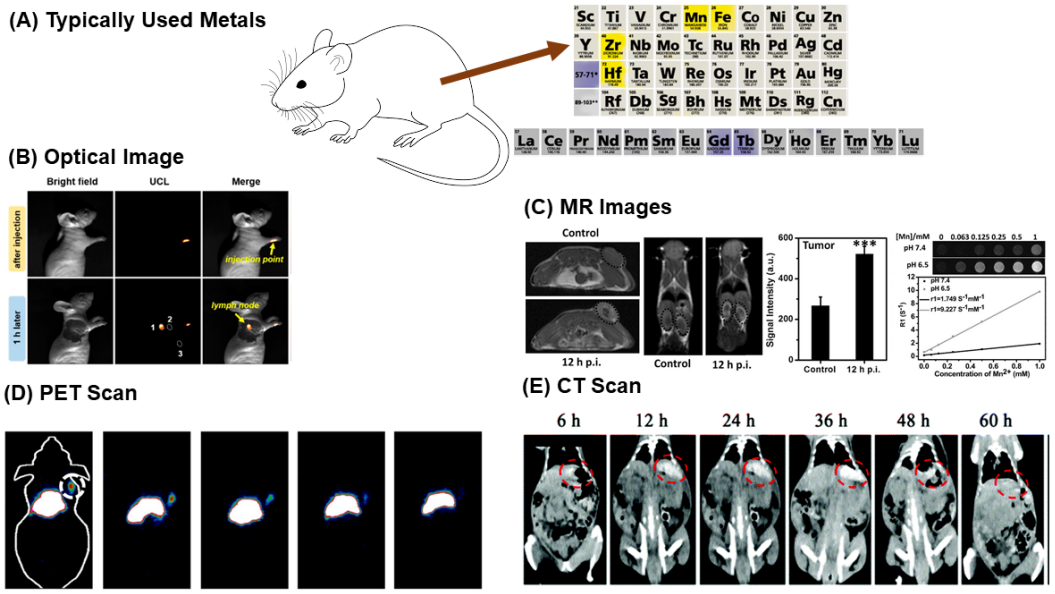

Figure 3. An overview of Metal-Organic Frameworks in biomedical imaging. Highlighted elements (yellow: transition metals, purple: lanthanides) typically used as metal clusters in MOFs for biomedical imaging such as (B) in-vivo optical imaging (C) MRI, (D) PET scanning and (E) in-vivo CT scan imaging

Gadolinium-based small molecules are the most commonly used contrast agents; thus, Gd-based MOFs arose as logical MRI contrast agent candidates. Lin and coworkers reported several experiments with Gd-containing nanomofs .[117] These Gd containing nanomofs possessed relaxation values about an order of magnitude higher than the widely clinically used contrast agent Omniscan.[118].In another approach, encapsulating superparamagnetic nanoparticles into MOFs may also produce effective contrast agents. [119] To avoid toxicity concerns with Gd, some researchers have switched their attention to other metal-based MOFs. Yang and coworkers developed Mn^{+2}-based MOFs with near-infrared dyes as

organic linkers which were shown to act as MRI contrast agents.[120] Chowdhuri and coworkers developed MOFs with internalized Fe_3O_4 nanoparticles.[121] Other Fe-based MOFs, such as Fe-MIL-53 carrying chemotherapeutics or oligonucleotides, have been tested as MRI contrast agents.[122] Another very important method X-ray computed tomography imaging, commonly referred to as CT scanning, provides a direct visualization of internal structures of a scanned object based on X-ray attenuation. X-rays are directed at an object at different orientations and a series of tomographic cross-sectional images are obtained to create a full 3D picture. Generally high atomic number elements such as iodine, barium, and bismuth are typically used as CT agents to contrast between tissues and using MOFs is advantageous as higher atomic number elements can be easily incorporated into MOFs. For example, Zhang and coworkers developed BODIPY-containing, UiO-based frameworks, named UiO-PDT. In-vivo CT imaging indicates preferential accumulation of MOF nanoparticles in tumor sites, providing enhanced contrast.[123] Sheng and coworkers reported a gold nanoparticle-incorporated MIL-88 MOF as a multifunctional diagnostic agent to give high-quality CT scans.[124] Another method termed Positron emission tomography (PET) relies on the accumulation of positron emitting radionucleotides at target organs which emit detectable gamma-ray photons upon decay. Capture data from detector panels can then be compiled to generate a three-dimensional image. Compared to other imaging techniques, PET imaging has better detection sensitivity in the picomolar range. MOFs with positron imaging radioisotopes are suitable choices for this technique. Hong and coworkers developed intrinsically radioactive UiO-66 with ^{89}Zr **SBU**s. These MOFs were further functionalized

with pyrene-derived polyethylene glycol (Py-PGA-PEG) and long peptide ligands.[125] These functionalized nano-MOFs demonstrated strong radiochemical and material stability in different biological media and acted as in-vivo, tumor-selective PET imaging agents. Given that the half-life of ^{89}Zr is much higher (78h) than traditionally used ^{19}F (2h), these Zr-based PET agents possess the potential for relatively long-term use. Finally, Optical imaging is a minimally invasive technique whereby light illumination is used to visualize tissue. However, this method suffers from the drawback of lower penetration depth. MOFs can play a role in upconverting wavelengths in affected tissues. Li and coworkers developed core-shell nanocomposite MOFs for luminescence imaging.[126] Cai and coworkers developed hyaluronic acid-coated MIL-100 MOFs loaded with dyes for imaging-guided cancer therapy.[127] Park and coworkers from Zhou group used a triplet-triplet annihilation up conversion system (TTA-UC) to harvest low energy photons in bioimaging. In their work, an anthracene-based Zr-MOF consisting of a porphyrinic photosensitizer was used. Due to the close proximity of the aligned chromophores, this system does an excellent job in increasing TTA-UC, particularly in aqueous media, demonstrative of an ideal in-vivo imaging system.[128]

Porous Materials as Therapeutic Reagents

Following developments in synthetic methodology for MOFs, formation of MOFs with specific functionality can be achieved through rational design of the organic linkers, metal clusters, and topology. MOFs can be utilized as superior platforms for therapeutic applications, whereby the therapeutic efficacy can be tuned and improved by a judicious modification to the structure. More importantly, the porosity of MOFs facilitates interaction between external species and active sites within the MOF structure and allows for encapsulation of therapeutic reagents to realize combined therapeutics. The most common therapeutic application of MOFs in the literature is to utilize MOFs as a photosensitizer in photodynamic therapy (PDT). PDT is a kind of non-invasive cancer treatment developed in recent decades. In this therapy, reactive oxygen species (ROS) are generated in the tumor cells by the excited photosensitizer under radiation of light, and then the ROS can cause tumor cell apoptosis and necrosis (**Figure 4a**). Compared to conventional therapies (chemotherapy, radiotherapy, and surgical tumor removal), PDT has minimal systemic side effects. However, the photosensitizers used are usually π-conjugated organic molecules with poor solubility and tendency to aggregate in cellular environments. Moreover, PDT cannot address metastasis of the tumor cells. MOFs can be integrated with photosensitizers on the organic linkers to then carry into the tumor cells. **Figure 4b** shows the common linkers integrated in MOFs for PDT. In 2014, Lin and coworkers[129] first applied MOF nanoparticles as photosensitizers in PDT. They constructed a UiO-type MOF, DBO-UiO, from 5,15-di(*p*-benzoato) porphyrin (H_2DBP) cores and Hf-oxo clusters. The nanoparticles of DPB-UiO were able to generate twice the

$^1O_2$ as the ligand alone under the same conditions. To test the performance of DBP-UiO as a PDT therapeutic, they carried out in vitro experiments on human head and neck cancer cells SQ20B and showed that cells treated with DBP-UiO had lower viability under light irradiation. To further enhance the PDT efficacy, Lin and coworkers[130] replaced the porphyrin core with a chlorin core and constructed a similar MOF, DBC-UiO [DBC = 5,15-di(*p*-benzoate) chlorin]. DBC-UiO has a red-shifted absorption spectrum and an 11-fold increase in extinction coefficient, resulting in a PDT efficiency three times that of DPC-UiO. To better target tumor cells, Park and coworkers modified the MOF, PCN-224, with folic acid (FA) to increase the affinity of PCN-224 for tumor cells.[131] Some tumor cells, such as cervical tumor cells, are known to overexpress folic acid receptors on their cellular membranes. Through the installation of FA on the Zr-oxo clusters, PCN-224 gains a higher affinity for ovarian cancer cells, indicated by the lower viability of ovarian cancer

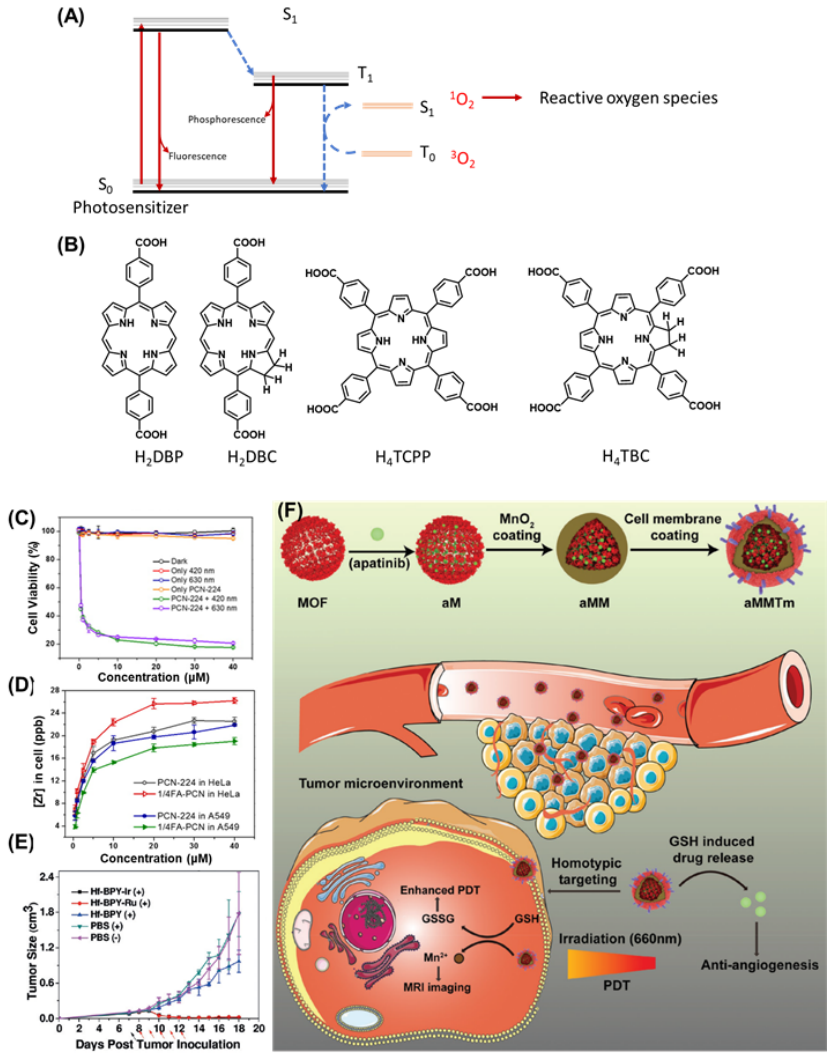

Figure 4. Metal-Organic Framework (MOFs) as therapeutic agents and a pictorial description of common mechanisms, Common porphyrin-based ligands and design and synthetic demonstration of multifunctional Photodynamic therapeutic systems in MOFs

cells compared to the FA receptor-negative cell line, A549, upon treatment with FA-PCN-224 **(Figure 4c&d)**. Apart from FA, more tumor-targeting molecules have also been utilized to increase the affinity of MOF nanoparticles for the tumor cells.[127, 132-134]

Limited by the penetration depth of visible light, PDT is mostly utilized to treat superficial tumors such as skin lesions and esophageal cancer. Unlike visible light, X-rays can penetrate soft tissue and potentially excite X-ray sensitizers to generate reactive oxygen species (ROS). Lan and coworkers constructed two-dimensional MOFs (Hf-BPY-Ir and Hf-BPY-Ru) with $[Hf_6O_4(OH)_4(HCO_2)_6]$ clusters and $[Ir(bpy)(ppy)_2]^+$- or $[Ru(bpy)_3]^{2+}$-derived tricarboxylate ligands.[135] The Hf-clusters in the 2D MOFs can effectively absorb X-rays and transfer the energy to the $[Ir(bpy)(ppy)_2]^+$ or $[Ru(bpy)_3]^{2+}$ moiety in the organic linker, subsequently generating $^1O_2$ from $^3O_2$. This energy transfer pathway was verified by radioluminescence, where the luminescence from the Ru/Ir moiety could excited by X-ray. Importantly, the 2 Gy X-ray dose is low compared to the 20-40 Gy doses used in radiotherapy. Moreover, the synthesized MOFs have nanosheet morphologies with thicknesses of about 1.2 nm, believed to be optimal for rapid ROS diffusion within the pores. In vitro experiments were conducted with CT26 (murine colorectal carcinoma cell) and MC38 (murine colon adenocarcinoma cell) cell lines to confirm the anticancer efficacy. These conclusions were further confirmed by in vivo experiments, whereby one week of the injection and X-ray treatment inhibited and reversed tumor growth (**Figure 4e)**. These results have shown that an X-ray PDT strategy can treat deeply seated tumors with a low X-ray dosage, broadening the applicability of PDT. has furthered the

development of this strategy by providing more examples of X-ray PDT. The same research groups with different MOFs and singlet O_2 generation moieties.[136-138]

Owing to their porous nature, MOFs offer the potential of bioactive molecule encapsulation to further enhance therapeutic activity. In pursuit of this advancement, researchers have been very creative in combining PDT-active MOFs with other therapeutic reagents to realize more advanced synergistic therapy. For example, Lin and coworkers[139] successfully combined immunotherapy and X-ray PDT using MOF nanoparticles. They designed an X-ray PDT-active MOF with an encapsulated immunoregulatory enzyme-inhibitor. The embedded inhibitor can trigger systemic immunity to prevent the regrowth of the tumor cell after the termination of X-ray PDT. In another example, Yang and coworkers combined photothermal therapy (PTT) with PDT by using a ferriporphyrin (FeP) MOF to encapsulate Hsp70 siRNA**.**[140] The decreased thermal tolerance endowed by Hsp70 siRNA in synergy with the ROS generation upon near-infrared (NIR) laser excitation of the FeP core results in effective damage to the tumor. More examples on the combined therapy of PTT and PDT have been widely reported in different MOF platforms, indicative of the versatility of the MOFs in combined PTT/PDT therapy.[141-143] Beside the combined therapy of PTT and PDT, a more complicated multicomponent system is represented by a recent example from Li and coworkers.[144](**Figure 4e)** Tumor cells can produce glutathione (GSH) to reduce damaging ROS. Furthermore, the long-term efficacy of PDT can be deterred by the product of the protumor factors after massive cell death, particularly the angiogenic factors. Therefore,

Zhang and coworkers furthered the PDT application of PCN-224 by equipping the MOF with a MnO_2 shell to oxidize GSH, after which apatinib, an antiangiogenic reagent guest molecule can be released. This sophisticated system has been proven highly efficient in reducing the size of several tumors by in vivo experiments.

The Goal of the Research Presented in This Dissertation

As this detailed discussion in this section about section Metal-Organic Frameworks and Porous Coordination Cages points out that they can be used in many diverse applications. They are easy to fine-tune to serve any purpose, which makes them excellent candidates to explore further. In this study, I used two approaches to tune two representative porous materials: **M**etal-**O**rganic **F**rameworks (MOFs) and **P**orous **C**oordination **C**ages (PCCs) via 1) post-synthetic modifications of pore environments and 2) self-assembly of required elements in framework structures, for sustainable environmental applications. Most modification approaches to optimize the pore environment of Metal-Organic Framework either suffer from great synthetic difficulty or lack of control in pore size distributions in frameworks. I aim to overcome these all complications via a novel method to create mesoporous defects in a stable Metal-Organic Framework and to dope the mesoporous defects with long alkyl chains to improve the nonpolar environment in the MOF pores (chapter II). I also try to develop another method to create systematic mesopores while providing non only non-polar interactions but ionic interactions in pores with methane molecules. Methane uptakes were validated by high-pressure gas sorption isotherms (chapter III). Finally, I try to develop a series of novel Porous Coordination Cages to

incorporate a cheap, abundant metal cluster into its pores, aiming to create a better catalyst for hydrogenation reactions (chapter IV). The results of this thesis will aid in developing new generation MOF and cage materials for gas storage and catalysis applications.

CHAPTER II

INCORPORATION OF HEAVY ALKANES IN METAL ORGANIC FRAMEWORKS FOR IMPROVED NATURAL GAS UPTAKE*

Introduction

Natural gas, the principal ingredient of which is methane, can either be directly used as a fuel or processed into other energy resources.[145] Many energy-intensive solutions have been proposed to capture, store, and transport natural gas into the US energy infrastructure.[146] For example, natural gas can be successfully compressed to higher pressures up to 250 bar (3,600 psi), which is commonly referred to as compressed natural gas (CNG). It can also be liquefied at the temperatures less than −160 °C, producing liquefied natural gas (LNG). These century-old technologies are known to improve the energy density of natural gas, to 9.2 MJ L^{-1} for CNG or 22.2 MJ L^{-1} for LNG, respectively. Still, they are subsequently downgraded by about 30 % volumetrically to account for their real cylindrical containment requirements.[147] In addition, both applications have intensive energy demands, creating critical cost issues. These issues have resulted in failure to fully utilize America's natural gas reserves.

---

*Parts and figures of this chapter are reprinted with permission from Fang, Y^{+}.; **Banerjee, S^{+}.**; Joseph, E. A^{+}.; Day, G. S.; Bosch, M.; Li, J.; Wang, Q.; Drake, H.; Ozdemir, O. K.; Ornstein, J. M..; Lu, T.-B.; Zhou, H.-C., Incorporating Heavy Alkanes in Metal-Organic Frameworks for Optimizing Adsorbed Natural Gas Capacity. *Chemistry. A European Journal* **2018,** *24* (64), 16977-16982. (+ represents equal contribution). Copyright Wiley 2018

Adsorbed natural gas (ANG) is an increasingly important method of improving natural gas storage.[26, 148] In the past few decades, a variety of candidate absorbents containing high surface areas, controlled pore diameters, and moderate binding energies have been developed for research.[149] As a precisely tunable porous material, metal-organic frameworks (MOFs) have attracted considerable interest recently with their potential to boost ANG technologies.[150] Theoretical works suggested a conceptual MOF, IRMOF-993, could have a volumetric methane storage capacity well above activated carbon.[78] However, the MOFs in the study suffers from low chemical stability, especially in the presence of trace natural gas pollutants like hydrogen sulfide or water vapor.[79, 151] Alternatively, an iron cluster-based MOF, PCN-250, is a radical departure from previously reported ANG MOFs due to its considerably higher stability. It is stable in boiling water as well as a wide range of pH conditions, maintaining its crystal structure and surface area. Moreover, PCN-250 exhibits a total reported methane storage capacity of 180 v (STP)/v , exhibiting a flat heat of adsorption curve, while also being capable of low-cost production.[152] Here, we provide a post-synthetic treatment of PCN-250, aiming to obtain an enhanced, regenerable methane storage absorbent. The addition of a small portion of high boiling point alkanes into natural gas to increase the compression and refrigeration storage has been used for CNG and LNG for many years.[153] The alkanes not only increased the boiling point of the liquefied methane but also dissolved the hydrophobic methane through hydrophobic interactions.[154] Inspired by this idea, we incorporated C_{10} and C_{14} hydrocarbons into the pores of PCN-250 as a method of improving the ANG concept. We have dubbed the combination of methane absorption in high alkanes at high pressures,

and its adsorption on the surface/pores of a porous material, HAANG (High Alkane Adsorbed Natural Gas). The doped system allows for a higher volume of methane to be stored as compared to the unmodified adsorbent at a given pressure. Most of the high alkane is also retained in and on the adsorbent through many working cycles of adsorption and desorption. This two-phase process, containing both liquid and vapor, can be achieved at suitable pressures (30–100 bar) and temperatures (260–323 K) for ANG technology.

Initial Testing with HAANG Process

To Realize the HAANG process, an apparatus was designed and constructed for direct volumetric measurement of methane uptake and delivery, as shown in **Figure 5** (A and B). The methane gas was first transported from the gas tank (②) to the charger unit ⑥. Then, the PCN-250 adsorbent (1 gram) was loaded into a test cell, ⑨. By controlling the valves (⑤, ⑦, and ⑧), methane gas can be transported to the test cell and adsorbed by PCN-250. Due to the presence of a pressure transducer (P/T) on the bottom of the charging unit, the final pressure (P_{fin}) can also be recorded. The initial pressure subjected to the methane supply inlet was assigned as P_{ini} (960 psi). By comparing the P_{ini} and P_{fin}, the adsorbed gas volume can be measured by the ΔP ($P_{ini} - P_{fin}$).

Furthermore, the adsorbed gas in the test cell was discharged from the system and released into an airbag (1 L). A flow of atmospheric air was then injected into the airbag until it was full (1 L) to dilute the methane gas. A gas syringe was then used to inject 10 mL of

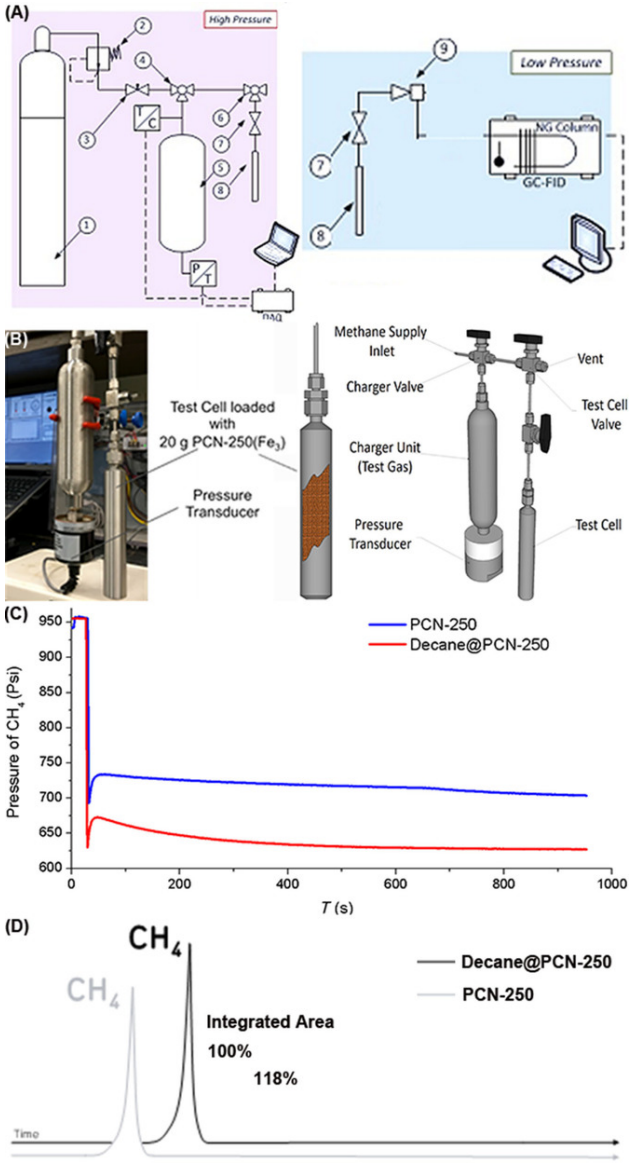

Figure 5. (A) Scheme of real-time gas monitoring station. (B) A detailed demonstration of charger unit. (C) Real-time monitoring of pressure drops of PCN-250 and PCN-250 doped with decane. (D) The GC-FID chromatogram shows the deliverable methane from PCN-250 and PCN-250 doped with decane.

the gas mixture into a gas chromatography-flame ionized detector (GC-FID). Due to the deliverable methane being different for every experiment and the total volume of the Airbag is a constant (1 L), the 10 mL in the syringe contains different amounts of methane. The injected methane gas was quantified by the integration area of the GC data. The integration area can represent the different ratios of deliverable methane in the airbag; thus, the variation of deliverable methane can be analyzed. By using this system, it was found that PCN-250 can absorb and deliver an almost equal amount of methane gas repeatedly.

The methane uptake capacity of the alkane-doped PCN-250 samples (defined as Decane@PCN-250) was also measured with their methane uptake properties according to the above procedure. A sample of 1 gram of PCN-250 was filled in the test cell and fully activated under vacuum at 160 °C. Then the test cell was taken into an inert atmosphere (glove box), and 60 μL of *n*-decane was injected. After standing for 20 min, the test cell was sealed with 2 μm VCR gasket for the following gas test. Methane gas at 960 psi (66.2 bar) pressure was stored in the charger unit and then injected into the test cell. The pressure drop ΔP for the PCN-250 sample was 275 psi, which could be translated into adsorbed methane. Surprisingly, when PCN-250 was doped with *n*-decane, we found there was a dramatic increase of 21.8 % for the ΔP (335 vs. 275 psi, **Figure 5 C**). This suggests that *n*-decane-doped PCN-250 has a storage capacity 21.8 % higher than that of pristine PCN-250. **Figure 5 D** shows a GC chromatogram comparing deliverable methane from PCN-250 at atmospheric pressure in the presence and absence of the doping agent (*n*-decane).

Similarly, when PCN-250 was doped with *n*-decane, an 18.0 % increase in the integrated area of the methane peak was observed. The pressure drops and GC results demonstrated an increase in total volumetric methane uptake of about 18 %

alongside the full desorption of methane, with the *n*-decane remaining in the PCN-250 adsorbent (not detectable by GC). It should be noted that the *n*-alkane loading was quite low (60 μL per 1 gram of adsorbent), accounting for 4.4 wt % of the MOF. When switched to a larger test tube filled with 20 grams of absorbents, a similar increase in methane uptake was observed. Also, increasing the loading of *n*-decane with the MOF tended to result in decreasing methane storage capacity. **(Fig 6)** We assume that too much *n*-decane would block the entrance of methane, thus inducing a decrease of methane uptake. Further screening of doping agents and engineering of the MOF–dopant interactions are needed to understand the system and demonstrate it as a proof-of-concept.

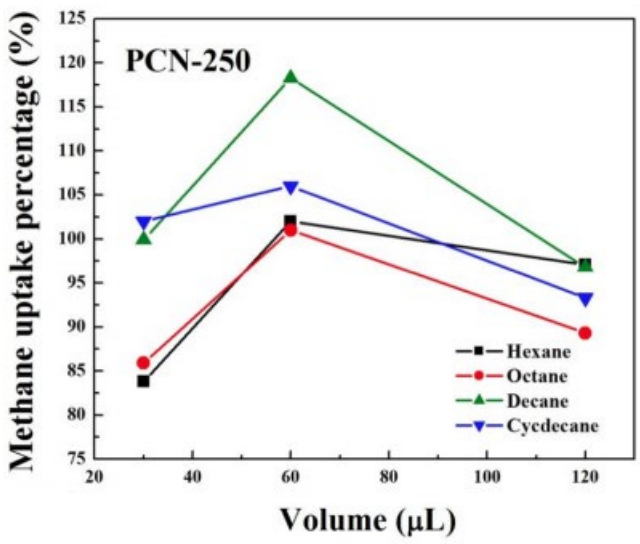

Figure 6. Capability of methane adsorption observed when PCN-250 is employed as adsorbent material in connection with different hydrocarbons with various amount.

Experimental Section

Instrumentation and Materials

Powder X-ray diffraction (PXRD) was carried out with a Bruker D8-Focus Bragg-Brentano Xray Powder Diffractometer was equipped with a Cu sealed tube (λ = 1.54178 Å) at 40 kV and 40 mA. Scanning Electron Microscopy (SEM) measurements were carried out on JEOL JSM-7500F. JEOL JSM-7500F is an ultra-high-resolution field emission scanning electron microscope (FESEM) equipped with a high brightness conical FE gun

and a low aberration conical objective lens. Thermal Gravimetric Analysis (TGA) was performed using a Mettler-Toledo TGA/DSC STAR*e*-1 system which was equipped with a GC100 gas controller. N_2 sorption measurements were conducted using a Micromeritics ASAP 2020 and 2420 system. High-Pressure real-time monitor equipment was built by our group. The equipment is consisting of cylinders valves, GC-FID and a PC. High-Pressure CH_4 adsorption isotherms were carried out on HPVA II high pressure volumetric analyzer from micromeritics. Solvents were purchased commercially and used without further purification.

Synthesis of PCN-250

PCN-250 is an iron-based MOF, also known as MIL-127, is an iron-based framework comprised of a trimeric metal cluster, formed by three Fe(III) octahedra sharing a central μ_3-oxo, linked by 6 ABTC ligands (ABTC = 3, 3‘, 5, 5‘-azobenzenetetracarboxylate), which each form four connections to the metal clusters via the carboxylate groups, resulting in a **soc** net. The preparation of the 3,3’,5,5’ Azobenzene-tetracarboxylic acid (H_4ABTC) can be accomplished on a 50-g scale using a standard reductive coupling reaction between 5-nitroisothalic acids in a single-step procedure. The preparation of PCN-250 can be executed using one of two approaches. In the first approach, metal clusters of $[Fe_2Fe(\mu_3\text{-}O)(CH_3\ COO)_6]$ are synthesized before the introduction of the organic ligand, forming the MOF, giving single crystals of the iron MOF. In the second approach (which is useful for large batch synthesis) we can use a one-pot method, combining the iron salt, organic ligand, and an acetic acid modulator to prepare PCN-250.

Synthesis of azobenzene-3,3',5,5'-tetracarboxylic acid (H_4ABTC)

To a mixture of 5-nitroisophthalic acid (2.1 g, 10 mmol), Zn (1.3 g, 20 mmol), and NaOH (0.8 g, 20 mmol) in a mixed solvent of ethyl alcohol (50 mL) and water (20 mL) was refluxed for atleast 12 h. A yellow precipitate was obtained and collected by filtration. The solid was dissolved in 50 mL of NaOH (aq, 1 M) and the solution was filtered to remove an insoluble residue. The filtrate was acidified to pH = 3 with 3 M HCl (aq) to afford 1.59 g of H_4ABTC

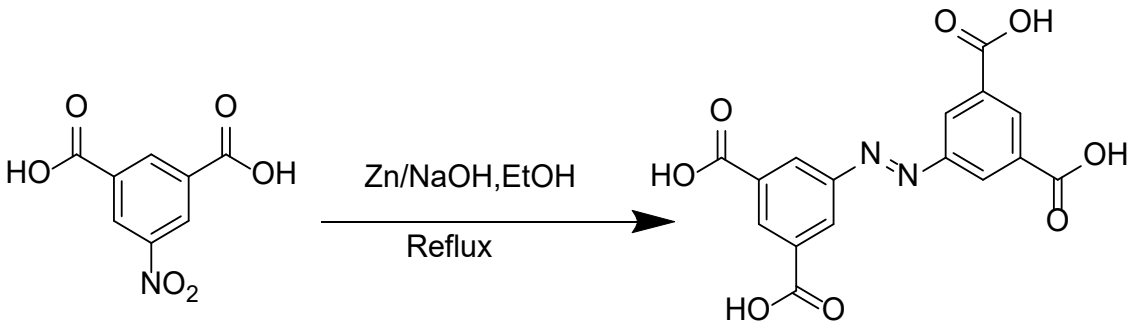

as a yellow solid (yield: 85%). The compound was recrystallized over hot DMF.^{1}H-NMR (DMSO-*d6*): 8.48 (t, 4*J* = 1 Hz, 1H), 8.65 (t, 4*J* = 1 Hz, 1H), 8.76 (d, 4*J* = 1 Hz, 2H), 8.90 (d, 4*J* = 1 Hz, 2H), 13.60 (s, br, 4H).

Synthesis of PCN-250 (small scale first method)

Iron (III) nitrate nonahydrate (8g, 0.02 mol) was dissolved in 70 ml of water in a 500 ml round bottom flask with a mechanical stirrer. This is mixed with a solution of sodium acetate trihydrate (42 g, 0.31 mol) in 70 ml water. The mixture is stirred in 80 °C for 12 hrs. a red-brown precipitate appears. The precipitate was filtered and dried in a vacuum

oven and used without further purification. 10 mg of ligand, 15 mg of preformed iron cluster, 2 ml DMF and 1 ml acetic acid was added in a vial, sonicated to dissolve entirely and heated in an oven for 12 h in 150 °C. MOF crystals will appear as dark brown crystals after 12 h. The vial was taken out and cooled down to room temperature. The MOF crystals were subjected to solvent exchange two times with DMF, the 1-time Methanol then final time acetone. Dried and taken for gas sorption.

Synthesis of PCN-250 (large scale, second method)

Fe $(NO_3)_3 \cdot 9H_2O$ (5.4 g), H_4ABTC (1.8 g), Acetic Acid (3 L), and DMF (6 L) were added into a jacketed 10 L Pyrex high-pressure reaction vessel. The vessel was then heated to 150 ºC for 12 h. The resulting reaction slurry was then removed and subjected to solvent exchange multiple times with DMF (2 times), Methanol (2 times), and acetone (1 time). Dried and taken for further analysis.

Creating Mesopores in PCN-250 via Mild Physical Treatment

5 g of PCN-250 is placed in a cellulose thimble, placed in the Soxhlet extractor. Ensure that the cellulose thimble is no more than half full. Fill a 500ml round bottom flask with 300 ml of methanol, add a magnetic stir bar and place the setup in a heated oil bath set to at least 85 °C. **(Fig 7)** Attach the Soxhlet extractor with the PCN-250 to the top of the round bottom flask, followed by a water condenser. Allow refluxing overnight. Product

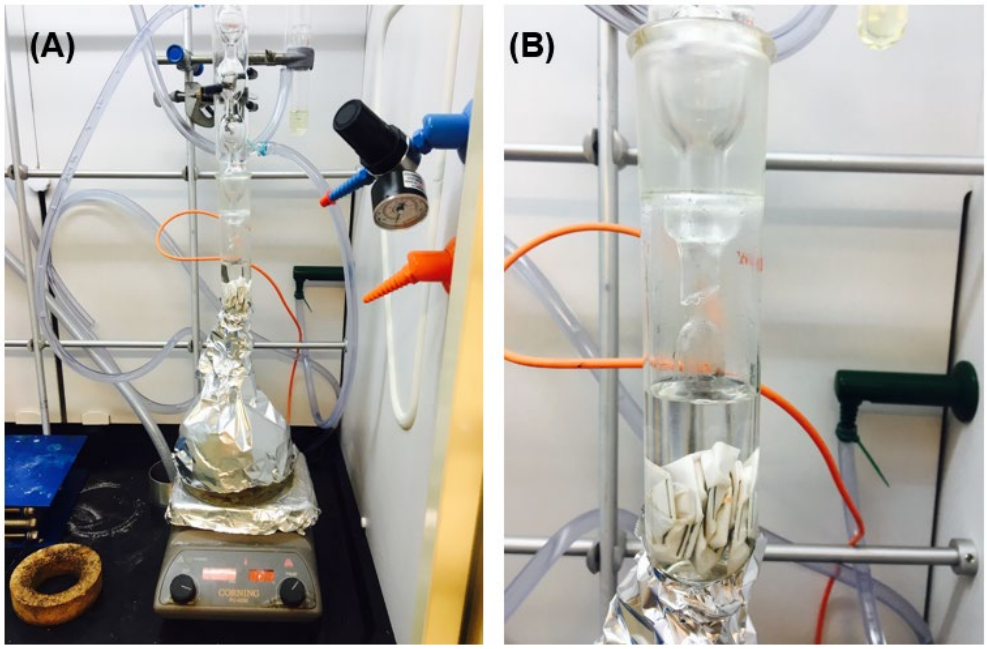

Figure 7. (A) Experimental setup of the mesopore generation reaction in PCN-250. (B) The PCN-250 can be put in cellulose paper wrap in batches.

can be filtered and dried with a Buchner filtration setup. The sample should be loosely covered and dried in a 70 °C oven overnight. The dried MOF to a sorption tube (Micromeritics) and activate the sample at 180 °C for 12h. Take a nitrogen isotherm at 77K of the sample to determine the sample quality for each day, and the mesoporous sample was taken for doping studies.

Alkane Doping in PCN-250

Fully Activated PCN-250 was taken in an inert atmosphere (Glovebox) and injected a designated amount of alkane. Kept for equilibrating for 20 minutes and then sealed with 2-micron VCR gasket for high-pressure absorption.

Fatty Acid Doping in PCN-250

500 milligrams (Excess amount) of myristic acid per gram of MOF was solubilized in methanol and then treated with fully activated PCN-250. After that, it was kept in a vacuum oven at 80 ºC for 5 hours for drying. After drying the MOF was washed with an excess amount to methanol to wash away any loosely attached myristic acid. After washing the MOF was activated fully for gas uptake measurements.

Results and Discussion

Considering that *n*-decane (van der Waals diameter ~14 Å) is too large to be accommodated within the cavity of PCN-250 (pore size 8 Å), we hypothesized that it could be located within the mesoporous defects of the MOF. Thus, we introduced mesoporous defects into PCN-250 by Soxhlet treatment to create mesoporous PCN-250 samples. The PCN-250 sample prepared according to reported literature is defined as

Micro-PCN-250. The Soxhlet treatment sample, Meso-PCN-250, maintained the same crystalline morphology **(Figure 8)** as Micro-PCN-250.

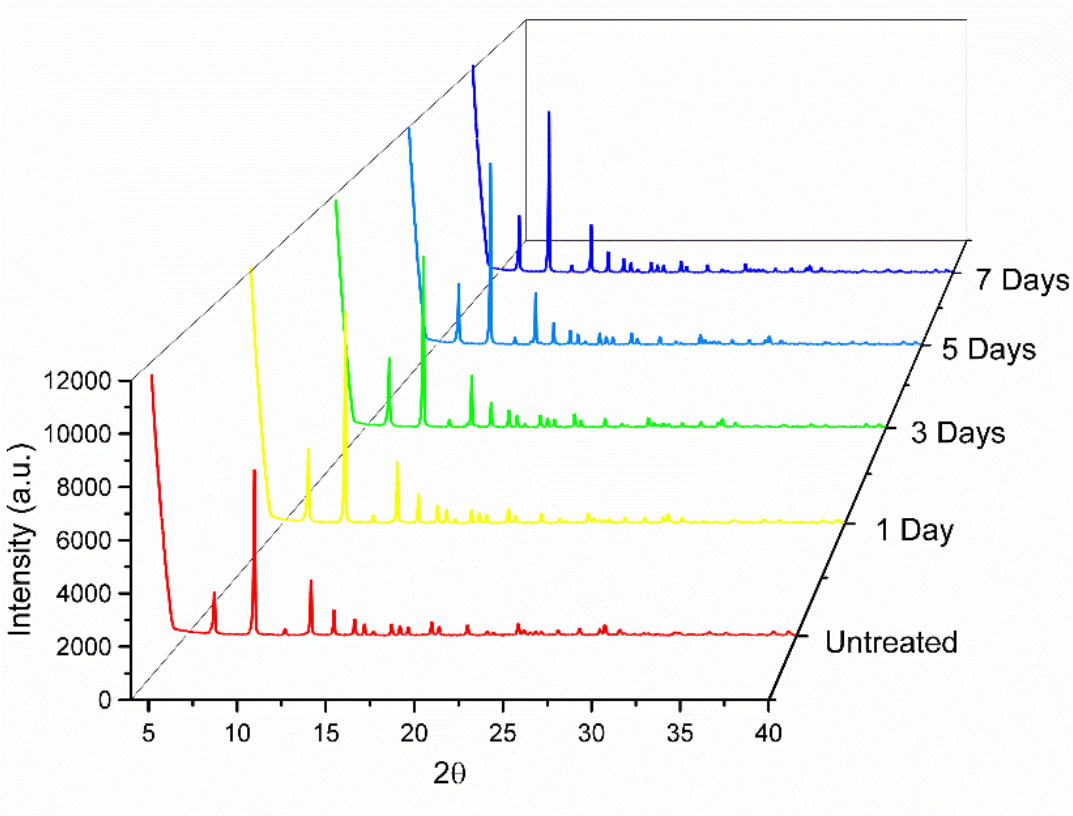

Figure 8. PXRD patterns of untreated PCN-250 samples (microporous) and Soxhlet treated samples over the days. Yellow (1 day), Green (3 days), Cyan (5 days) and Blue (7 days) Soxhlet washed samples show no change in crystallinity.

However, high-resolution scanning electron microscopy (SEM) imaging revealed that the mesoporous defects (about 3–5 nm) were generated at the surface of Meso-PCN-250 **(Fig 9).**

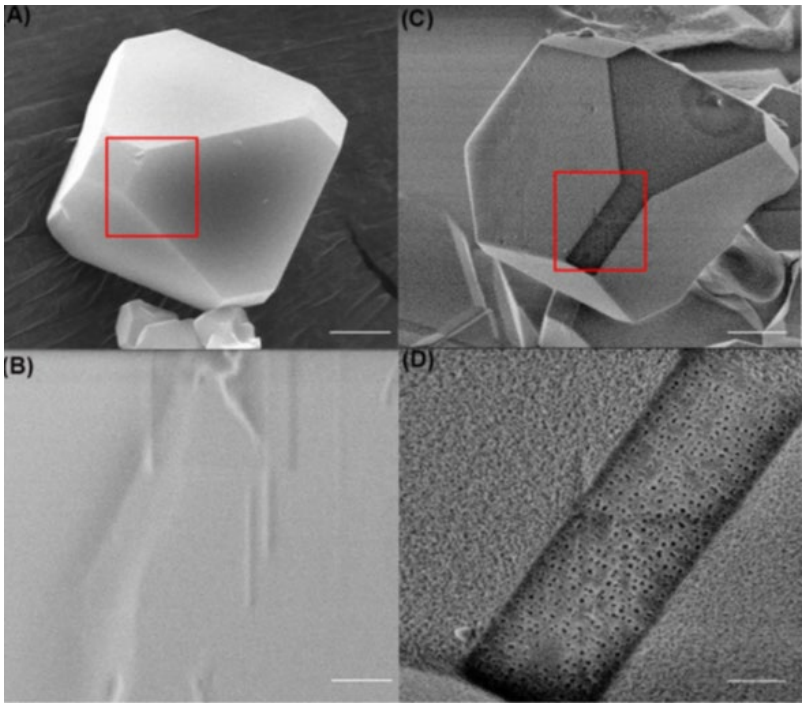

Figure 9. (A) SEM images for micro PCN-250 (C) SEM image of meso-PCN-250. (B) & (D) Enlarged SEM image of the red reticular zone in micro-PCN-250 (A) and meso-PCN-250 (C). Scale bar for (A) and (B): 1 µm. Scale bar for (C) and (D): 200 nm.

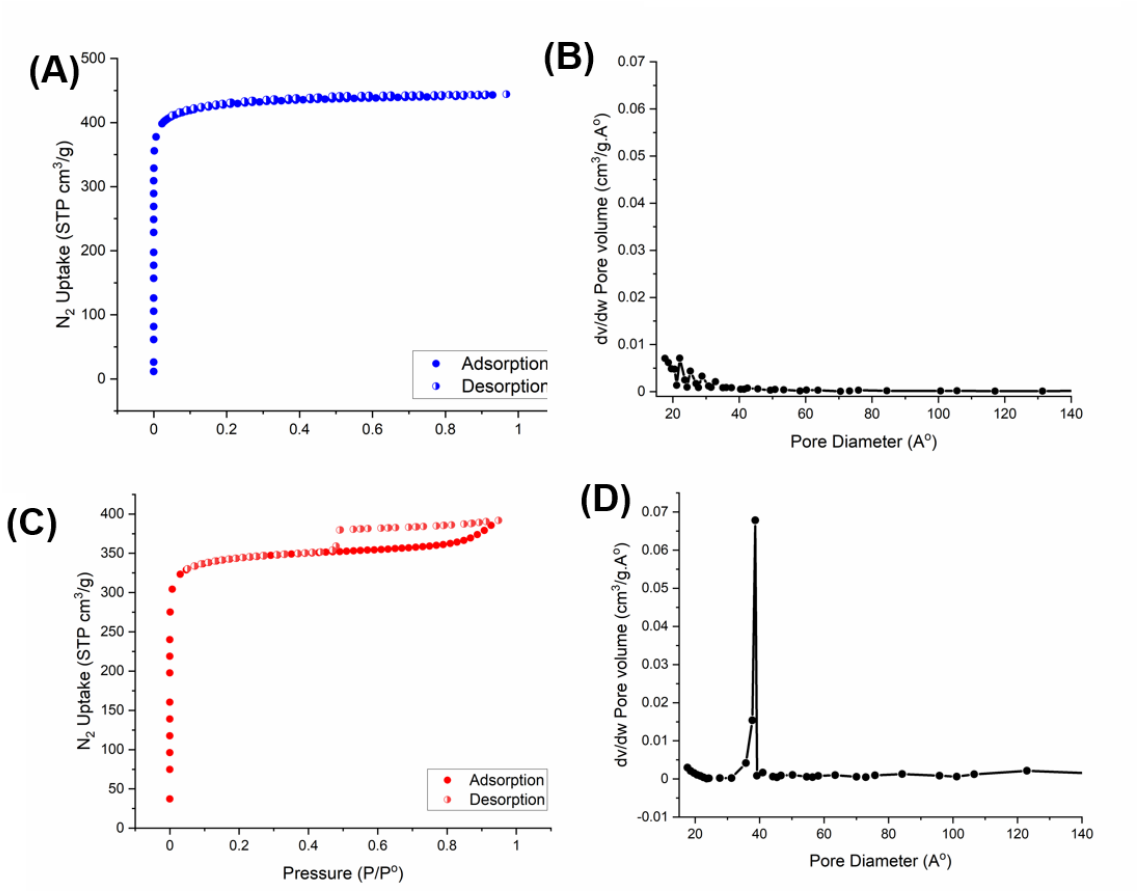

Figure 10. N_2 **isotherm of (A) Micro-PCN-250 and (C) Meso-PCN-250. BJH desorption pore size distribution of (B) Micro-PCN-250 and (D) Meso-PCN-250 (only the mesoporous region is shown).**

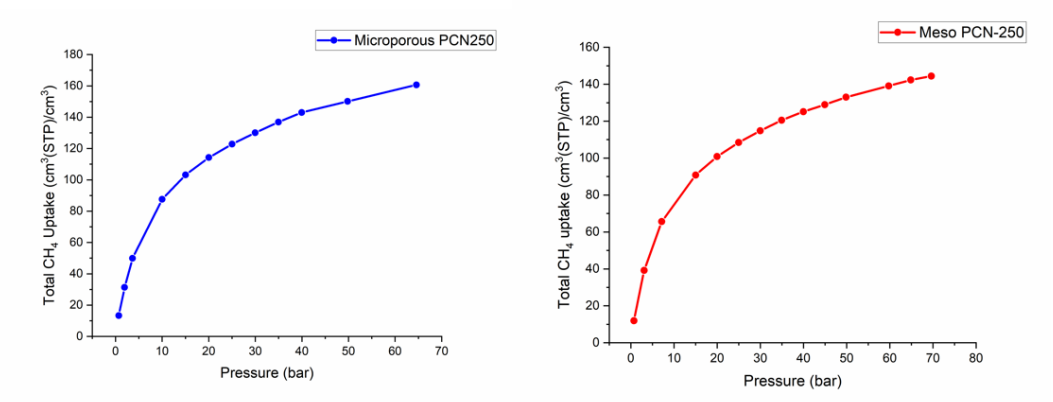

Figure 11. High-pressure methane uptake of (Left blue isotherm) Micro-PCN-250 and (Right red isotherm) Meso-PCN-250.

The total N_2 uptake capacity of Meso-PCN-250 (398 $cm^3\ g^{-1}$ STP) is largely similar to Micro-PCN-250 (405 $cm^3\ g^{-1}$ STP). Notably, the N_2 adsorption-desorption isotherm (**Figure 10**) at 77 K displays a type-IV isothermal with hysteresis loops characteristic of large constricted mesopores for Meso-PCN-250, providing evidence for Soxhlet-induced mesopores within the framework. The pore-size distribution **(Figure 10 (B) and (D))** as determined by the Barrett–Joyner–Halenda (BJH) desorption model, unambiguously shows that Meso-PCN-250 has ordered 3.8 nm mesopores, whereas Micro-PCN-250 does not.

The high-pressure methane uptake of both PCN-250 adsorbents was measured at 298 K using a Micromeritics HPVA-II **(Fig 11).** The Meso-PCN-250 has a methane uptake of 142 $cm^3\ cm^{-3}$ at 65 bar, 11.8 % lower than Micro-PCN-250 (161 $cm^3\ cm^{-3}$). It is well-known that mesoporous MOFs tend to have poor methane storage capabilities due to the large pore openings not being optimized for binding methane molecules.[155, 156] From the above characterization, we realized that Meso-PCN-250 maintains similar crystallinity and gas adsorption performance to Micro-PCN-250. However, Meso-PCN-250 exhibited a distinct pore-size distribution. The ordered and uniform mesopores of Meso-PCN-250 make it a suitable candidate for the investigation of hydrocarbon loading in PCN-250. As the loaded alkanes investigated for the phenomenon tend to be in the gaseous or liquid phase and are easily desorbed, it is difficult to determine the actual loading within the MOF during tests. To prevent this ease of desorption, we opted to investigate fatty acid incorporation into MOFs. Considering that fatty acids are capable of coordinating with the metal cluster of the MOFs, they will have more durable binding to the MOF frameworks. Doped samples of *n*-decane and myristic acid, Decane@Meso-PCN-250 (4.4 wt % loaded) and Myristic@Meso-PCN-250 (50 wt % loaded), were prepared accordingly. A PXRD of the doped absorbents found to be a very similar pattern to that of as-synthesized PCN-250 and the simulated pattern. The IR (infrared) spectrum **(Figure 12)** of Myristic@Meso-PCN-250 shows a representative peak for myristic acid at 2800–2900 cm^{-1}, indicative of the successful binding of myristic acid to the MOF framework.[157] As seen in **(Figure 12)**, the thermal stability of samples before and after doping was analyzed by thermal gravity analysis (TGA). The TGA curve of Meso-PCN-250 displays a mass

loss of 5.6 % below 100 °C, likely resulting from the removal of methanol from the framework. From 100–400 °C, the mass loss of Meso-PCN-250 is 17.0 %, corresponding to the loss of residual guest DMF molecules. The Decane@Meso-PCN-250 sample demonstrated a similar TGA curve, but with one more weight loss step (12.1 %) starting from 220 °C, which resulted from the loss of decane (boiling point of 174 °C). However, the TGA of Myristic@Meso-PCN-250 exhibited significant differences when compared to the above two samples in TGA. Below 150 °C, there is a significant mass loss of 19.2 %, corresponding to the loss of methanol used in the loading of myristic acid (boiling point of 326 °C). In the range of 150–400 °C, the mass loss of Myristic@Meso-PCN-250 is only 7.3 %, which is the smallest of the three compared samples. This showcases the relatively slow desorption of myristic acid as compared to *n*-decane and DMF. There is also a slight shift in framework decomposition temperature in the Myristic@Meso-PCN-250, from 400 °C to 410 °C. This shift suggests that the myristic acid attached to the MOF increases the thermal stability of the structure.

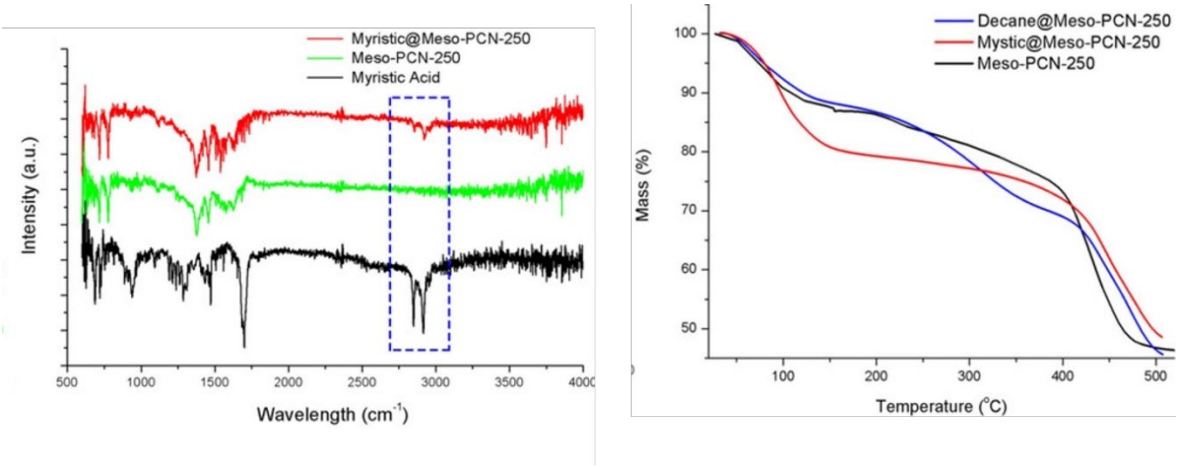

Figure 12. FT-IR spectrum of Meso-PCN-250 and Myrstic@Meso-PCN-250, and compared with myristic acid authentic sample. (Right) TGA curve of Meso-PCN-250, Decane@Meso-PCN-250, and Myristic@Meso-PCN-250.

After doping with *n*-decane and myristic acid, both PCN-250 adsorbents were measured for high-pressure methane uptake at 298 K using the HPVA-II from Micromeritics **(Figure 13 A and B)**. The two doping reagents, *n*-decane and myristic acid, have minimal volumetric methane uptakes in the absence of the framework at 65 bars (10 $cm^3\ cm^{-3}$ *v /v)*. When Micro-PCN-250 was doped with *n*-decane and myristic acid, a decrease in methane uptake at 65 bars was observed (132 and 121 $cm^3\ cm^{-3}$ *v /v,* respectively). In contrast, when Meso-PCN-250 was doped with *n*-decane, the methane uptake at 65 bar improved from 142 to 203 $cm^3\ cm^{-3}$ *v /v*, which is a 43.0 % increase compared to pristine Meso-PCN-250 **(Figure 13 A).** When compared to the pristine Micro-PCN-250, the increased

value is 26.1 %, which is comparable to the 18 % increase for deliverable methane. In addition, the working capacity (5–65 bar) of Decane@Meso-PCN-250 was also elevated, reaching 159 compared to 110 $cm^3\ cm^{-3}$ *v* /*v* for Micro-PCN-250. Myristic@Meso-PCN-250 can reach a total methane uptake capacity of 173 $cm^3\ cm^{-3}$ *v* /*v* at 65 bars **(Figure 13 B)**, and 192 $cm^3\ cm^{-3}$ *v* /*v* at 95 bars. To the best of our knowledge, the 192–203 $cm^3\ cm^{-3}$ *v* /*v* values represent record-high methane uptake of mesoporous PCN-250 adsorbents reported so far.[158, 159] It was also noted that the methane uptake increased faster for *n*- decane than that for myristic-acid-doped samples when increasing the pressure **(Figure 13 C and D**). This can likely be ascribed to the stronger interactions between methane and high alkanes, such as *n*- decane.[160, 161] Although *n*-decane doping has better methane adsorption performance than myristic acid doping, the recyclability follows the reverse trend **(Figure 13 E and F).** After three cycles, the performance of *n*-decane-doped samples was reduced to 50 % of the initial cycle. Due to the lack of strong interactions

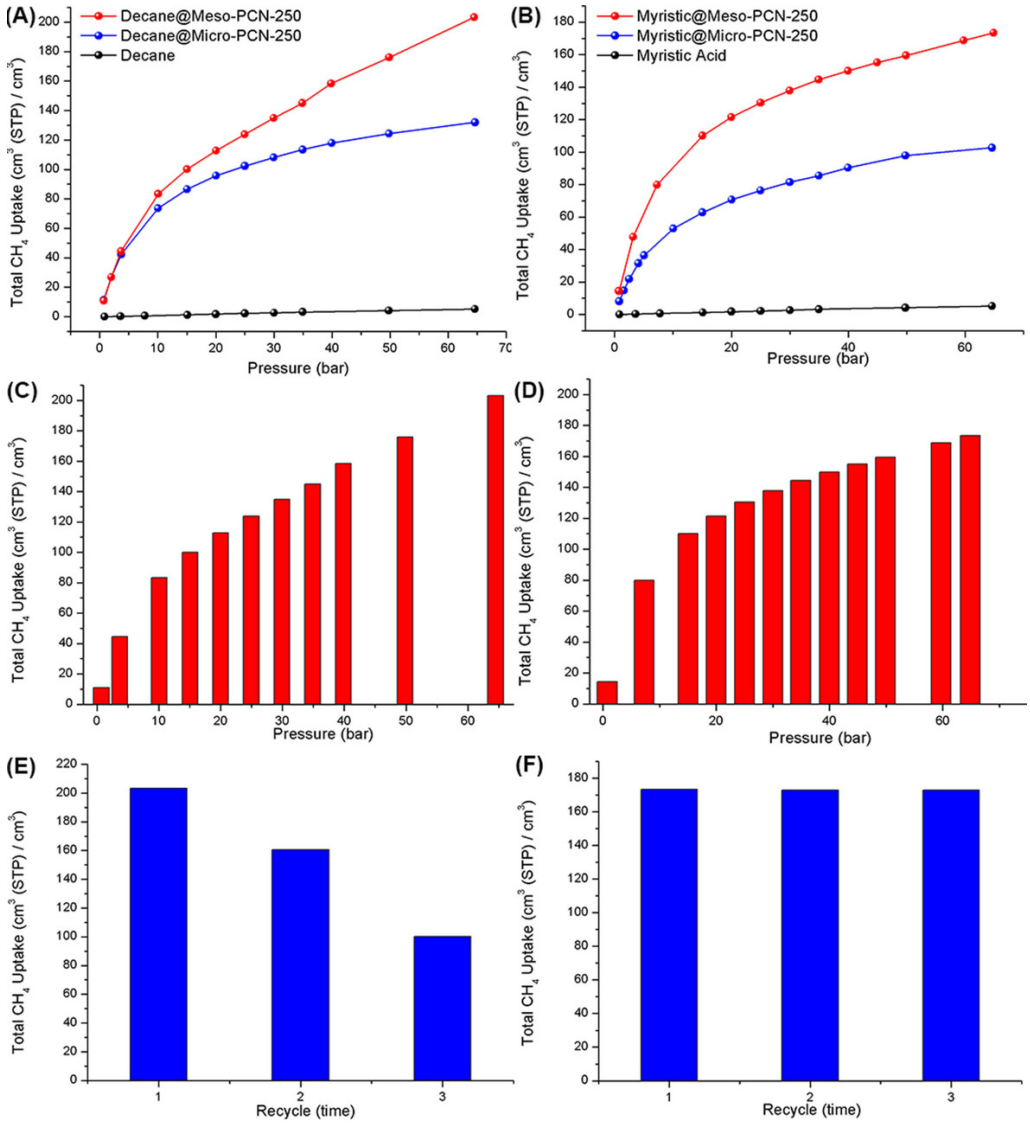

Figure 13. High-pressure methane uptake of Micro-PCN-250 and Meso-PCN-250 doped with n-decane or myristic acid. Volumetric total methane uptake of Micro-PCN-250 and Meso-PCN-250 doped with (A) *n*-decane and (B) myristic acid. Total methane uptake of Meso-PCN-250 doped with (C) *n*-decane and (D) myristic acid at each pressure. Recyclability test of Decane@Meso-PCN-250 doped (E) and Myristic@Meso-PCN-250 (F).

between *n*-decane and the MOF, it is difficult to prevent the *n*-decane from leaching from the framework during the regeneration process, which included vacuum-assisted heating. After three cycles, the subsequent two cycles maintained a performance that was 45 % that of the original. In contrast, myristic-acid-doped Meso-PCN-250 showed consistent performance even after three cycles. As expected, the carboxylic acid moieties of the fatty acid can bind to the metal cluster of the MOF adsorbent, reducing the loss of dopant during the desorption process.[162] The weight of myristic acid doped Meso-PCN-250 for each cycle was also measured, and no weight loss was found. This strongly indicated the retention of fatty acids within the framework throughout the gas storage cycle. According to the results obtained above. Through Soxhlet treatment, defects were created in the microporous PCN-250, yielding mesoporous PCN-250. Considering that mesopores have no significant interactions with small molecules, such as methane, methane uptake of undoped mesoporous PCN-250 was lower than that of undoped microporous PCN-250. In contrast, myristic acid strongly binds to the open metal sites of PCN-250, with long alkane chains located in the Mesopores. By taking advantage of hydrophobic interactions and efficient space partition, methane molecules were packed into the mesopores, resulting in enhanced uptake capability **(Fig 14).** Although there are several pre- or post-synthetic methods to introduce mesoporous defects in MOFs, a MOF rarely shows increased methane uptake after the

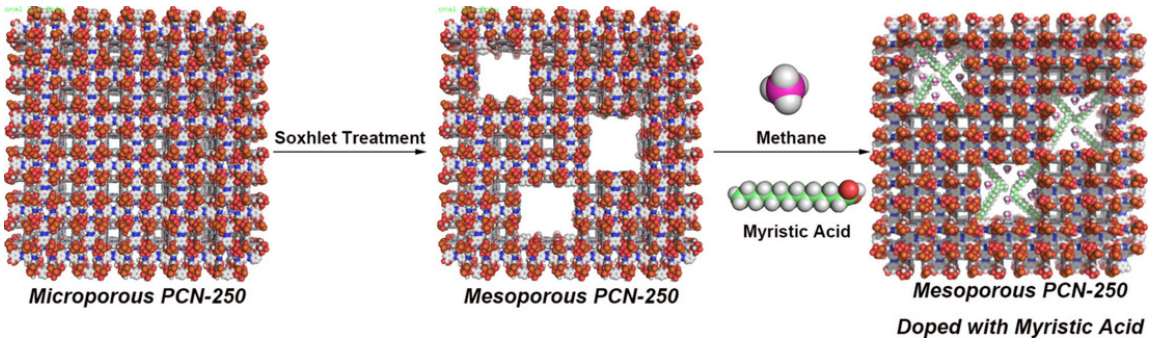

Figure 14. Schematic illustration of mesoporous PCN-250 doped with myristic acid for enhanced methane uptake.

treatment.[163-169] Furthermore, compared to conventional methods previously reported, the HAANG method can produce enhanced methane storage and is more straightforward and more highly recyclable.

Conclusion

In conclusion, we applied a post-synthetic treatment method, termed HAANG, to MOF adsorbents and obtained MOF-hydrocarbon composites with improved methane uptake performance and excellent recyclability. By applying two forms of the same MOF, microporous and mesoporous PCN-250, we observed that doping reagents only improve the methane-uptake performance for Meso-PCN-250 and reduce the performance for

Micro-PCN-250. This result indicates that the doping reagents are presumably located within the mesopores or at defect sites in the adsorbent, utilizing the void space and dissolving additional methane molecules. Through doping weakly (*n*-decane) and strongly (myristic acid) binding agents, the Meso-PCN-250 can produce a robust reusable adsorbent composite with increased methane uptake performance. Our findings shed light on the potential for post-synthetic treatment of MOF absorbents to obtain high performing and sustainable natural gas resources.

CHAPTER III

INCORPORATION OF FUNCTIONALIZED MESOPORES INTO PCN-250

Introduction

As I am discussing in this thesis, Metal-Organic Frameworks are porous crystalline materials which are assembled through coordination between mainly two types of building blocks: First is Metal clusters, and second is organic linkers. The pore size and structures can be tuned by altering these building blocks[170] and leading to diverse applications of MOFs as in gas separation and gas storage[76, 81, 171], and catalysis.[172] Generally, the functionalization of MOF interiors has relied on the pre-installation of ligands with desired functional groups[173] or post-modification of ligands bearing reactive groups[174] or doping of chemical compounds which can induce more affinity towards guest molecules.[175] Despite their success in many aspects, both functionalization of MOF building blocks before synthesis and post-modification of synthesized MOFs generally suffer from the limitation that the pore size of the modified MOF is reduced compared to that of the parent MOF because of the additional functional groups point toward the pores and occupying free volume. This reduction of pore sized generally results in reduction of both the surface area and pore volume thus reduce the guest molecules uptake in practical applications. However, Zhou group reported in 2012 a versatile strategy to introduce not only functional groups but also functionalized cavities into microporous MOFs via one pot assembly of a primitive ligand and its fragments **(Fig 15)**. This method was termed as Metal-Ligand Fragment Coassembly and has been successfully demonstrated in a NbO-type topological

MOF PCN-125 .[176] This functionalization approach leads to the nice formation of mesopores decorated with several functional groups in originally microporous MOFs.

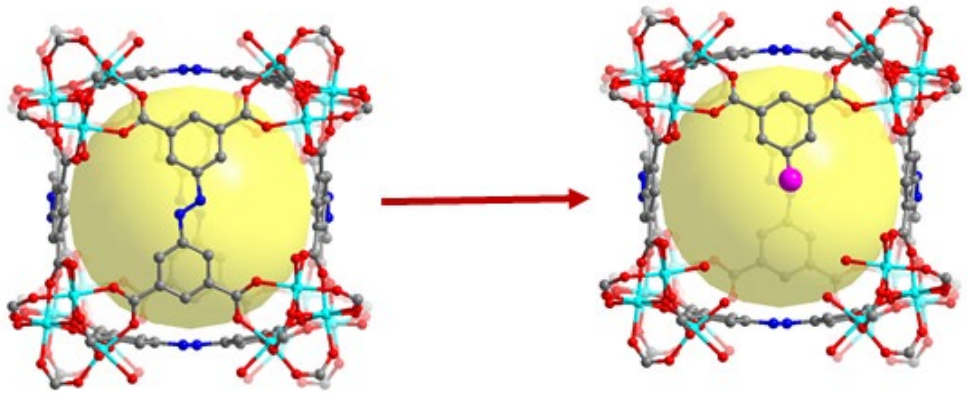

Figure 15. Schematic representation of the Ligand Fragment Co-assembly (LFCA) process in PCN-250. When fragmented ligands and the parent ligands are copolymerized together functionalized mesopores were introduced

There has been a well-established mixed-ligand approach to generate functionalized mesopores in MOF previously demonstrated by Yaghi group.[177] However, it is quite challenging to synthesize complex ligands with various substituent groups; this kind of functionalization method cannot be generally used in diverse structural MOFs. Another approach which is previously demonstrated by Matzger group[178, 179] which uses coordination copolymerization of structurally distinct ligands, such as extended ligands,

creates MOFs with functionalized mesoporous MOFs which are generally not isostructural to the parent MOF, making it very hard to predict the outcome and the structure of daughter MOFs after the reaction. However, the in metal-ligand–fragment co-assembly method demonstrated by the Zhou group, the first ligand, and its fragment, are crystallized into MOFs that are isostructural to the parent MOF makes it a easy and predictable MOF synthetic approach. Moreover, Ligand Fragment Co-assembly to introduce mesopores in MOFs allows inner pores of the MOFs to be decorated by a variety of functional groups on the ligand fragments, including polar, non-polar and ionic ones. Also, the functionalized MOFs maintain similar structures than with the parent MOFs allowing a systematic study on the functional groups and MOF structures and helps to create a more predictable model.[180-182] These hierarchical porous MOFs are suitable for both high guest uptake and efficient mass transport into and out of the pores, and very useful in applications such as catalysis, separation, and fuel gas storage.[183, 184] This truncated ligand approach is also very well-known and studied in other porous materials such as porous polymers where the truncated sites contain several added functionalities while retaining the structures of the parent polymer.[185, 186]

Current pioneers in this area of research have been dedicated to the MOFs with first-row late transition metals, especially zinc and copper-based MOFs. LFCA was first demonstrated in a Cu based MOF (PCN-125), and the poor moisture stability of these MOFs limited their utility for industrial application, especially in raw natural gas storage and transport.[187] Iron-Based MOFs, which I am discussing in this thesis, have exhibited remarkable chemical and thermal stability[188], which makes them more applicable for

commercialization and industrial applications.[189] So, I focused on PCN-250 (PCN stands for Porous Coordination Network), an iron-based MOF with Fe_2Fe (μ3 -O)] metal oxide clusters and 3,3',5,5' Azobenzene-tetra carboxylic acid and applied Ligand Fragment Co-assembly to create functionalized mesopores to increase guest-host interactions in its pores.

Experimental Section

Instruments

^{1}H nuclear magnetic resonance (NMR) data to confirm the ligand were recorded on a Bruker Avance Neo 400 spectrometer at the Department of Chemistry, Texas A&M University. IR data were collected by use of an IRAffinity-1 instrument. To obtain the TGA data, a Shimadzu thermogravimetric analyzer was used. The PXRD patterns were recorded by a Bruker ECO D8-Focus Bragg–Brentano X-ray powder diffractometer equipped with a Cu sealed tube (λ = 1.54178 Å) at a scan rate of 0.5 s deg^{-1}. All gas adsorption measurements were done by Micromeritics' ASAP 2020 instrument with extra-pure-quality gases. High-Pressure Measurement was performed by Micromeretics HPVA-II cryo gas analyzer. Based on the adsorption and desorption branch of N_2 adsorption isotherms of R-PCN-250, the pore size distributions were calculated by using DFT method or the Barrett–Joyner–Halenda (BJH) algorithm[190, 191] provided in the ASAP 2020 software.

Synthesis of azobenzene-3,3',5,5'-tetracarboxylic acid (H_4ABTC)

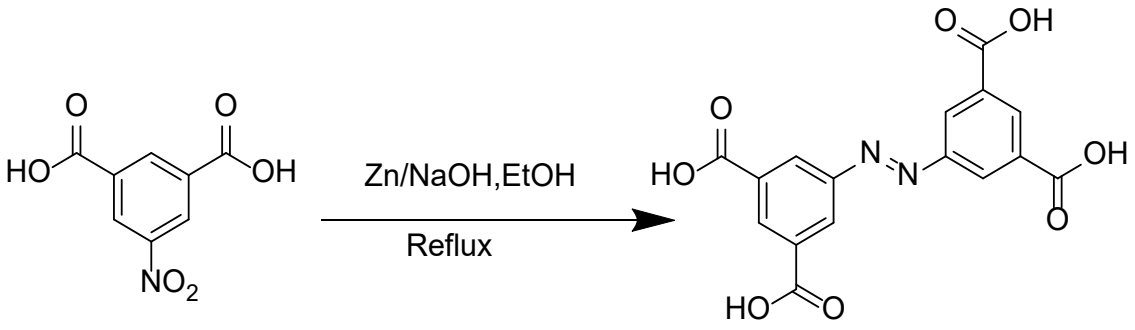

A mixture of 5-nitroisophthalic acid (2.1 g, 10 mmol), Zn (1.3 g, 20 mmol), and NaOH (0.8 g, 20 mmol) in a mixed solvent of ethanol (50 mL) and water (20 mL) was refluxed for 12 h. A yellow precipitate was obtained and collected by filtration. The solid was dissolved in 50 mL of NaOH (aq, 1 M) and the solution was filtered to remove an insoluble residue. The filtrate was acidified to pH = 3 with 3 M HCl (aq) to precipitate out 1.59 g of H_4ABTC as a yellow solid (yield: 85%). The compound was recrystallized over hot DMF.^{1}H-NMR (DMSO-*d6*): 8.48 (t, 4*J* = 1 Hz, 1H), 8.65 (t, 4*J* = 1 Hz, 1H), 8.76 (d, 4*J* = 1 Hz, 2H), 8.90 (d, 4*J* = 1 Hz, 2H), 13.60 (s, br, 4H).

Synthesis of 5-(Aminomethyl) isophthalic acid (CH_2NH_2-isoph)

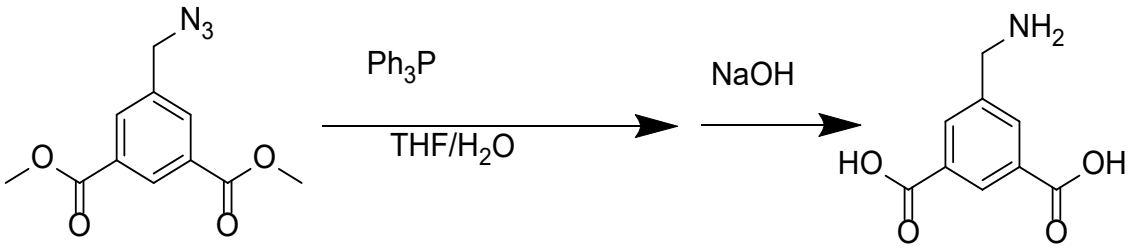

A solution of dimethyl 5- (azidomethyl)isophthalate[192] (0.52 g, 2.1 mmol) was added in THF (10 mL) and was added water (2 mL) and triphenylphosphine (0.61 g, 2.3 mmol). The resulting solution was stirred at room temperature overnight. NaOH (1.0 (N), 8.0 mL was added, and the mixture was stirred at room temperature for another 10 h. The mixture was diluted with water (10 mL) and extracted with DCM (40 mL) and then EtOAc (40 mL) to leave a slightly milky solution. This solution was acidified with HCl (1.0 N, ~10 mL) to give a clear solution (pH ~5). THF (40 mL) was then added followed by frezeing at -20°C. overnight. After that filtration, washing , and drying in high vacuum yields the desired product (0.36 g, 60% yield for 2 steps) as a whitish solid. ^{1}H NMR (in D_2O), 300 MHz) δ 8.13 7.86(d, 2 H, J = 1.5 Hz), 3.81 (s, 2 H), (t, 1 H, J = 1.7 Hz)

Synthesis of R-PCN-250 and gas sorption

A mixture of H_4ABTC (36 mg, 0.1 mmol), R-isoph (0.1mmol, amounts indicated are respectively H-isoph, NH_2-isoph, NO_2-isoph, CH_2NH_2-isoph, CH_3-isoph are 17 mg, 18 mg, 21 mg, 20 mg and 18 mg respectively, and $FeCl_3$,$6H_2O$ (135 mg, 0.5 mmol) in 20 mL of *N,N*-dimethylformamide (DMF) was placed in a glass vial. The vial was tightly capped and kept in a 120 °C oven for 24 h to yield dark brown powders. For subsequent analysis, such as gas adsorption, PXRD, the crystalline powder samples were washed with fresh DMF (20 mL) and then immersed in fresh DMF (20 mL) for one day. PXRD evaluated the phase purity of all products. Gas adsorption measurements were performed using an ASAP 2020 volumetric adsorption analyzer. A high-purity grade of gases was used throughout the adsorption experiments. Before adsorption, the sample was immersed in dry methanol for 72 h to remove the nonvolatile solvates. After the methanol was drained, acetone was subsequently added, and the sample was allowed to sit for 72 h. After the removal of acetone, the sample was dried under a vacuum at room temperature overnight and then activated again at 200 °C by using the degassing port in ASAP 2020. After that gas analysis experiment was performed. Once the low-pressure gas sorption measurement was completed the sample was transferred to a metal cell and activated again before the high-pressure gas sorption

Results and Discussion

We started a ligand–fragment coassembly strategy in which a creating a soc-net topology with ABTC ligands and Fe_2Fe (μ3 -O)] metal oxide clusters were chosen as a model structure. 5-R isophthalate (R-isoph, where R represents functional groups such as nitro, methyl, amino, aminomethyl groups) can be considered like a truncated fragment of ABTC as it is structurally prepared by one half of ABTC, namely biphenyl dicarboxylate, with R substituents. In R-isoph, its carboxylate moieties will coordinate with (μ3 -O) Fe cluster, and the various R groups will modify the pore interior. As R-isophalate fragments are shorter than ABTC, the introduction for these truncated fragments into the frameworks will result in the formation of larger pores. For this approach to be successful, some things should be kept in mind. Firstly, the MOF structure should be stable enough to withstand the incomplete connectivity. Secondly, the complete ligand and the ligand fragments should have comparable reactivity toward metal ions; otherwise, the fragments may be excluded from the MOF crystal formation. In this method, because R-isoph and ABTC have the same basic coordination moiety, they behave similarly during the crystal formation and are distributed throughout the crystals and providing functionalized cavities in the MOFs and this kind of heterogeneity, originating from the additional ligands (here R-isoph), has rarely been reported in iron-based MOFs.[193, 194]

Newly assembled MOFs with ABTC and R-isoph are designated as R-PCN-250. PCN represents porous coordination network. In general, R-PCN-250 was prepared by adding $FeCl_3$,$6H_2O$ into an *N*,*N*-dimethylacetamide solution of H_4ABTC and H_2R-isoph mixtures and details are explained in experimental section. Synthesized R-PCN-250 was

characterized by powder X-ray diffraction (PXRD) and N_2 gas adsorption measurements to study its crystallinity, its permanent porosity, and the formation of micro- and mesopores and compared with the parent.

First, we start with the incorporation of the simplest ligand fragment, isophthalate acid (H-isoph), to check the feasibility of our approach. The resultant MOF crystals were formed are isostructural with feed ratios of H_4ABTC and H_2H-isoph from 1:0 to 1:4 as confirmed by the PXRD patterns of the crystalline powders (H-PCN-250). **(Fig 16).** Based on the PXRD patterns and peak intensity, we determined that lower feed ratios 1:4 of H_4ABTC to H_2R-isoph is optimal to synthesize functionalized MOFs via this approach. Ratios beyond 1:4 (higher the truncated ligand yielded noncrystalline product). It is worth mentioning that pure H-isoph can crystallize in a totally different phase under identical conditions and create a different Metal-Organic Framework termed PCN 234.[195] Thus, if the truncated ligand is not incorporated in the parent structure, the peaks from a crystal solely with H-isoph and Fe cluster should appear in a mixed PXRD pattern[196] which is not the case here. Our PXRD patterns that confirm phase purity the possibility of the formation of two different MOFs with each ABTC and H-isoph was ruled out. Once the

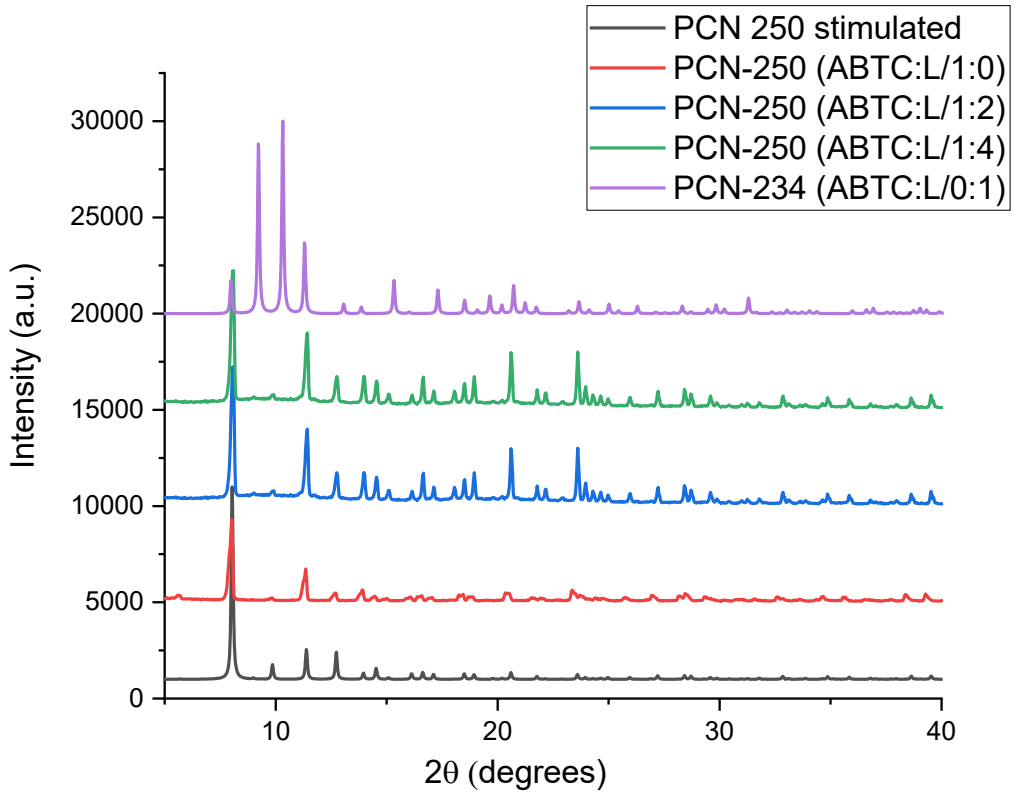

Figure 16. PXRD measurement of R-PCN-250 prepared from different ratios (1:0,1:2,1:4,0:1) of ABTC and H-isoph

successful incorporation of H-isoph into the MOFs without collapsing or changing the overall structure was optimized, we tried other R-isoph with useful functional groups for gas storage at the 5-position, such as methyl, amine, methylamine, nitro groups. These functionalized MOFs crystallized in the same PCN-250 crystal system, as evidenced by PXRD measurements**. (Fig 17)**

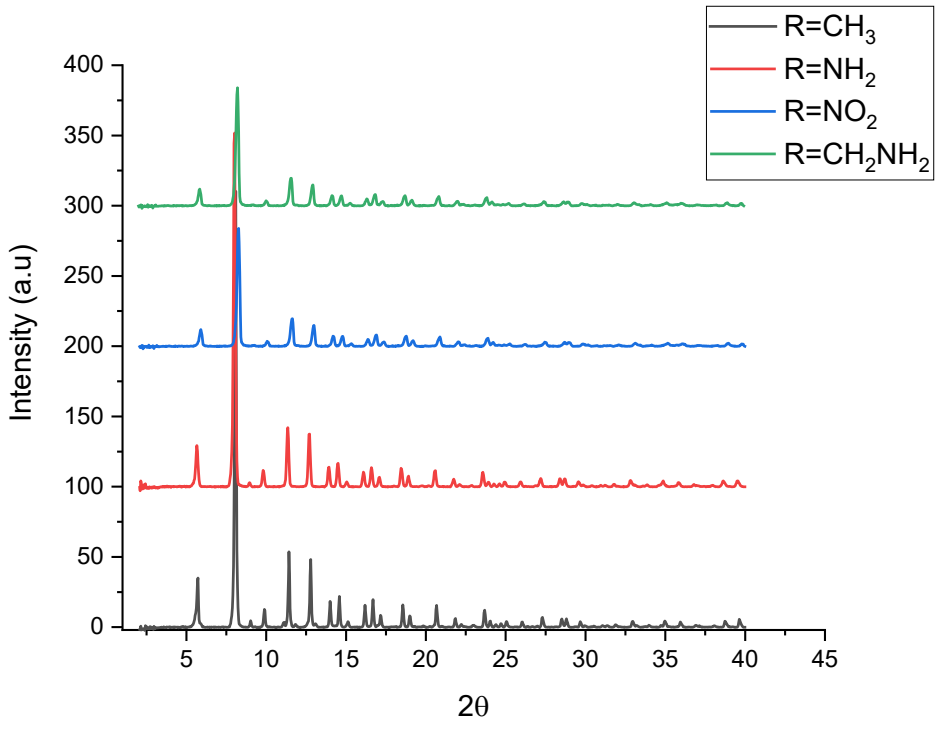

Figure 17. PXRD measurements of R-PCN250 MOFs prepared from different fragmented ligands. PXRD patterns showing all R-PCN-250 are isostructural.

N_2 adsorption isotherms at 77 K for two samples of H-PCN-250 prepared in different molar ratios of H_4ABTC to H_2H-isoph (4:1 and 1:2) were measured to determine their permanent porosity and pore size distribution. **(Fig 18)** The 4:1 ratio resulted in almost the same N_2 uptake as that of unfunctionalized PCN-250 showing a type I isotherm. However, when

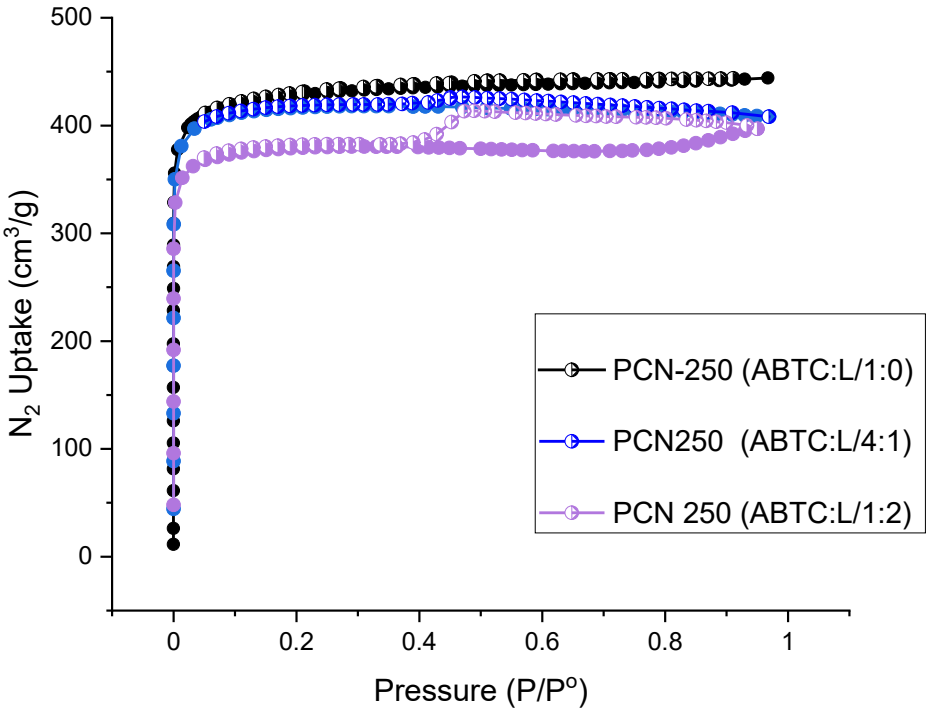

Figure 18. N_2 isotherm at 77K for unaltered microporous PCN-250 (black) and R-PCN-250 (R=H in this case) in different ligand and ligand fragment ratios (blue and purple ABTC: L/ 4:1 and 1:2)

the H_4ABTC/H_2H-isoph ratio was increased to 1:2, H-PCN-250 still retained high surface areas (around 1690 m^2/g) while showing hysteresis type IV N_2 adsorption isotherm[197] with a decrease in total uptake capacity and the pore widths gradually increased.

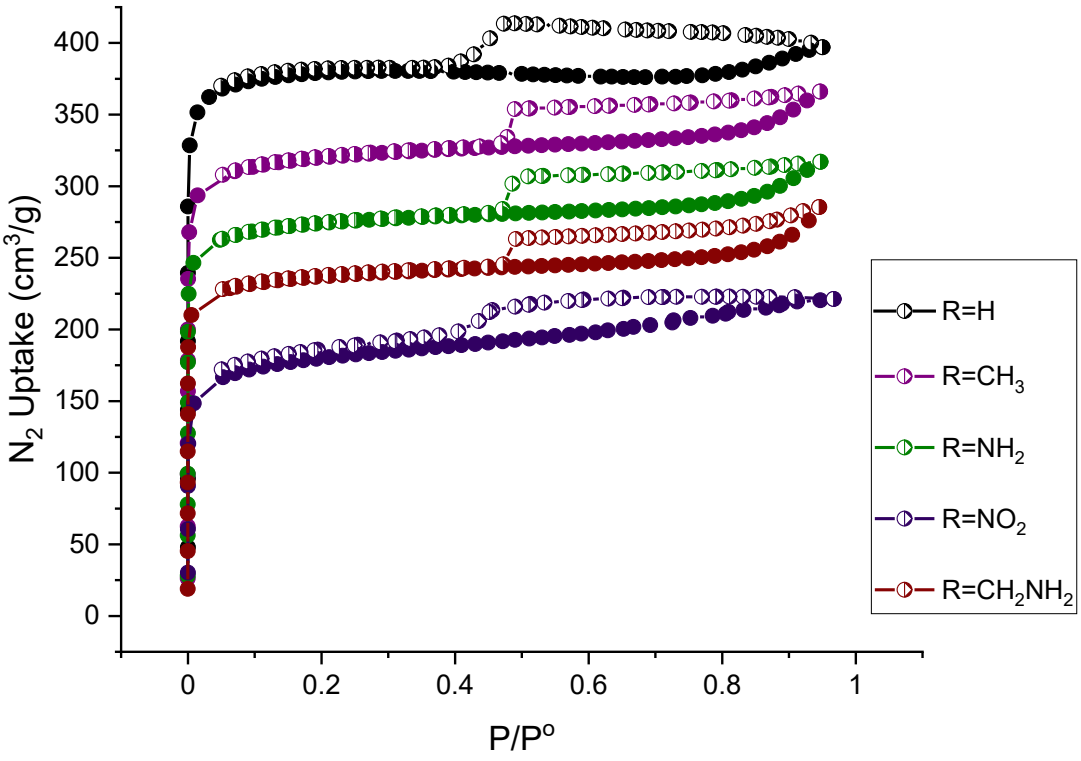

Figure 19. N_2 isotherm at 77K for different functional group modified (Black: H, Purple: CH_3, Green: NH_2, Blue: NO_2, and Brown: CH_2NH_2) fragment assembled R-PCN-250 MOFs. Hysteresis indicates the mesoporosity in these MOFs

This is a stark difference between this approach and other traditional surface functionalization methods. In other methods functional groups tend to dangle into pores and result in decreased pore sizes however in this method the functional groups are pointing toward the pores generated via the incorporation of R-isoph, leading to increased pore size with the desired functionalities.

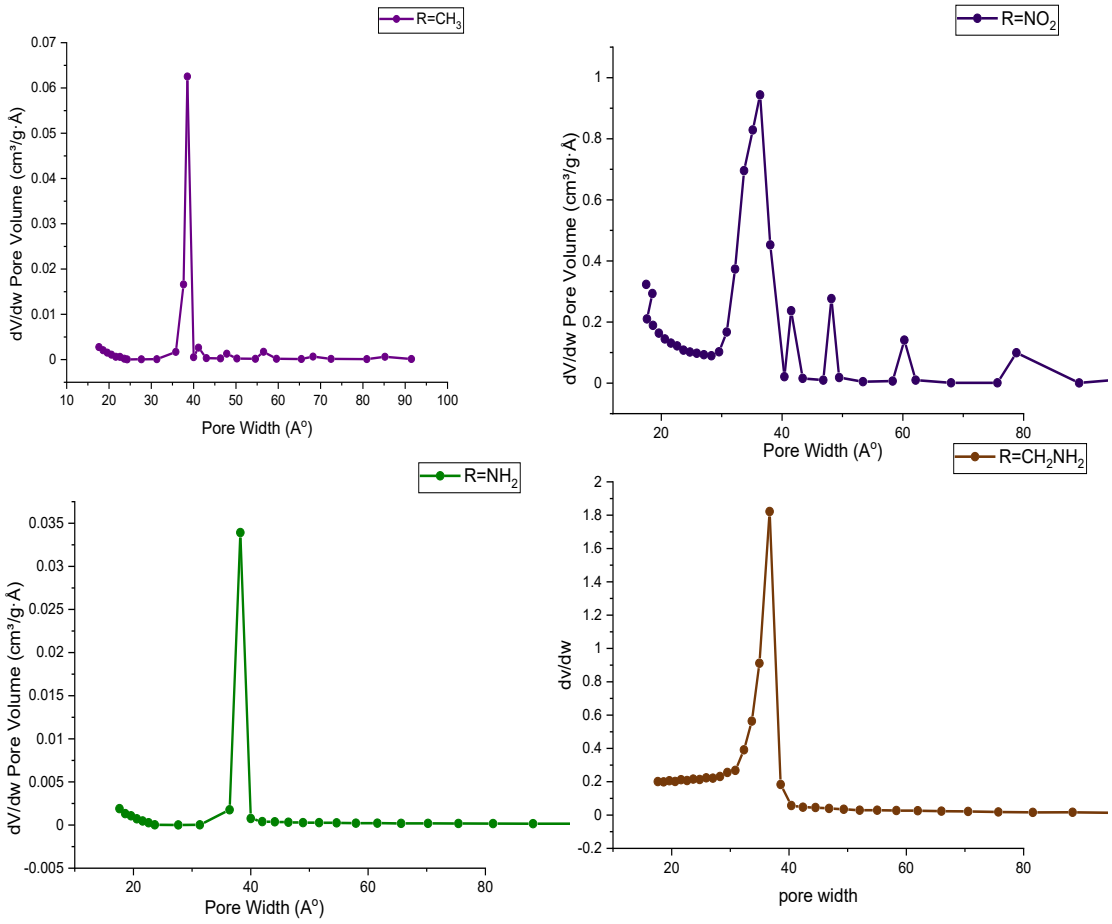

Figure 20. Pore size distributions of different R-PCN-250 MOFs. (Purple: CH_3, Green: NH_2, Blue: NO_2, and Brown: CH_2NH_2). Pore size distribution is calculated by BJH method

We also tried to incorporate various functional R-isoph, having polar, ionic, or bigger functional groups, to increase the interaction between guest molecules and pore environment. In general, these functional groups, when added in an organic linker during MOF synthesis, occupy more space in the pores, leading to a significant decrease of pore size. In contrast, the MOFs functionalized via this LFCA approach shows that the introduced functionalities in terms of the truncated ligand can be increased up to the mesoporous region. CH_3, CH_2NH_2 NH_2 and NO_2-PCN-250 were found to have type IV N_2 adsorption isotherms **(Fig 19)** and mesopores in around 40 Å **(Fig 20)** which are a characteristic of mesoporous materials in contrast to unfunctionalized PCN-250.[198, 199]

The Brunauer–Emmett–Teller (BET) and Langmuir surface areas and pore volumes of all R-PCN-250 prepared in different feed ratios are presented in **Table 1.**

Table 1 Sample table summarizes BET and Langmuir surface area of different R-PCN-250.

MOF	**Ligand**	**Ligand Fragment (isoph)**	**BET surface area (m^2/g)**	**Langmuir surface area(m^2/g)**
PCN-250	ABTC	Nil	1691	1920
H-PCN-250	ABTC	H (4:1)	1639	1813
H-PCN-250	ABTC	H (1:2)	1527	1645
CH_3-PCN-250	ABTC	CH_3	1178	1519
NH_2-PCN250	ABTC	NH_2	1093	1314
NO_2-PCN-250	ABTC	NO_2	688	886
CH_2NH_2-PCN250	ABTC	CH_2NH_2	547	1110

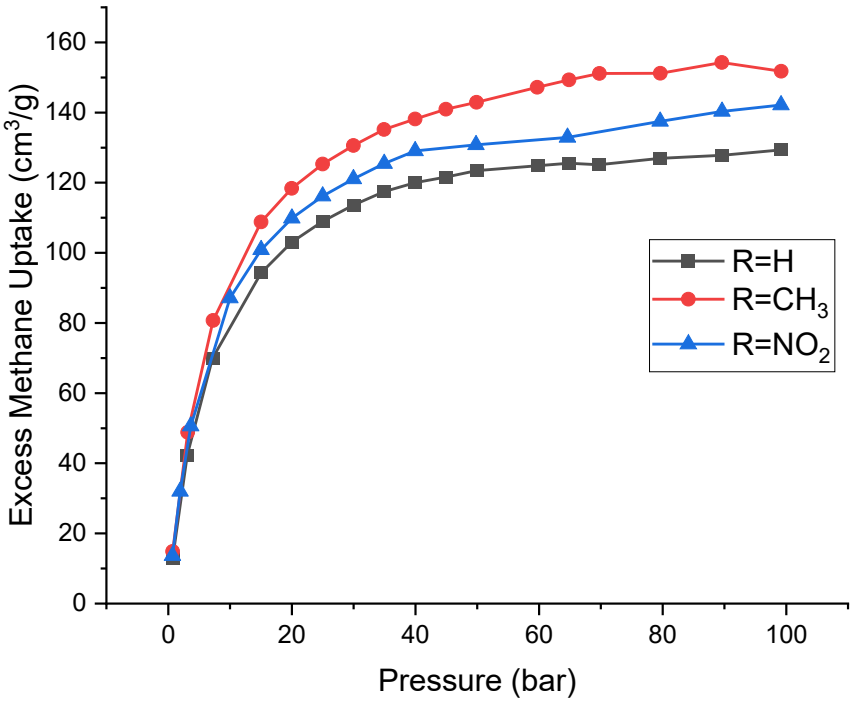

Figure 21 Calculated excess uptake of methane in cc/g in high-pressure methane of R-PCN-250. Adsorption isotherm (Black=H, Red=CH_3, Blue=NO_2) indicates polar nonpolar interaction in pores.

We tried to examine the enhanced interaction with guest molecules due to the introduced functionalities in these modified PCN-250 MOFs. CH_4 adsorption in the high-pressure range was performed to see the enhanced interactions. Although CH_3-, and NO_2-PCN-250 possessed lower surface areas, their CH_4 uptake at 298 K was either higher or similar compared with those of their unfunctionalized counterparts **(Figure 21)** mainly because of increased hydrophobic interaction and increases ionic interaction between guest

molecules and functionalized groups. Moreover, H- PCN-250 also showed increased methane storage. This increase is attributed to uncoordinated carboxylate groups of ABTC or metal clusters which might be serving as additional favorable gas adsorption sites.[200]

Summary

In summary, the metal–ligand–fragment coassembly strategy was performed to introduce functionalized mesopores in iron-based MOF called PCN-250. The primitive ligand (ABTC) and its ligand fragment (R-isoph) were co-assembled together via solvothermal methods to generate a series of the isostructural MOFs with functional groups (R) and depending on the functional groups. Mesopores were generated in the microporous structure, confirmed by N_2 adsorption isotherms. The hierarchical micro- and mesopores in MOFs can improve the binding interactions with the guest molecules in the pores demonstrated by low- and high-pressure methane adsorption isotherms.

CHAPTER IV

ENCAPSULATION OF HIGHLY REACTIVE COBALT NANOCLUSTER IN A SERIES OF POROUS COORDINATION CAGES FOR CATALYSIS

Introduction to Porous Cages and Supramolecular Catalysis

Coordination Cages" are also known as in several names such as Porous Coordination Cages (PCCs), Metal-Organic Super Container (MOSC), Metal-Organic Polyhedron (MOPs) uses principles of coordination chemistry between Metal clusters and Organic Linkers.[201-206] Their structural diversity and intrinsic pores and structures make them very unique programmable nanoreactors for catalysis. Encapsulations of catalysts inside molecular cages are just like enzymes where active sites and guest binding pockets provide a unique microenvironment for reaction and can provide unique, Regio and Stereoselectivity.[207, 208] Cages alone can provide catalytic activity in the reaction via providing either suitable pore environment or via incorporation of catalytically active organic ligands in the cage structures.[209-214] However, in this chapter, we provide another approach where catalytically active compounds are encapsulated in the pores of a series of novel coordination cages.

Cage crystal structure and the catalytic study reported in this chapter was performed in collaboration with Dr.Yu Fang, and Zhifeng Xiao and TEM analysis was performed by Dr Jialuo Li.

This approach has been extensively studied before in Metal-Organic Frameworks[215, 216], zeolites[217-219], graphene[220, 221] and sometimes in cage compounds as well.[222-224] However, encapsulations and enhancement of catalytic activity for first-row transition metal nanoclusters are very difficult and have not been studied so well.[225] Especially encapsulation of ultra-thin nanoclusters inside porous materials is still challenging as they tend to agglomerate.[226] This chapter describes efforts towards achieving uniformly encapsulated first-row transition metal nanoclusters inside a porous coordination cage.

Design and Structures of Porous Coordination Cage

In this chapter, we designed and synthesized three novel porous coordination cages PCC-2a, PCC-2b, and PCC-2c. All three cages PCC-2a, 2b and 2c cages were assembled by six V ligands as capping vertices, eight L ligands as planner faces, and six tetranuclear Co clusters as knots between four L ligands and one V ligand **(Figure 22).** By reacting vertex ligand ($Na_4H_4V^1$ and H_4V^2) and panel ligand (H_3L_1 and L_2) with $CoCl_2$ at solvothermal conditions in methanol cages were synthesized (Detailed experimental details are discussed later in this chapter). Single crystal Xray diffraction analysis reveals that PCC-2a adopted an octahedral hollow structure in the trigonal $R\bar{3}$ space group. Similarly, Similarly, PCC-2b and PCC-2c were prepared by reacting vertex ligand (H_4V^2) and panel ligand (H_3L_1 and L_2) with $CoCl_2$ under solvothermal conditions in DMF for 24 h. (Detailed experimental procedure discussed later in this chapter). PCC-2b and PCC-2c both adopted a similar octahedral hollow cage structure but in the tetragonal *I* 4/*m* space group **(Figure 23).**

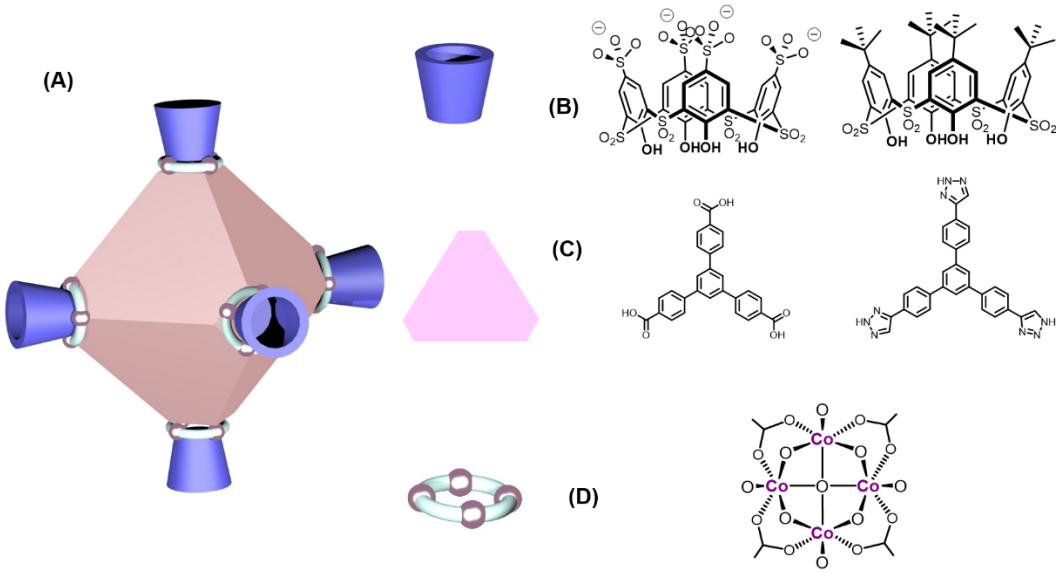

Figure 22. (A) Design and structural characteristics of synthesized cages. (B) vertex ligands (C) trigonal panel ligands and (D) cobalt clusters.

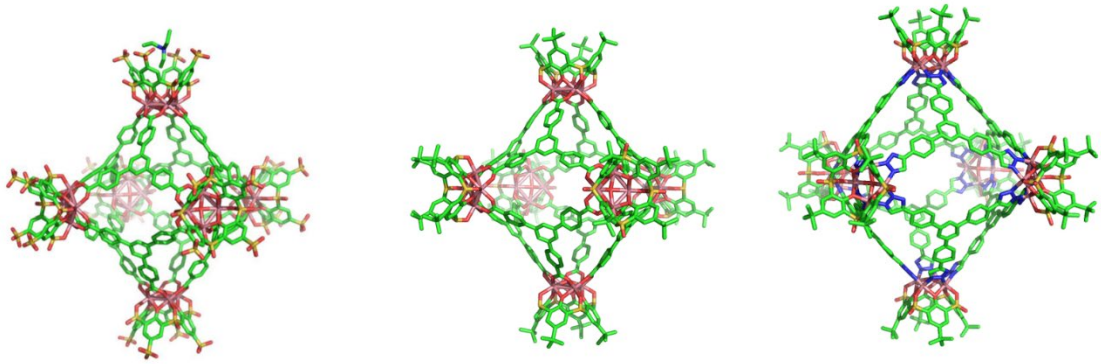

Figure 23. Structures of synthesized porous coordination cages (left to right) PCC-2a, PCC-2b and PCC-2c

We can see these PCC-2b and 2c shares the same structure as CIAC-106.[227] Each cobalt atom in the cluster was held in an octahedral configuration by coordinating with one sulfonic oxygen and two phenolate oxygen atoms from V, two carboxylate oxygens from two adjacent L, and a μ_4-OH at the center of the cluster. The assignment of the central oxygen atom to be μ_4-OH or μ_4-OH_2 depends on the synthetic conditions.[202]. Similar coordination was achieved via N-atoms in the case of PCC-2c. Based on the crystal structures of three PCC-2 cages, we find the longest inner-cavity distance is 25.1–24.6 Å (the distance between two μ_4-OH of two opposite Co_4 clusters), and the largest outer diameter of them are 42.2–42.7 Å. From the packing diagram, we revealed micro- to mesoporosity in the solid-state, which indicates that PCC-2 are porous materials. Regardless of their structural similarity, the charge property of PCC-2a,2b and 2c are totally different. From the literature survey it is found that PCC-2a is one of the most negatively charged coordination cages.[228] For most, in general, for cationic or anionic coordination cages, the charge originates from the coordination site.[229, 230] However, for PCC-2 series, the 48 positive charges from the Co^{2+} metal ions are fully compensated by the phenolate groups from V^2 (24 negative charges) and the carboxylate groups or azolate groups from panel ligand L (24 negative charges). Thus, the negative charge of PCC-2b and 2c is only attributed to the six μ_4-OH groups in the Co cluster. For PCC-2a however, the negative charge is derived from a combination of sulfate groups from the V^1 ligand (24 additional negative charges) and the OH group (6 negative charges) in the Co cluster itself. Molecular simulations and N_2 isotherm results visualized the porous nature of these cages. **(Fig 24)** Based on the crystal structure of PCC-2a and similar structures, the helium-

accessible void fraction is calculated to be an enormous 74.3 % which suggests it as a stable permanent porous material Also simulated N_2 uptake of 640 $cm^3\ g^{-1}$ (STP) at 77 K and P/P_0=0.94.

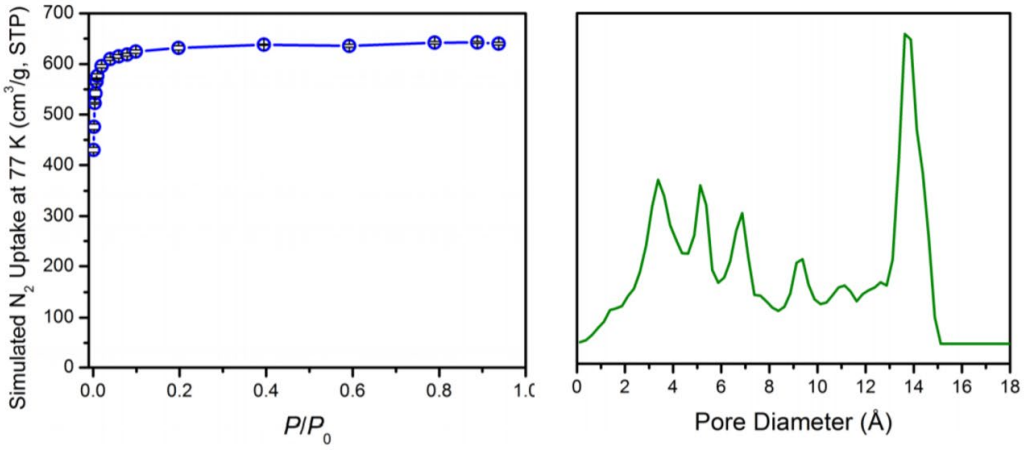

Figure 24. Stimulated N_2 isotherm and pore size distribution at 77K for PCC-2a cage. Reprinted with permission from 231 .

Nanocluster Incorporation

These synthesized cages were used as a potent cation container, especially for Co^{2+} cation and NC stabilization for Ammonia-borane ($NH_3.BH_3$, AB) dehydrogenation reaction. $CoCl_2$ (20.8 mg) was added to the DMF solution (1.0 mL) containing 0.44×10^{-3} mmol dried PCC-2a/b/c crystals. After 30 minutes incubation at room temperature, the mixture was added to a 1:2 DMF/Methanol solution (total was 1.5 mL) containing sodium

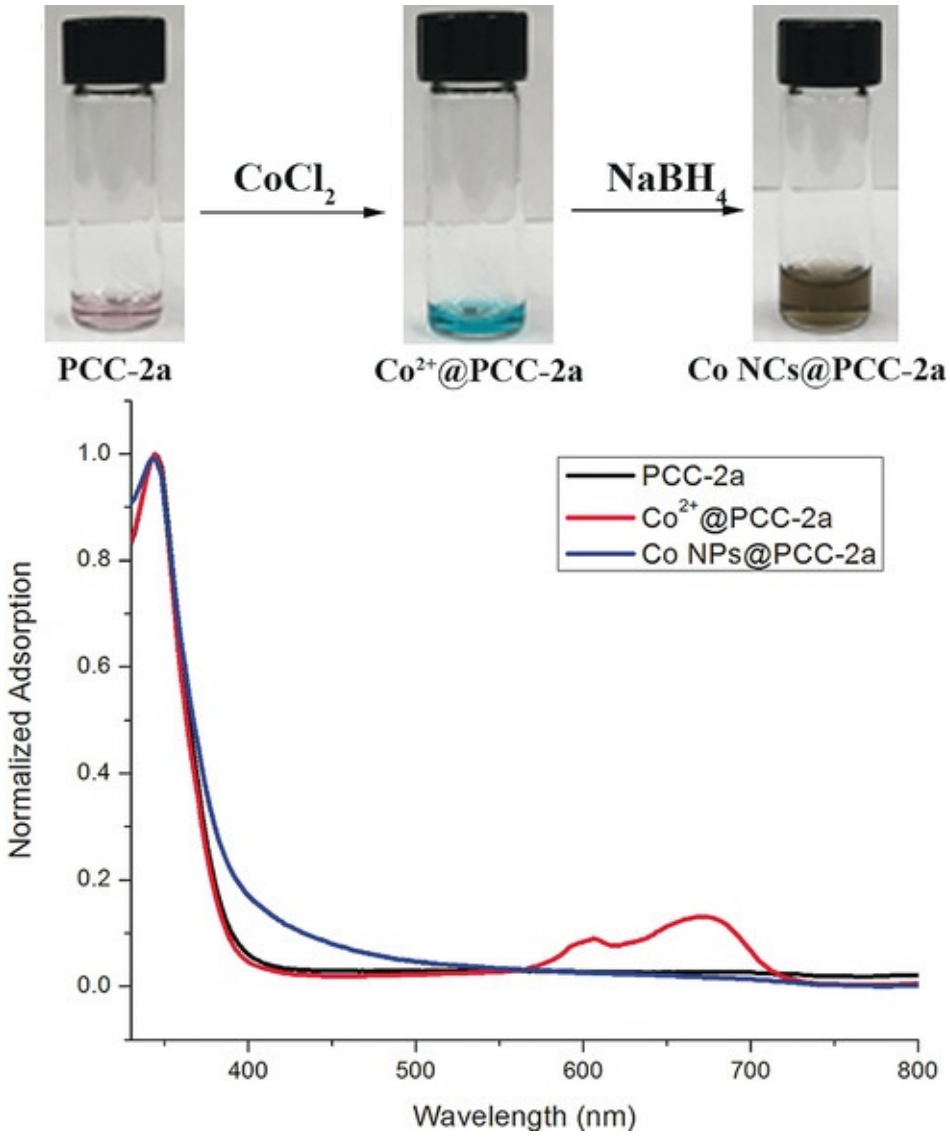

Figure 25. The preparation of Co NCs by PCC-2a. And UV/Vis spectrum of PCC-2a after adding Co salt and after adding $NaBH_4$. Reprinted with permission from 231.

borohydride (0.9 mg). The solution containing PCC-2a undergoes an immediate color change without any precipitate formation **(Figure 25).** This phenomenon demonstrates the generation of well-dispersed Co NCs encapsulated by PCC-2a. The reduction of Co^{II} to Co^{0} was monitored by UV/Vis spectroscopy as the adsorption band of Co^{II} from 600 to 700 nm disappeared upon addition of $NaBH_4$.[232] Co NCs@PCC-2a also demonstrated excellent colloidal stability as this homogeneous nature is maintained even after a month in room temperature. In contrast, for the solution containing PCC-2b and PCC-2c, the addition of $NaBH_4$ led to instantaneous black precipitation, which demonstrates NC aggregation. The incapability of these PCCs in terms of NCs stabilization is attributed to lower negative charges of these cages does not have strong interaction with Co^{2+} ions resulting in the reduction outside the cavity of cages and agglomerate instantly. The Co NCs@PCC-2a was characterized by transmission electron microscopy (TEM). The Co NCs inside the coordination cages were found to be uniform and very well-dispersed, with an average diameter of 2.5 nm **(Figure 26).** The high-resolution TEM (HRTEM) image shows the lattice spacing of Co NCs@PCC-2a to be 2.01 Å (111) plane, which corresponds to the *fcc* crystal face on Co NCs.[233-235] Notably. However, *hcp* type Co NCs are normally obtained from low-temperature synthesis, the *fcc* type of Co NCs is more favorable when their size is below 20 nm and more probable in this octahedral cage as a previous study reported similar lattice type of Ru-Nanocrystals in these cages.[236] The size distribution of Co NCs@PCC-2a is quite narrow and near the diameter of the internal cavity of the porous cage (2.5 nm), which indicates the formed Co NCs were encapsulated

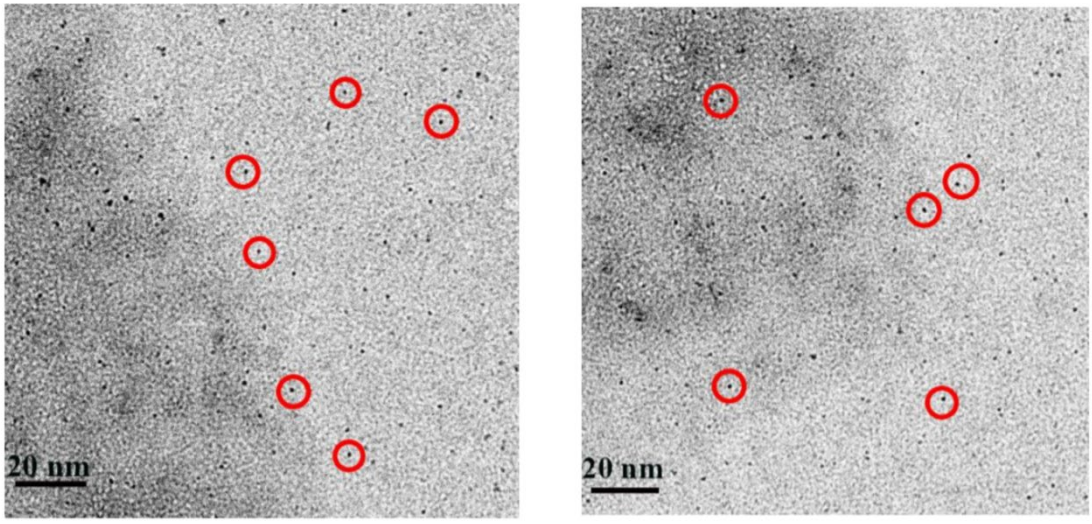

Figure 26. TEM images of Co NCs@PCC-2a (red cycles indicate single NCs) Reprinted with Permission from 231.

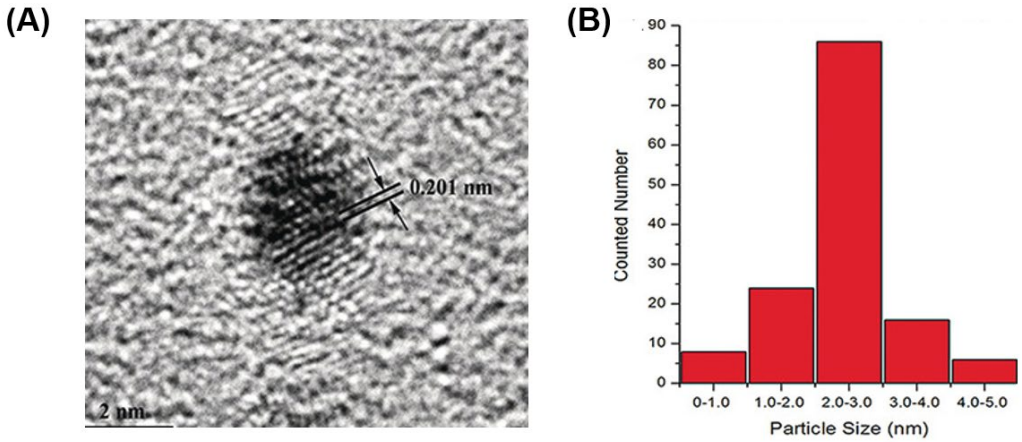

Figure 27. (A) HRTEM image of single NC of Co NCs@PCC-2a showing the (1,1,1) crystal surface. (B) The size distribution of Co NCs@PCC-2a. Reprinted with permission from 231.

and regulated by PCC-2a. **(Fig 27)** These data establish the PCC-2a successfully encapsulate and modulate a well-dispersed first-row transition metal catalyst in its pores.

Catalytic Activity Study

Among all the clean and sustainable energy sources, hydrogen is the best for many reasons[237] and often termed as the best fuel for a sustainable future.[238] Since physisorption of hydrogen is very difficult to even in porous media in ambient temperature.[239] Scientists tried to optimize chemisorption hydrogen platforms for hydrogen generation. Ammonia Borane (NH_3BH_3) is one of those platforms which have very high hydrogen content of 19.6% and is a very promising hydrogen storage reagent for energy applications.[240] There has been many studies involving - noble metal NC catalyst for dehydrogenation of AB, however they come with their own cons such as low abundance and high cost.[226, 241] In this section I will study catalytic activity of Co NCs stabilized by PCC-2a/b/c in the hydrolysis of ammonia–borane shown below.

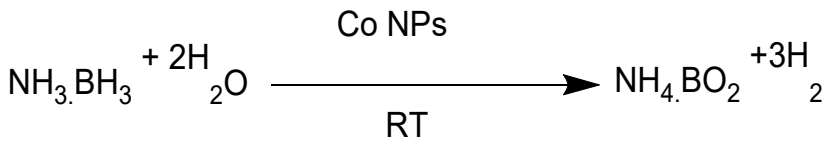

When the reaction was initiated by these homogenous catalysts, hydrogen gas was gathered in a graduated cylinder, and the volume was recorded according to time. **(Fig 28)** The catalytic activity was evaluated and compared in **Table 2.** Co NCs@PCC-2a achieved

a maximum turn-over frequency (TOF) of 90.1 min^{-1}. According to previous reports, the record-high result (TOF=41) was achieved by immobilizing Ni NCs on 3D graphene.[219] Besides, PVP protected Co NCs gave a moderate TOF of 38.9 min^{-1}. It has

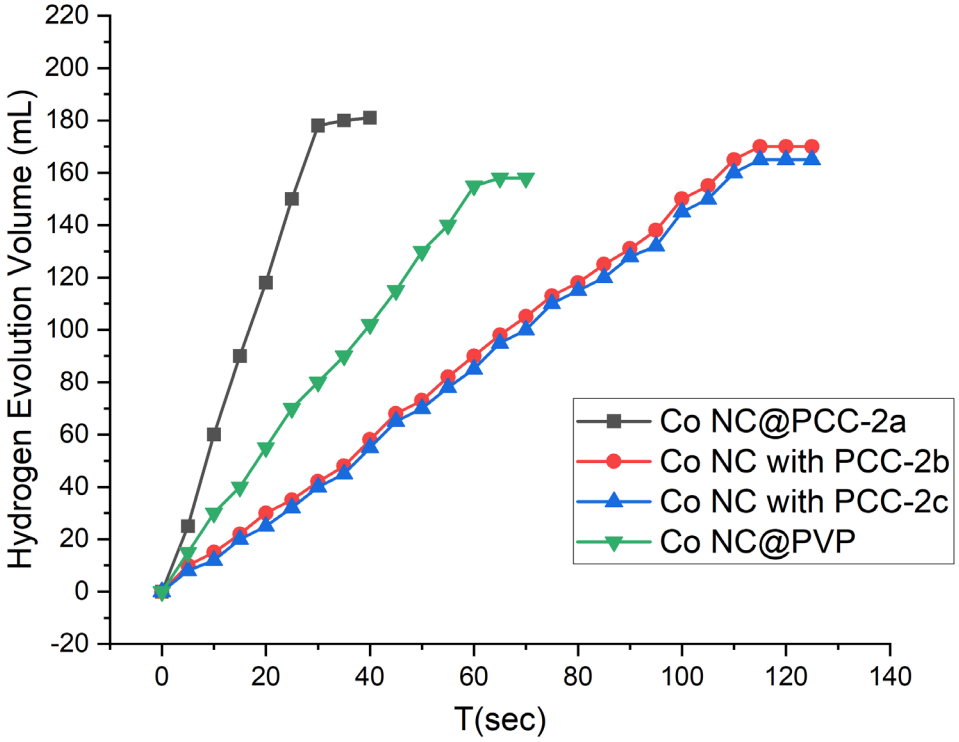

Figure 28. Time course plots of H_2 generation for the hydrolysis of AB by Co NCs@PCC-2a, Co NCs/PCC-2b, Co NCs/PCC-2c. and Co NCs@PVP

been reported that the alkane chain in PVP sometimes blocks the active site of encapsulated NCs, which is a common issue for surfactants.[242] Co NCs/PCC-2b catalyst only give a TOF of 22.5 min^{-1}. Co NCs/PCC-2c give a similar TOF of 21.1 min^{-1}

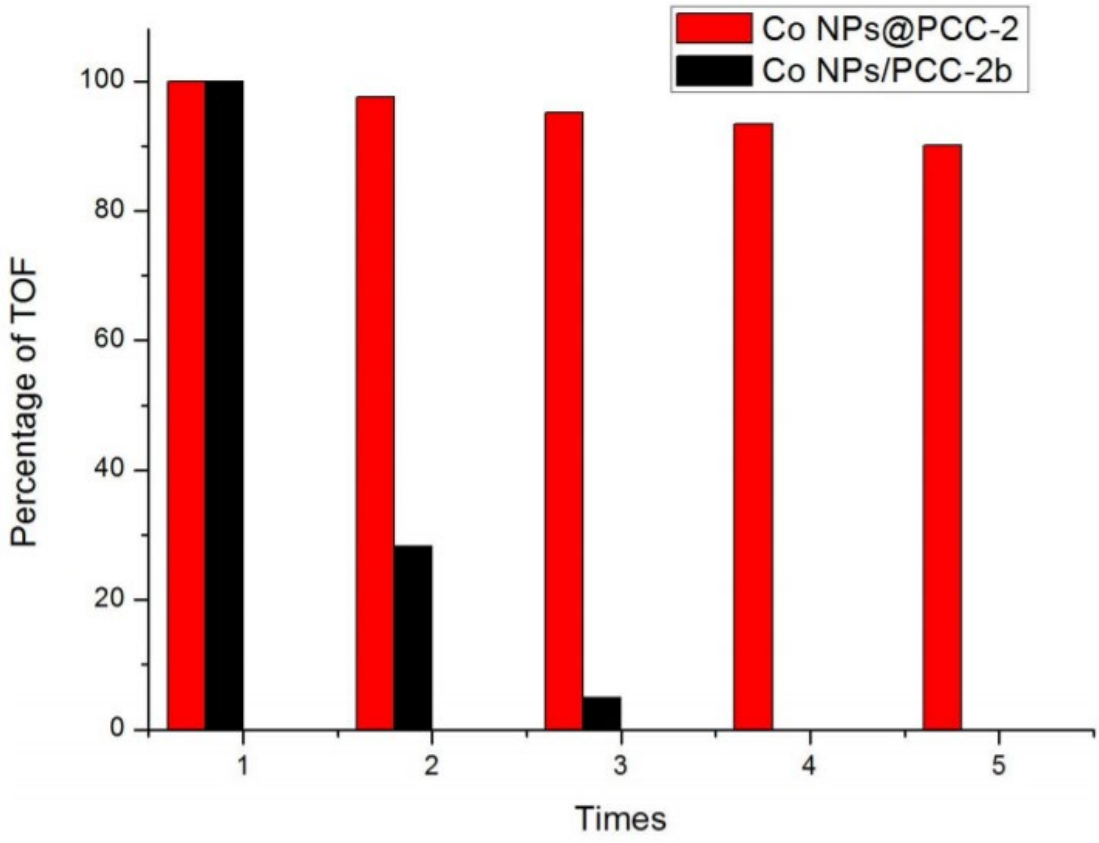

Figure 29. Recyclability tests of Co NPs@PCC-2 and Co NCs/PCC-2b.Reprinted with permission from 231.

which is very obvious as they are unable to encapsulate and stabilize the nanoparticles inside the pores. Control experiments were performed with an empty PCC-2a cage (without any Co), and it was observed that hydrogen gas was barely generated. Since the vertex ligand ($Na_4H_4V^1$) is mainly responsible for all the negative charges in the cage, we then replaced

PCC-2a with $Na_4H_4V^1$ in the reaction with $CoCl_2$ and $NaBH_4$. The TOF of the reaction measured as 19.1 min^{-1}. This experiment excluded the possibility that the surface charges of the vertex ligand can stabilize the NCs and firmly establishes the fact that nanoparticles were stabilized inside the cage pores. Furthermore, Co NCs@PCC-2a catalyst can be recycled (**Fig 29**) more than five times with the negligible loss of activity which demonstrates the anionic cage pore helps to stabilize the nanoparticles from aggregate and from catalyst poisoning. The experimental observation with some of the similar catalyst from the literature is summarized in **Table 2**

Table 2. Catalysis performance of PCC-2 and other compounds for the hydrolysis of Ammonia-Borane

Catalyst	**Particle Size (nm)**	**T (min)**	**Catalyst (%)**	**TOF (min^{-1})**	**Reference**
Co NP@PCC-2a	2.5	0.5	7	90.1	This work
CoNP and PCC-2b	100	2.0	7	22.5	This work
Co NP and PCC-2c	100	2.1	7	21.1	This work
Co NP @PVP	10-20	1.2	7	38.9	This work
PCC-2a	>100	>60	0.4	<1	Reference[236]
Ru NP@ PCC-2	<3	4.5	7	304	Reference[236]
Pd@MIL-101	<3	6.5	0.3	51	Reference[243]

Experimental Section

Materials and Instruments

$CoCl_2$, p-tert-butylsulfonylcalix[4]arene (H_4V_2), 1,3,5-Tris(4-Carboxyphenyl)Benzene (H_3L) and tri-(p-bromophenyl)–benzene (L_2 ligand precursor),$NaBH_4$, N,N-dimethylformamide (DMF), acetone, and ethanol were purchased commercially and used without further purification. Single crystal X-ray diffraction was carried out on a Bruker Quest diffractometer equipped with a MoKα sealed-tube X-ray source (graphite radiation monochromator, λ = 0.71073 nm) and a low-temperature device (110 K). TEM was performed on a FEI Tecnai G2 F20 ST microscope at 200 kV equipped with a field emission gun.

Synthesis of Sulfonate Vertex Ligand ($Na_4H_4V^1$)

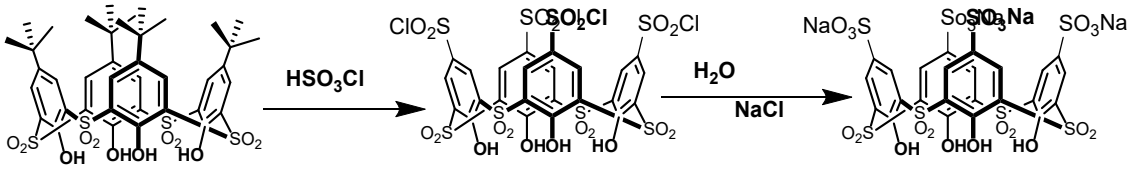

The procedure was slightly modified from the reported procedure in Reference[244] .To a mixture of p-tert-butylsulfonylcalix[4]arene (187 mg,0.22 mmol) ,chlorosulfonic acid (10 cc) was added and stirred for 36 hours for 140 °C. The reaction mixture was then poured into ice-water mixture and the precipitate was collected through filtration. The product

was dissolved in water and refluxed for 12 hours and after cooling to room temp the compound was filtered to remove any insoluble impurity. To the filtrate, NaCl was added to salt out the product pentasodium trihydroxy-octaoxo tetrathiacalix[4]arene-tetrasulfonate was then collected by filtration and dried in vacuum. ^{1}H NMR (with D_2O, 400 MHz) 8.04(s,8H, ArH).

Synthesis of TBP-Triazolate (L_2)

Solid 1,3,5-tri-(p-bromophenyl)-benzene) (16.2 g, 30.0 mmol) was dissolved in 250 mL of freshly distilled diethylamine under a nitrogen atmosphere. Copper(I) iodide (50 mg)

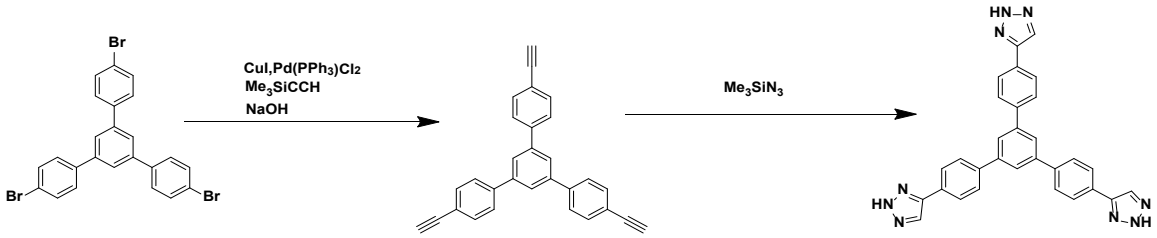

and dichlorobis(triphenylphosphine)palladium (II) catalyst (400 mg) were added to the solution. Trimethysilylacetylene (10.6 g, 108 mmol) was added, and the mixture was heated at 50 °C for 8 h. After cooling, the resulting precipitate was removed by filtration and washed with ether. The combined filtrates were evaporated under reduced pressure

and the residue was chromatographed to yield 9.1 g (77%) of 1,3,5-tris(p-trimethylsilylethynylphenyl) benzene as an intermediate product. Hydrolysis of this compound (9.50 g, 26.0 mmol) was carried out under alkaline condition, by treatment with a mixture consisting of 20 mL of CH_2Cl_2, 50 mL of MeOH, and 30 mL of 1 M NaOH (aq) under stirring at room temperature for 3 h. After a standard work-up procedure and removal of the solvent under reduced pressure yielded 2.65 g of white powder containing 1,3,5-(triethynylphenyl)-benzene. Under an inert atmosphere, trimethylsilyl azide (9.16 g, 79.5 mmol) was added to a solution of CuI (500 mg, 2.60 mmol) and 1,3,5-triethynylphenyl) benzene (6.65 g, 17.6 mmol) in a mixture with 100 mL of DMF and 10 mL of methanol. The reaction mixture was heated at 100 °C for 36 h. The hot mixture was filtered and concentrated under reduced pressure to afford a pale-yellow precipitate. The solid was collected by filtration, washed with diethyl ether, and dried under reduced pressure to yield the final product.

Synthesis of PCC-2a

$Na_4H_4V_1$ (14.5 mg, 0.014 mmol), H_3L_1 (14.5 mg, 0.033 mmol), and $CoCl_2$ (13.3 mg, 0.103 mmol) were suspended in 2 mL MeOH with 2 drops of Et_3N. The mixture was heated at 85 °C. in an oven for 12 h. After cooling to ambient temperature, large purple crystals

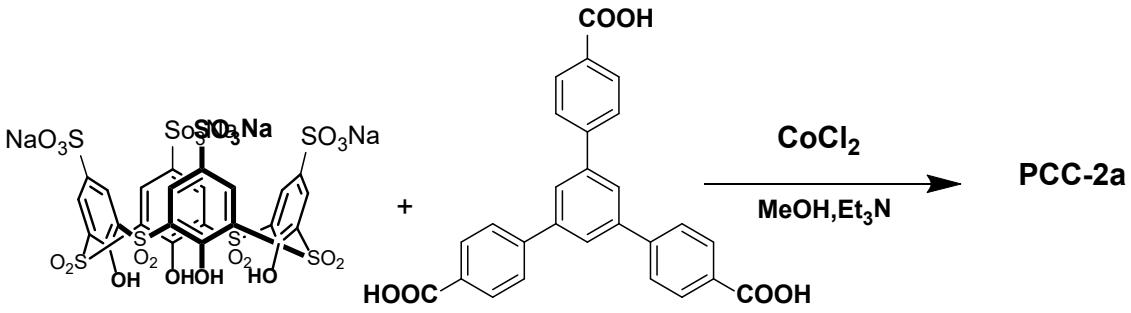

were collected and washed with methanol to yield PCC-2a in about 95% (according to $Na_4H_4V_1$). Elemental analysis: calculated (%) for $Na_{24}[Et_3NH]_6[C_{360}H_{222}S_{48}O_{198}Co_{24}] \cdot 5$ MeOH · 10 H_2O, C 39.56, H 2.96, N 0.69, S 12.64; found (%):C 39.28, H 2.92, N 0.70 S 12.86.

Synthesis of PCC-2b

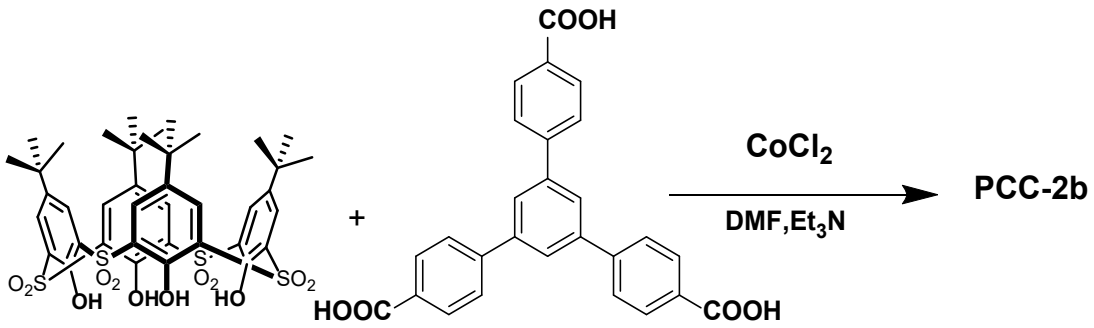

H_4V_2 (11.9 mg, 0.014 mmol), H_3L_1 (14.5 mg, 0.033 mmol), and $CoCl_2$ (13.3 mg, 0.103

mmol) were suspended in 1 mL DMF with 2 drops of Et_3N. The mixture was heated at 130 °C. in an oven for 24 h. After cooling to ambient temperature, large purple crystals were collected and washed with methanol to yield PCC-2b in about 99% (according to H_4V_2).

Synthesis of PCC-2c

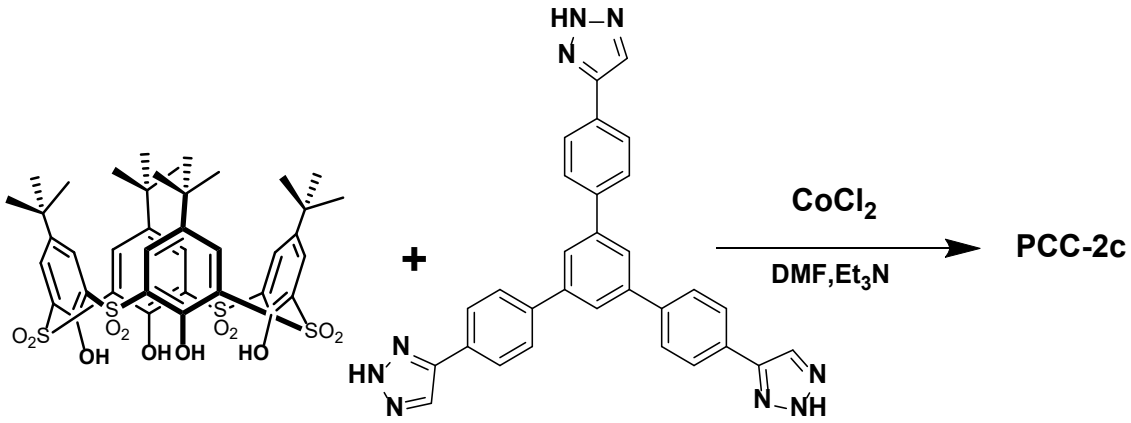

H_4V_2 (11.9 mg, 0.014 mmol), H_3L_2 (16.7 mg, 0.033 mmol), and $CoCl_2$ (13.3 mg, 0.103 mmol) were suspended in 1 mL DMF with 2 drops of Et_3N. The mixture was heated at 130°C.in an oven for 24 h. After cooling to ambient temperature, large purple crystals were collected and washed with methanol to yield PCC-2b in about 90%.

Hydrogen Generation Reaction and TOF Calculation

A gas burette filled with water was connected to the reaction flask to measure the volume of hydrogen. The reaction started when 1 mL aqueous solution of ammonia borane (30 mg, 1 mmol) was injected into the flask containing Co NCs@PCC-2 prepared above. The volume of the evolved hydrogen gas was monitored by recording the displacement of water in the gas burette. The reaction was completed when the gas generation ceased.

The turnover frequency (TOF) is based on the amount of Ru atoms, which was calculated from the equation below: $TOF = \boldsymbol{VH_2}/(\ Vm \cdot n\text{Co} \cdot \boldsymbol{t})$ where VH_2 is the total volume of generated H_2, VH_2 is calculated by P_{atm}/RT (P_{atm} is 101.325 kPa, R is 8.3145 $m^3 \cdot Pa \cdot mol^{-1} \cdot K^{-1}$, and T is 298 K), nCo is the total number of moles of Co in the catalyst and t is the completion time of the reaction in minutes.

Summary

In summary, three porous coordination cages (PCC-2a PCC- 2b and PCC-2c) sharing a similar structure were synthesized, and their Co-Nanoparticle encapsulation with catalytic activity in hydrogenation reaction was studied. We found that the highly negative PCC-2a is very efficient in encapsulating the Co NCs via evenly dispersing them in the pores. PCC-2b and PCC-2c cannot encapsulate these Co nanoclusters inside pores due to less charge of the cages. The composite Co NCs inside PCC-2a showed high catalytic activity in the hydrolysis of $NH_3 \cdot BH_3$, which is rare in first-row transition metal catalysis. The

study in this chapter demonstrates an efficient way to utilize Metal-Organic Cage compounds to encapsulate and stabilize nanoclusters for clean energy applications.

CHAPTER V

CONCLUSIONS AND OUTLOOK

In this dissertation work, I studied pore environment modifications of Metal-Organic Frameworks and Porous Coordination Cages to further optimize them for applications such as gas storage/separation and hydrogenation reaction catalysis. In chapter two, two new methods were described. Firstly, it created steady mesopores via Soxhlet extraction, which is an easy and scalable method. Also, we discuss the consequence of higher alkane doping in pores of a Metal-Organic Framework. We see higher alkane and long-chain fatty acid doping, such as decane in the Metal-Organic Framework increases the natural gas uptake. Fatty acid-MOF composite retains the performance after three cycles make it a good scalable, solid natural gas adsorbent during transportation and stationary storage of methane. In the next chapter, we discuss creating functionalize mesopores in PCN-250 via a method called Ligand Fragment Coassembly (LFCA). Fragmented ligand already possesses functional groups that provides interactions in MOF pores simultaneously generates mesopores in Metal-Organic Frameworks. This method's effectiveness was tested with high pressure methane uptake where nitro decorated ligand fragment shows high methane uptake despite having a lower surface area. In the fourth chapter, we focused our attention to another significant class of porous material called Porous Coordination Cage (PCCs). Its design and synthesis were discussed. These cages were tested to effectively encapsulate and stabilize a first-row transition metal nanoparticle (i.e., cobalt nanoparticle). It was concluded that PCC-2a was able to stabilize the nanoparticle inside the pores due to its high negative charge, whereas the other two cages were unable to

stabilize it. The catalytic performance also reflected this fact, and PCC-2a showed the highest catalytic activity.

Future studies that would be beneficial to this aim of creating better porous materials for sustainable energy applications and the research described herein include an extrapolation of in-depth structural studies of binding sites and interactions of functional groups of mesoporous MOFs with guest molecules with neutron diffraction studies. This structural study would able to clearly demonstrate a pathway to optimize balance porosity and gas sorption in Metal-Organic Frameworks and reach goals set by the Department of Energy. This proposed structural characterization will be continued via a valuable collaboration with the Zhou group and Oak Ridge National Laboratory (ORNL). Additionally, these studies were done in Fe based U3 oxo clusters; a reasonable next step would concern the study of a similar strategy to other topologies and check the universality of these methods. Lastly, regarding studies of Metal-Organic Cages, although PCC-2c did not perform well in these catalytic studies. However, PCC-2c having a unique structural feature. It has a nitrogen-based coordination site, unlike its sister structures of carboxylate-based sites. These nitrogen-based donor sites would be beneficial in providing soft-soft interactions, and it is hypothesized to be quite stable under basic conditions. Follow up studies should be carried out to find applications of this cage materials in water pollutant contamination capture. It should be able to perform where water pH is alkaline such as in industrial zones[245], where other cage-based filters degrade. This extrapolation would provide PCC-2c's aptitude as water purifying porous material.

The overall theme of this dissertation work can be best described as an attempt to modify porous materials for improved gas storage and catalytic applications. Through the first project, modifications were done post-synthetically via Soxhlet treatment and doping of hydrocarbons, to improve the natural gas storage application side of porous material chemistry. The second project focuses on creating more systemic mesopores that can potentially bring insightful guest-host interaction inside the mesopores environment. In the last project, we tuned the charge of the porous cage to tune its encapsulating behavior, which leads to develop a new class of catalytic systems in sustainable energy science.

REFERENCES

1. Nakanishi, K.; Hierarchically Structured Porous Materials: Application to Separation Sciences. In *Hierarchically Structured Porous Materials*, Su, Bao. L.;Sanchez, Clement.;Wiley-VCH: New York, 2011; pp 517-529.

2. Casson, S., Origins and Development of Applied Chemistry by J. R. Partington. Longmans, Green & Co., 1935. pp. XII and 597. 45s. *Antiquity* **1935,** *9* (36), 502-504.

3. Scheele, C. W.; Priestley, J.; Bergman, T.; Kirwan, R.; Forster, J. R.; Johnson, J.; Real Colegio de Cirugía de San, C., *Chemical Observations and Experiments on Air and Fire*. printed for J. Johnson . London, 1780; p XL, 259.

4. Woodhead, G. S.; Wood, G. E. C., An Inquiry into the Relative Efficiency of Water Filters in the Prevention of Infective Disease: A Special Report to the "British Medical Journal.". *Br Med J* **1894,** *2* (1767), 1053-1059.

5. Derlet, R. W.; Albertson, T. E., Activated charcoal--past, present and future. *West J Med* **1986,** *145* (4), 493-496.

6. Weckhuysen, B. M.; Yu, J., Recent advances in zeolite chemistry and catalysis. *Chemical Society Reviews* **2015,** *44* (20), 7022-7024.

7. Narayan, R.; Nayak, U. Y.; Raichur, A. M.; Garg, S., Mesoporous Silica Nanoparticles: A Comprehensive Review on Synthesis and Recent Advances. *Pharmaceutics* **2018,** *10* (3), 118.

8. Bragg, W. H.; Bragg, W. L., The structure of the diamond. *Proc. R. Soc. Lond.* **1913,** *89* (610), 277-291.

9. Batten, S. R.; Champness, N. R.; Chen, X.-M.; Garcia-Martinez, J.; Kitagawa, S.; Öhrström, L.; O'Keeffe, M.; Suh, M. P.; Reedijk, J., Coordination polymers, metal–organic frameworks and the need for terminology guidelines. *CrystEngComm* **2012,** *14* (9), 3001-3004.

10. Kauffman, G. B. Coordination Chemistry: History. In *Encyclopedia of Inorganic and Bioinorganic Chemistry*.**2011**.

11. Buser, H. J.; Schwarzenbach, D.; Petter, W.; Ludi, A., The crystal structure of Prussian Blue: Fe4[Fe(CN)6]3.xH2O. *Inorganic Chemistry* **1977,** *16* (11), 2704-2710.

12. Hantzsch, A.; Werner, A., Ueber räumliche Anordnung der Atome in stickstoffhaltigen Molekülen. *Berichte der deutschen chemischen Gesellscaft* **1890,** *23* (1), 11-30.

13. Constable, E. C.; Housecroft, C. E., Coordination chemistry: the scientific legacy of Alfred Werner. *Chemical Society Reviews* **2013,** *42* (4), 1429-1439.

14. Cooper, J. N.; McCoy, J. D.; Katz, M. G.; Deutsch, E., Trans effect in octahedral complexes. 4. Kinetic trans effect induced by the S-bonded thiosulfato ligand in bis(ethylenediamine)cobalt(III) complexes. *Inorganic Chemistry* **1980,** *19* (8), 2265-2271.

15. Shaw, J. L.; Dockery, C. R.; Lewis, S. E.; Harris, L.; Bettis, R., The Trans Effect: A Guided-Inquiry Experiment for Upper-Division Inorganic Chemistry. *Journal of Chemical Education* **2009,** *86* (12), 1416.

16. Pearson, R. G., Hard and Soft Acids and Bases. *Journal of the American Chemical Society* **1963,** *85* (22), 3533-3539.

17. Wilkinson, G., The Long Search for Stable Transition Metal Alkyles. *Imperial College of Science & Technology* **1973**.

18. Kauffman, G. B.; Girolami, G. S.; Busch, D. H., John C. Bailar, Jr. (1904–1991): father of coordination chemistry in the United States. *Coordination Chemistry Reviews* **1993,** *128* (1), 1-48.

19. Robson, R., *Crystal Engineering of Novel Materials Composed of Infinite Two- and Three-Dimensional Frameworks Supramolecular Architecture*. ACS Synposium Series 499; American Chemical Society: Washington, DC, 1992; p 256.

20. Fujita, M.; Kwon, Y. J.; Washizu, S.; Ogura, K., Preparation, Clathration Ability, and Catalysis of a Two-Dimensional Square Network Material Composed of Cadmium(II) and 4,4'-Bipyridine. *Journal of the American Chemical Society* **1994,** *116* (3), 1151-1152.

21. Zheng, C.; Greer, H. F.; Chiang, C.-Y.; Zhou, W., Microstructural study of the formation mechanism of metal–organic framework MOF-5. *CrystEngComm* **2014,** *16* (6), 1064-1070.

22. Contant, R.; Yaghi, O. M., Potassium Octadecatungstodiphosphates(V) and Related Lacunary Compounds. In *Inorganic Syntheses*, Wiley-VCH: New York, 2011 pp 104-111.

23. Klemperer, W. G.; Marquart, T. A.; Yaghi, O. M., New Directions in Polyvanadate Chemistry: From Cages and Clusters to Baskets, Belts, Bowls, and Barrels. *Angew. Chem. Int. Ed.* **1992,** *31* (1), 49-51.

24. Li, H.; Eddaoudi, M.; O'Keeffe, M.; Yaghi, O. M., Design and synthesis of an exceptionally stable and highly porous metal-organic framework. *Nature* **1999,** *402* (6759), 276-279.

25. Kitagawa, S.; Munakata, M.; Shimono, H.; Matsuyama, S.; Masuda, H., Synthesis and crystal structure of hexanuclear copper(I) complexes of μ3-pyridine-2-thionate. *Dalton Transactions* **1990,** (7), 2105-2109.

26. Kondo, M.; Yoshitomi, T.; Matsuzaka, H.; Kitagawa, S.; Seki, K., Three-Dimensional Framework with Channeling Cavities for Small Molecules:{[M2(4, 4′-bpy)3(NO3)4]·xH2O}n (M : Co, Ni, Zn). *Angew. Chem. Int. Ed.* **1997,** *36* (16), 1725-1727.

27. Eddaoudi, M.; Kim, J.; Rosi, N.; Vodak, D.; Wachter, J.; Keeffe, M.; Yaghi, O. M., Systematic Design of Pore Size and Functionality in Isoreticular MOFs and Their Application in Methane Storage. *Science* **2002,** *295* (5554), 469.

28. Liu, X.; Zhou, Y.; Zhang, J.; Tang, L.; Luo, L.; Zeng, G., Iron Containing Metal–Organic Frameworks: Structure, Synthesis, and Applications in Environmental Remediation. *ACS Applied Materials & Interfaces* **2017,** *9* (24), 20255-20275.

29. Ding, M.; Cai, X.; Jiang, H.-L., Improving MOF stability: approaches and applications. *Chemical Science* **2019,** *10* (44), 10209-10230.

30. Bai, Y.; Dou, Y.; Xie, L.-H.; Rutledge, W.; Li, J.-R.; Zhou, H.-C., Zr-based metal–organic frameworks: design, synthesis, structure, and applications. *Chemical Society Reviews* **2016,** *45* (8), 2327-2367.

31. Zhang, J.-P.; Zhang, Y.-B.; Lin, J.-B.; Chen, X.-M., Metal Azolate Frameworks: From Crystal Engineering to Functional Materials. *Chemical Reviews* **2012,** *112* (2), 1001-1033.

32. Park, K. S.; Ni, Z.; Côté, A. P.; Choi, J. Y.; Huang, R.; Uribe-Romo, F. J.; Chae, H. K.; O'Keeffe, M.; Yaghi, O. M., Exceptional chemical and thermal stability of zeolitic imidazolate frameworks. *Proceedings of the National Academy of Sciences* **2006,** *103* (27), 10186.

33. Wang, K.; Feng, D.; Liu, T.-F.; Su, J.; Yuan, S.; Chen, Y.-P.; Bosch, M.; Zou, X.; Zhou, H.-C., A Series of Highly Stable Mesoporous Metalloporphyrin Fe-MOFs. *Journal of the American Chemical Society* **2014,** *136* (40), 13983-13986.

34. Feng, L.; Wang, K.-Y.; Willman, J.; Zhou, H.-C., Hierarchy in Metal–Organic Frameworks. *ACS Central Science* **2020,** *6* (3), 359-367.

35. Gropp, C.; Canossa, S.; Wuttke, S.; Gándara, F.; Li, Q.; Gagliardi, L.; Yaghi, O. M., Standard Practices of Reticular Chemistry. *ACS Central Science* **2020,** *6* (8),1255-1273.

36. Asgari, M.; Jawahery, S.; Bloch, E. D.; Hudson, M. R.; Flacau, R.; Vlaisavljevich, B.; Long, J. R.; Brown, C. M.; Queen, W. L., An experimental and computational study of CO2 adsorption in the sodalite-type M-BTT (M = Cr, Mn, Fe, Cu) metal–organic frameworks featuring open metal sites. *Chemical Science* **2018,** *9* (20), 4579-4588.

37. Stuart, R. B.; Neil, R. C.; Xiao-Ming, C.; Javier, G.-M.; Susumu, K.; Lars, Ö.; Michael, O. K.; Myunghyun Paik, S.; Jan, R., Terminology of metal–organic frameworks

and coordination polymers (IUPAC Recommendations 2013). *Pure and Applied Chemistry* **2013,** *85* (8), 1715-1724.

38. Frensdorff, H. K., Salt complexes of cyclic polyethers. Distribution equilibriums. *Journal of the American Chemical Society* **1971,** *93* (19), 4684-4688.

39. Krakowiak, K.; Bradshaw, J., Syntheses of the Cryptands. A Short Review. *Israel Journal of Chemistry* **1992,** *32* (1), 3-13.

40. von-Schnering, H. G.; Saalfrank, R.; Stark, A.; Peters, K.; von Schnering, H., The First Adamantoid Alkaline Earth Metal Chelate Complex: Synthesis, Structure, and Reactivity. *Angewandte Chemie International Edition* **1988,** *27* (6), 851-853.

41. Fujita, M.; Nagao, S.; Ogura, K., Guest-Induced Organization of a Three-Dimensional Palladium(II) Cagelike Complex. A Prototype for "Induced-Fit" Molecular Recognition. *Journal of the American Chemical Society* **1995,** *117* (5), 1649-1650.

42. Fujita, M.; Oguro, D.; Miyazawa, M.; Oka, H.; Yamaguchi, K.; Ogura, K., Self-assembly of ten molecules into nanometre-sized organic host frameworks. *Nature* **1995,** *378* (6556), 469-471.

43. Olenyuk, B.; Whiteford, J.; Fechtenkötter, A.; Stang, P., Self-assembly of nanoscale cuboctahedra by coordination chemistry. *Nature* **1999,** *398* (6730), 796-799.

44. Cotton, F. A.; Lin, C.; Murillo, C. A., Supramolecular Arrays Based on Dimetal Building Units. *Accounts of Chemical Research* **2001,** *34* (10), 759-771.

45. Oliveri, C.; Ulmann, P.; Wiester, M.; Mirkin, C., Heteroligated Supramolecular Coordination Complexes Formed via the Halide-Induced Ligand Rearrangement Reaction. *Accounts of Chemical Research* **2008,** *41* (12), 1618-1629.

46. Eddaoudi, M.; Kim, J.; Wachter, J. B.; Chae, H. K.; O'Keeffe, M.; Yaghi, O. M., Porous Metal−Organic Polyhedra: 25 Å Cuboctahedron Constructed from 12 Cu2(CO2)4 Paddle-Wheel Building Blocks. *Journal of the American Chemical Society* **2001,** *123* (18), 4368-4369.

47. Hosono, N.; Gochomori, M.; Matsuda, R.; Sato, H.; Kitagawa, S., Metal–Organic Polyhedral Core as a Versatile Scaffold for Divergent and Convergent Star Polymer Synthesis. *Journal of the American Chemical Society* **2016,** *138* (20), 6525-6531.

48. Zhang, Y.; Crawley, M.; Hauke, C.; Friedman, A.; Cook, T., Phosphorescent Decanuclear Bimetallic Pt6M4(M = Zn, Fe) Tetrahedral Cages. *Inorganic Chemistry* **2017,** *56* (8), 4258-4262.

49. Ke, Y.; Collins, D. J.; Zhou, H. C., Synthesis and structure of cuboctahedral and anticuboctahedral cages containing 12 quadruply bonded dimolybdenum units. *Inorg Chem* **2005,** *44* (12), 4154-6.

50. Gosselin, E. J.; Rowland, C. A.; Bloch, E. D., Permanently Microporous Metal–Organic Polyhedra. *Chemical Reviews* **2020,** *120* (16) 8987-9014.

51. Cook, T. R.; Zheng, Y.-R.; Stang, P. J., Metal–Organic Frameworks and Self-Assembled Supramolecular Coordination Complexes: Comparing and Contrasting the Design, Synthesis, and Functionality of Metal–Organic Materials. *Chemical Reviews* **2013,** *113* (1), 734-777.

52. Briggs, M. E.; Cooper, A. I., A Perspective on the Synthesis, Purification, and Characterization of Porous Organic Cages. *Chemistry of Materials* **2017,** *29* (1), 149-157.

53. Chatterjee, B.; Noveron, J. C.; Resendiz, M. J. E.; Liu, J.; Yamamoto, T.; Parker, D.; Cinke, M.; Nguyen, C. V.; Arif, A. M.; Stang, P. J., Self-Assembly of Flexible Supramolecular Metallacyclic Ensembles: Structures and Adsorption Properties of Their Nanoporous Crystalline Frameworks. *Journal of the American Chemical Society* **2004,** *126* (34), 10645-10656.

54. Park, J.; Chen, Y. P.; Perry, Z.; Li, J. R.; Zhou, H. C., Preparation of core-shell coordination molecular assemblies via the enrichment of structure-directing "codes" of bridging ligands and metathesis of metal units. *J Am Chem Soc* **2014,** *136* (48), 16895-901.

55. Young, M. D.; Zhang, Q.; Zhou, H.-C., Metal–organic polyhedra constructed from dinuclear ruthenium paddlewheels. *Inorganica Chimica Acta* **2015,** *424*, 216-220.

56. Li, J. R.; Zhou, H. C., Metal-organic hendecahedra assembled from dinuclear paddlewheel nodes and mixtures of ditopic linkers with 120 and 90 degrees bend angles. *Angewandte Chemie International Ed.* **2009,** *48* (45), 8465-8.

57. Li, J. R.; Yakovenko, A. A.; Lu, W.; Timmons, D. J.; Zhuang, W.; Yuan, D.; Zhou, H. C., Ligand bridging-angle-driven assembly of molecular architectures based on quadruply bonded Mo-Mo dimers. *J Am Chem Soc* **2010,** *132* (49), 17599-610.

58. Rowland, C. A.; Lorzing, G. R.; Gosselin, E. J.; Trump, B. A.; Yap, G. P. A.; Brown, C. M.; Bloch, E. D., Methane Storage in Paddlewheel-Based Porous Coordination Cages. *Journal of the American Chemical Society* **2018,** *140* (36), 11153-11157.

59. Inokuma, Y.; Kawano, M.; Fujita, M., Crystalline molecular flasks. *Nature Chemistry* **2011,** *3* (5), 349-358.

60. Li, J. R.; Zhou, H. C.; Li, J.-R.; Yakovenko, A.; Lu, W.; Timmons, D.; Zhuang, W.; Yuan, D.; Zhou, H.-C., Ligand Bridging-Angle-Driven Assembly of Molecular Architectures Based on Quadruply Bonded Mo−Mo Dimers. *Journal of the American Chemical Society* **2010,** *132* (49), 17599-17610.

61. Fang, Y.; Powell, J. A.; Li, E.; Wang, Q.; Perry, Z.; Kirchon, A.; Yang, X.; Xiao, Z.; Zhu, C.; Zhang, L.; Huang, F.; Zhou, H.-C., Catalytic reactions within the cavity of coordination cages. *Chemical Society Reviews* **2019,** *48* (17), 4707-4730.

62. Kuppler, R. J.; Timmons, D. J.; Fang, Q.-R.; Li, J.-R.; Makal, T. A.; Young, M. D.; Yuan, D.; Zhao, D.; Zhuang, W.; Zhou, H.-C., Potential applications of metal-organic frameworks. *Coordination Chemistry Reviews* **2009,** *253* (23), 3042-3066.

63. Schlapbach, L., Hydrogen as a Fuel and Its Storage for Mobility and Transport. *MRS Bulletin* **2002,** *27* (9), 675-679.

64. Rowsell, J. L. C.; Yaghi, O. M., Strategies for Hydrogen Storage in Metal–Organic Frameworks. *Angew Chem Int Ed* **2005,** *44* (30), 4670-4679.

65. Runčevski, T.; Kapelewski, M. T.; Torres-Gavosto, R. M.; Tarver, J. D.; Brown, C. M.; Long, J. R., Adsorption of two gas molecules at a single metal site in a metal–organic framework. *Chemical Communications* **2016,** *52* (53), 8251-8254.

66. Kaye, S. S.; Dailly, A.; Yaghi, O. M.; Long, J. R., Impact of Preparation and Handling on the Hydrogen Storage Properties of Zn4O(1,4-benzenedicarboxylate)3 (MOF-5). *Journal of the American Chemical Society* **2007,** *129* (46), 14176-14177.

67. Wong-Foy, A. G.; Matzger, A. J.; Yaghi, O. M., Exceptional H2 Saturation Uptake in Microporous Metal−Organic Frameworks. *Journal of the American Chemical Society* **2006,** *128* (11), 3494-3495.

68. Lee, Y.-G.; Moon, H. R.; Cheon, Y. E.; Suh, M. P., A Comparison of the H2 Sorption Capacities of Isostructural Metal–Organic Frameworks With and Without Accessible Metal Sites: [{Zn2(abtc)(dmf)2}3] and [{Cu2(abtc)(dmf)2}3] versus [{Cu2(abtc)}3]. *Angewandte Chemie International Edition* **2008,** *47* (40), 7741-7745.

69. Tan, C.; Yang, S.; Champness, N. R.; Lin, X.; Blake, A. J.; Lewis, W.; Schröder, M., High capacity gas storage by a 4,8-connected metal–organic polyhedral framework. *Chemical Communications* **2011,** *47* (15), 4487-4489.

70. Sun, D.; Ma, S.; Ke, Y.; Collins, D. J.; Zhou, H.-C., An Interweaving MOF with High Hydrogen Uptake. *Journal of the American Chemical Society* **2006,** *128* (12), 3896-3897.

71. Feng, D.; Wang, K.; Wei, Z.; Chen, Y. P.; Simon, C. M.; Arvapally, R. K.; Martin, R. L.; Bosch, M.; Liu, T. F.; Fordham, S.; Yuan, D.; Omary, M. A.; Haranczyk, M.; Smit, B.; Zhou, H. C., Kinetically tuned dimensional augmentation as a versatile synthetic route towards robust metal-organic frameworks. *Nat Commun* **2014,** *5*, 5723.

72. Wang, X.-S.; Ma, S.; Forster, P. M.; Yuan, D.; Eckert, J.; López, J. J.; Murphy, B. J.; Parise, J. B.; Zhou, H.-C., Enhancing H2 Uptake by "Close-Packing" Alignment of Open Copper Sites in Metal–Organic Frameworks. *Angew Chem Int Ed* **2008,** *47* (38), 7263-7266.

73. Chen, Z.; Li, P.; Anderson, R.; Wang, X.; Zhang, X.; Robison, L.; Redfern, L. R.; Moribe, S.; Islamoglu, T.; Gómez-Gualdrón, D. A.; Yildirim, T.; Stoddart, J. F.; Farha, O. K., Balancing volumetric and gravimetric uptake in highly porous materials for clean energy. *Science* **2020,** *368* (6488), 297.

74. Allendorf, M. D.; Hulvey, Z.; Gennett, T.; Ahmed, A.; Autrey, T.; Camp, J.; Seon Cho, E.; Furukawa, H.; Haranczyk, M.; Head-Gordon, M.; Jeong, S.; Karkamkar, A.; Liu, D.-J.; Long, J. R.; Meihaus, K. R.; Nayyar, I. H.; Nazarov, R.; Siegel, D. J.; Stavila, V.; Urban, J. J.; Veccham, S. P.; Wood, B. C., An assessment of strategies for the development of solid-state adsorbents for vehicular hydrogen storage. *Energy & Environmental Science* **2018,** *11* (10), 2784-2812.

75. Armor, J. N., Emerging importance of shale gas to both the energy & chemicals landscape. *Journal of Energy Chemistry* **2013,** *22* (1), 21-26.

76. Mason, J. A.; Veenstra, M.; Long, J. R., Evaluating metal–organic frameworks for natural gas storage. *Chemical Science* **2014,** *5* (1), 32-51.

77. Wu, H.; Zhou, W.; Yildirim, T., High-Capacity Methane Storage in Metal−Organic Frameworks M2(dhtp): The Important Role of Open Metal Sites. *Journal of the American Chemical Society* **2009,** *131* (13), 4995-5000.

78. Ma, S.; Sun, D.; Simmons, J. M.; Collier, C. D.; Yuan, D.; Zhou, H.-C., Metal-Organic Framework from an Anthracene Derivative Containing Nanoscopic Cages Exhibiting High Methane Uptake. *Journal of the American Chemical Society* **2008,** *130* (3), 1012-1016.

79. Peng, Y.; Krungleviciute, V.; Eryazici, I.; Hupp, J. T.; Farha, O. K.; Yildirim, T., Methane Storage in Metal–Organic Frameworks: Current Records, Surprise Findings, and Challenges. *Journal of the American Chemical Society* **2013,** *135* (32), 11887-11894.

80. Jiang, Y.; Park, J.; Tan, P.; Feng, L.; Liu, X.-Q.; Sun, L.-B.; Zhou, H.-C., Maximizing Photoresponsive Efficiency by Isolating Metal–Organic Polyhedra into Confined Nanoscaled Spaces. *Journal of the American Chemical Society* **2019,** *141* (20), 8221-8227.

81. Li, H.; Wang, K.; Sun, Y.; Lollar, C. T.; Li, J.; Zhou, H.-C., Recent advances in gas storage and separation using metal–organic frameworks. *Materials Today* **2018,** *21* (2), 108-121.

82. Sumida, K.; Rogow, D. L.; Mason, J. A.; McDonald, T. M.; Bloch, E. D.; Herm, Z. R.; Bae, T.-H.; Long, J. R., Carbon Dioxide Capture in Metal–Organic Frameworks. *Chemical Reviews* **2012,** *112* (2), 724-781.

83. McDonald, T. M.; D'Alessandro, D. M.; Krishna, R.; Long, J. R., Enhanced carbon dioxide capture upon incorporation of N,N′-dimethylethylenediamine in the metal–organic framework CuBTTri. *Chemical Science* **2011,** *2* (10), 2022-2028.

84. McDonald, T. M.; Lee, W. R.; Mason, J. A.; Wiers, B. M.; Hong, C. S.; Long, J. R., Capture of Carbon Dioxide from Air and Flue Gas in the Alkylamine-Appended Metal–Organic Framework mmen-Mg2(dobpdc). *Journal of the American Chemical Society* **2012,** *134* (16), 7056-7065.

85. Fracaroli, A. M.; Furukawa, H.; Suzuki, M.; Dodd, M.; Okajima, S.; Gándara, F.; Reimer, J. A.; Yaghi, O. M., Metal–Organic Frameworks with Precisely Designed

Interior for Carbon Dioxide Capture in the Presence of Water. *Journal of the American Chemical Society* **2014,** *136* (25), 8863-8866.

86. McDonald, T. M.; Mason, J. A.; Kong, X.; Bloch, E. D.; Gygi, D.; Dani, A.; Crocellà, V.; Giordanino, F.; Odoh, S. O.; Drisdell, W. S.; Vlaisavljevich, B.; Dzubak, A. L.; Poloni, R.; Schnell, S. K.; Planas, N.; Lee, K.; Pascal, T.; Wan, L. F.; Prendergast, D.; Neaton, J. B.; Smit, B.; Kortright, J. B.; Gagliardi, L.; Bordiga, S.; Reimer, J. A.; Long, J. R., Cooperative insertion of CO2 in diamine-appended metal-organic frameworks. *Nature* **2015,** *519* (7543), 303-308.

87. Peng, Y.; Li, Y.; Ban, Y.; Jin, H.; Jiao, W.; Liu, X.; Yang, W., Metal-organic framework nanosheets as building blocks for molecular sieving membranes. *Science* **2014,** *346* (6215), 1356.

88. Sanz-Pérez, E. S.; Murdock, C. R.; Didas, S. A.; Jones, C. W., Direct Capture of CO2 from Ambient Air. *Chemical Reviews* **2016,** *116* (19), 11840-11876.

89. Sinha, A.; Darunte, L. A.; Jones, C. W.; Realff, M. J.; Kawajiri, Y., Systems Design and Economic Analysis of Direct Air Capture of CO2 through Temperature Vacuum Swing Adsorption Using MIL-101(Cr)-PEI-800 and mmen-Mg2(dobpdc) MOF Adsorbents. *Industrial & Engineering Chemistry Research* **2017,** *56* (3), 750-764.

90. Bigdeli, F.; Lollar, C. T.; Morsali, A.; Zhou, H.-C., Switching in Metal–Organic Frameworks. *Angewandte Chemie International Edition* **2020**, *59* 4652.

91. Dong, Z.; Sun, Y.; Chu, J.; Zhang, X.; Deng, H., Multivariate Metal–Organic Frameworks for Dialing-in the Binding and Programming the Release of Drug Molecules. *Journal of the American Chemical Society* **2017,** *139* (40), 14209-14216.

92. Hermenegildo García , S. N., Metal-Organic Frameworks: Applications in Separations and Catalysis. In *Metal-Organic Frameworks: Applications in Separations and Catalysis*, García, H., Ed. John Wiley and Sons: 2018; pp 1-28.

93. Howarth, A. J.; Liu, Y.; Li, P.; Li, Z.; Wang, T. C.; Hupp, J. T.; Farha, O. K., Chemical, thermal and mechanical stabilities of metal–organic frameworks. *Nature Reviews Materials* **2016,** *1* (3), 15018.

94. Li, N.; Xu, J.; Feng, R.; Hu, T.-L.; Bu, X.-H., Governing metal–organic frameworks towards high stability. *Chemical Communications* **2016,** *52* (55), 8501-8513.

95. Brock, D. J.; Kustigian, L.; Jiang, M. Q.; Graham, K.; Wang, T. Y.; Erazo-Oliveras, A.; Najjar, K.; Zhang, J. J.; Rye, H.; Pellois, J. P., Efficient cell delivery mediated by lipid-specific endosomal escape of supercharged branched peptides. *Traffic* **2018,** *19* (6), 421-435.

96. Wang, X.; Chen, X. Z.; Alcantara, C. C. J.; Sevim, S.; Hoop, M.; Terzopoulou, A.; de Marco, C.; Hu, C.; de Mello, A. J.; Falcaro, P.; Furukawa, S.; Nelson, B. J.; Puigmarti-Luis, J.; Pane, S., MOFBOTS: Metal-Organic-Framework-Based Biomedical Microrobots. *Adv Mater* **2019**, *31*,1901592.

97. Kamaly, N.; Yameen, B.; Wu, J.; Farokhzad, O. C., Degradable Controlled-Release Polymers and Polymeric Nanoparticles: Mechanisms of Controlling Drug Release. *Chemical Reviews* **2016,** *116* (4), 2602-2663.

98. Zhang, S.; Chu, Z.; Yin, C.; Zhang, C.; Lin, G.; Li, Q., Controllable Drug Release and Simultaneously Carrier Decomposition of SiO2-Drug Composite Nanoparticles. *Journal of the American Chemical Society* **2013,** *135* (15), 5709-5716.

99. Öztürk-Atar, K.; Eroğlu, H.; Çalış, S., Novel advances in targeted drug delivery. *Journal of Drug Targeting* **2018,** *26* (8), 633-642.

100. Miao, Y.; Zhao, X.; Qiu, Y.; Liu, Z.; Yang, W.; Jia, X., Metal–Organic Framework-Assisted Nanoplatform with Hydrogen Peroxide/Glutathione Dual-Sensitive On-Demand Drug Release for Targeting Tumors and Their Microenvironment. *ACS Applied Bio Materials* **2019,** *2* (2), 895-905.

101. Chen, T. T.; Yi, J. T.; Zhao, Y. Y.; Chu, X., Biomineralized Metal-Organic Framework Nanoparticles Enable Intracellular Delivery and Endo-Lysosomal Release of Native Active Proteins. *J Am Chem Soc* **2018,** *140* (31), 9912-9920.

102. Wang, H.; Chen, Y.; Wang, H.; Liu, X.; Zhou, X.; Wang, F., DNAzyme-Loaded Metal-Organic Frameworks (MOFs) for Self-Sufficient Gene Therapy. *Angew Chem Int Ed Engl* **2019** *58* (22) 7380-7384

103. Tan, L.-L.; Song, N.; Zhang, S. X.-A.; Li, H.; Wang, B.; Yang, Y.-W., Ca2+, pH and thermo triple-responsive mechanized Zr-based MOFs for on-command drug release in bone diseases. *Journal of Materials Chemistry B* **2016,** *4* (1), 135-140.

104. Carrillo-Carrion, C.; Martinez, R.; Navarro Poupard, M. F.; Pelaz, B.; Polo, E.; Arenas-Vivo, A.; Olgiati, A.; Taboada, P.; Soliman, M. G.; Catalan, U.; Fernandez-Castillejo, S.; Sola, R.; Parak, W. J.; Horcajada, P.; Alvarez-Puebla, R. A.; Del Pino, P., Aqueous Stable Gold Nanostar/ZIF-8 Nanocomposites for Light-Triggered Release of Active Cargo Inside Living Cells. *Angew Chem Int Ed Engl* **2019,** *58* (21), 7078-7082.

105. Sharma, S.; Mittal, D.; Verma, A. K.; Roy, I., Copper-Gallic Acid Nanoscale Metal–Organic Framework for Combined Drug Delivery and Photodynamic Therapy. *ACS Applied Bio Materials* **2019**, *2*, (5) 2092-2101

106. Jiang, K.; Zhang, L.; Hu, Q.; Zhao, D.; Xia, T.; Lin, W.; Yang, Y.; Cui, Y.; Yang, Y.; Qian, G., Pressure controlled drug release in a Zr-cluster-based MOF. *Journal of Materials Chemistry B* **2016,** *4* (39), 6398-6401.

107. Fang, J.; Yang, Y.; Xiao, W.; Zheng, B.; Lv, Y. B.; Liu, X. L.; Ding, J., Extremely low frequency alternating magnetic field-triggered and MRI-traced drug delivery by optimized magnetic zeolitic imidazolate framework-90 nanoparticles. *Nanoscale* **2016,** *8* (6), 3259-63.

108. Samanta, D.; Roy, S.; Sasmal, R.; Saha, N. D.; K, R. P.; Viswanatha, R.; Agasti, S. S.; Maji, T. K., Solvent Adaptive Dynamic Metal-Organic Soft Hybrid for Imaging and Biological Delivery. *Angew Chem Int Ed Engl* **2019,** *58* (15), 5008-5012.

109. Peng, S.; Bie, B.; Sun, Y.; Liu, M.; Cong, H.; Zhou, W.; Xia, Y.; Tang, H.; Deng, H.; Zhou, X., Metal-organic frameworks for precise inclusion of single-stranded DNA and transfection in immune cells. *Nat Commun* **2018,** *9* (1), 1293.

110. Gandara-Loe, J.; Ortuno-Lizaran, I.; Fernandez-Sanchez, L.; Alio, J. L.; Cuenca, N.; Vega-Estrada, A.; Silvestre-Albero, J., Metal-Organic Frameworks as Drug Delivery Platforms for Ocular Therapeutics. *ACS Appl Mater Interfaces* **2019,** *11* (2), 1924-1931.

111. Lian, X.; Huang, Y.; Zhu, Y.; Fang, Y.; Zhao, R.; Joseph, E.; Li, J.; Pellois, J. P.; Zhou, H. C., Enzyme-MOF Nanoreactor Activates Nontoxic Paracetamol for Cancer Therapy. *Angew Chem Int Ed Engl* **2018,** *57* (20), 5725-5730.

112. Gao, X.; Zhai, Q.; Hu, M.; Li, S.; Song, J.; Jiang, Y., Design and preparation of stable CPO/HRP@H-MOF(Zr) composites for efficient bio-catalytic degradation of organic toxicants in wastewater. *Journal of Chemical Technology & Biotechnology* **2019,** *94* (4), 1249-1258.

113. Gkaniatsou, E.; Sicard, C.; Ricoux, R.; Benahmed, L.; Bourdreux, F.; Zhang, Q.; Serre, C.; Mahy, J. P.; Steunou, N., Enzyme Encapsulation in Mesoporous Metal-Organic Frameworks for Selective Biodegradation of Harmful Dye Molecules. *Angew Chem Int Ed Engl* **2018,** *57* (49), 16141-16146.

114. Lian, X.; Chen, Y. P.; Liu, T. F.; Zhou, H. C., Coupling two enzymes into a tandem nanoreactor utilizing a hierarchically structured MOF. *Chem Sci* **2016,** *7* (12), 6969-6973.

115. Rojas, S.; Baati, T.; Njim, L.; Manchego, L.; Neffati, F.; Abdeljelil, N.; Saguem, S.; Serre, C.; Najjar, M. F.; Zakhama, A.; Horcajada, P., Metal-Organic Frameworks as Efficient Oral Detoxifying Agents. *J Am Chem Soc* **2018,** *140* (30), 9581-9586.

116. Kato, S.; Otake, K.; Chen, H. Y.; Akpinar, I.; Buru, C. T.; Islamoglu, T.; Snurr, R. Q.; Farha, O. K., Zirconium-Based Metal-Organic Frameworks for the Removal of Protein-Bound Uremic Toxin from Human Serum Albumin. *Journal of the American Chemical Society* **2019,** *141* (6), 2568-2576.

117. Taylor, K. M. L.; Jin, A.; Lin, W., Surfactant-Assisted Synthesis of Nanoscale Gadolinium Metal–Organic Frameworks for Potential Multimodal Imaging. *Angewandte Chemie International Edition* **2008,** *47* (40), 7722-7725.

118. Rieter, W. J.; Taylor, K. M. L.; An, H.; Lin, W.; Lin, W., Nanoscale Metal−Organic Frameworks as Potential Multimodal Contrast Enhancing Agents. *Journal of the American Chemical Society* **2006,** *128* (28), 9024-9025.

119. Wu, M.-X.; Yang, Y.-W., Metal–Organic Framework (MOF)-Based Drug/Cargo Delivery and Cancer Therapy. *Advanced Materials* **2017,** *29* (23), 1606134.

120. Yang, Y.; Liu, J.; Liang, C.; Feng, L.; Fu, T.; Dong, Z.; Chao, Y.; Li, Y.; Lu, G.; Chen, M.; Liu, Z., Nanoscale Metal–Organic Particles with Rapid Clearance for Magnetic Resonance Imaging-Guided Photothermal Therapy. *ACS Nano* **2016,** *10* (2), 2774-2781.

121. Ray Chowdhuri, A.; Bhattacharya, D.; Sahu, S. K., Magnetic nanoscale metal organic frameworks for potential targeted anticancer drug delivery, imaging and as an MRI contrast agent. *Dalton Transactions* **2016,** *45* (7), 2963-2973.

122. Gao, X.; Zhai, M.; Guan, W.; Liu, J.; Liu, Z.; Damirin, A., Controllable Synthesis of a Smart Multifunctional Nanoscale Metal–Organic Framework for Magnetic Resonance/Optical Imaging and Targeted Drug Delivery. *ACS Applied Materials & Interfaces* **2017,** *9* (4), 3455-3462.

123. Zhang, T.; Wang, L.; Ma, C.; Wang, W.; Ding, J.; Liu, S.; Zhang, X.; Xie, Z., BODIPY-containing nanoscale metal–organic frameworks as contrast agents for computed tomography. *Journal of Materials Chemistry B* **2017,** *5* (12), 2330-2336.

124. Shang, W.; Zeng, C.; Du, Y.; Hui, H.; Liang, X.; Chi, C.; Wang, K.; Wang, Z.; Tian, J., Core–Shell Gold Nanorod@Metal–Organic Framework Nanoprobes for Multimodality Diagnosis of Glioma. *Advanced Materials* **2017,** *29* (3), 1604381.

125. Chen, D.; Yang, D.; Dougherty, C. A.; Lu, W.; Wu, H.; He, X.; Cai, T.; Van Dort, M. E.; Ross, B. D.; Hong, H., In Vivo Targeting and Positron Emission Tomography Imaging of Tumor with Intrinsically Radioactive Metal–Organic Frameworks Nanomaterials. *ACS Nano* **2017,** *11* (4), 4315-4327.

126. Li, Y.; Tang, J.; He, L.; Liu, Y.; Liu, Y.; Chen, C.; Tang, Z., Core–Shell Upconversion Nanoparticle@Metal–Organic Framework Nanoprobes for Luminescent/Magnetic Dual-Mode Targeted Imaging. *Advanced Materials* **2015,** *27* (27), 4075-4080.

127. Cai, W.; Gao, H.; Chu, C.; Wang, X.; Wang, J.; Zhang, P.; Lin, G.; Li, W.; Liu, G.; Chen, X., Engineering Phototheranostic Nanoscale Metal–Organic Frameworks for Multimodal Imaging-Guided Cancer Therapy. *ACS Applied Materials & Interfaces* **2017,** *9* (3), 2040-2051.

128. Park, J.; Xu, M.; Li, F.; Zhou, H.-C., 3D Long-Range Triplet Migration in a Water-Stable Metal–Organic Framework for Upconversion-Based Ultralow-Power in Vivo Imaging. *Journal of the American Chemical Society* **2018,** *140* (16), 5493-5499.

129. Lu, K.; He, C.; Lin, W., Nanoscale Metal–Organic Framework for Highly Effective Photodynamic Therapy of Resistant Head and Neck Cancer. *Journal of the American Chemical Society* **2014,** *136* (48), 16712-16715.

130. Lu, K. D.; He, C. B.; Lin, W. B., A Chlorin-Based Nanoscale Metal-Organic Framework for Photodynamic Therapy of Colon Cancers. *Journal of the American Chemical Society* **2015,** *137* (24), 7600-7603.

131. Park, J.; Jiang, Q.; Feng, D.; Mao, L.; Zhou, H.-C., Size-Controlled Synthesis of Porphyrinic Metal–Organic Framework and Functionalization for Targeted Photodynamic Therapy. *Journal of the American Chemical Society* **2016,** *138* (10), 3518-3525.

132. Zhu, W.; Liu, Y.; Yang, Z.; Zhang, L.; Xiao, L.; Liu, P.; Wang, J.; Yi, C.; Xu, Z.; Ren, J., Albumin/sulfonamide stabilized iron porphyrin metal organic framework nanocomposites: targeting tumor hypoxia by carbonic anhydrase IX inhibition and T1–T2 dual mode MRI guided photodynamic/photothermal therapy. *Journal of Materials Chemistry B* **2018,** *6* (2), 265-276.

133. Liu, Y.; Hou, W.; Xia, L.; Cui, C.; Wan, S.; Jiang, Y.; Yang, Y.; Wu, Q.; Qiu, L.; Tan, W., ZrMOF nanoparticles as quenchers to conjugate DNA aptamers for target-induced bioimaging and photodynamic therapy. *Chem Sci* **2018,** *9* (38), 7505-7509.

134. Liu, J.; Zhang, L.; Lei, J.; Shen, H.; Ju, H., Multifunctional Metal–Organic Framework Nanoprobe for Cathepsin B-Activated Cancer Cell Imaging and Chemo-Photodynamic Therapy. *ACS Applied Materials & Interfaces* **2017,** *9* (3), 2150-2158.

135. Lan, G. X.; Ni, K. Y.; Xu, R. Y.; Lu, K. D.; Lin, Z. K.; Chan, C.; Lin, W. B., Nanoscale Metal-Organic Layers for Deeply Penetrating X-ray-Induced Photodynamic Therapy. *Angewandte Chemie-International Edition* **2017,** *56* (40), 12102-12106.

136. Lan, G. X.; Ni, K. Y.; Veroneau, S. S.; Song, Y.; Lin, W. B., Nanoscale Metal-Organic Layers for Radiotherapy-Radiodynamic Therapy. *Journal of the American Chemical Society* **2018,** *140* (49), 16971-16975.

137. Ni, K. Y.; Lan, G. X.; Chan, C.; Quigley, B.; Lu, K. D.; Aung, T.; Guo, N. N.; La Riviere, P.; Weichselbaum, R. R.; Lin, W. B., Nanoscale metal-organic frameworks

enhance radiotherapy to potentiate checkpoint blockade immunotherapy. *Nature Communications* **2018,** *9*.

138. Ni, K. Y.; Lan, G. X.; Veroneau, S. S.; Duan, X. P.; Song, Y.; Lin, W. B., Nanoscale metal-organic frameworks for mitochondria-targeted radiotherapy-radiodynamic therapy. *Nature Communications* **2018,** *9*. 4321

139. Lu, K. D.; He, C. B.; Guo, N. N.; Chan, C.; Ni, K. Y.; Lan, G. X.; Tang, H. D.; Pelizzari, C.; Fu, Y. X.; Spiotto, M. T.; Weichselbaum, R. R.; Lin, W. B., Low-dose X-ray radiotherapy-radiodynamic therapy via nanoscale metal-organic frameworks enhances checkpoint blockade immunotherapy. *Nature Biomedical Engineering* **2018,** *2* (8), 600.

140. Zhang, K.; Meng, X.; Cao, Y.; Yang, Z.; Dong, H.; Zhang, Y.; Lu, H.; Shi, Z.; Zhang, X., Metal-Organic Framework Nanoshuttle for Synergistic Photodynamic and Low-Temperature Photothermal Therapy. *Advanced Functional Materials* **2018,** *28* (42), 1804634.

141. Zheng, X.; Wang, L.; Liu, M.; Lei, P.; Liu, F.; Xie, Z., Nanoscale Mixed-Component Metal–Organic Frameworks with Photosensitizer Spatial-Arrangement-Dependent Photochemistry for Multimodal-Imaging-Guided Photothermal Therapy. *Chemistry of Materials* **2018,** *30* (19), 6867-6876.

142. Wang, S.; Chen, W.; Jiang, C.; Lu, L., Nanoscaled porphyrinic metal–organic framework for photodynamic/photothermal therapy of tumor. *ELECTROPHORESIS* **2019** *40* 2204-2210

143. Liu, C.; Luo, L.; Zeng, L.; Xing, J.; Xia, Y.; Sun, S.; Zhang, L.; Yu, Z.; Yao, J.; Yu, Z., Porous Gold Nanoshells on Functional NH2-MOFs: Facile Synthesis and Designable Platforms for Cancer Multiple Therapy. *Small* **2018,** *14* (35), 1801851.

144. Min, H.; Wang, J.; Qi, Y.; Zhang, Y.; Han, X.; Xu, Y.; Xu, J.; Li, Y.; Chen, L.; Cheng, K.; Liu, G.; Yang, N.; Li, Y.; Nie, G., Biomimetic Metal–Organic Framework Nanoparticles for Cooperative Combination of Antiangiogenesis and Photodynamic Therapy for Enhanced Efficacy. *Advanced Materials* **2019,** *31* (15), 1808200.

145. Brandt, A. R.; Heath, G. A.; Kort, E. A.; Sullivan, F.; Pétron, G.; Jordaan, S. M.; Tans, P.; Wilcox, J.; Gopstein, A. M.; Arent, D.; Wofsy, S.; Brown, N. J.; Bradley, R.; Stucky, G. D.; Eardley, D.; Harriss, R., Methane Leaks from North American Natural Gas Systems. *Science* **2014,** *343* (6172), 733.

146. Menon, V. C.; Komarneni, S., Porous Adsorbents for Vehicular Natural Gas Storage: A Review. *Journal of Porous Materials* **1998,** *5* (1), 43-58.

147. Makal, T. A.; Li, J.-R.; Lu, W.; Zhou, H.-C., Methane storage in advanced porous materials. *Chemical Society Reviews* **2012,** *41* (23), 7761-7779.

148. Fu, J.; Tian, Y.; Wu, J., Seeking metal–organic frameworks for methane storage in natural gas vehicles. *Adsorption* **2015,** *21* (6), 499-507.

149. Celzard, A.; Fierro, V., Preparing a Suitable Material Designed for Methane Storage: A Comprehensive Report. *Energy & Fuels* **2005,** *19* (2), 573-583.

150. Düren, T.; Sarkisov, L.; Yaghi, O. M.; Snurr, R. Q., Design of New Materials for Methane Storage. *Langmuir* **2004,** *20* (7), 2683-2689.

151. Low, J. J.; Benin, A. I.; Jakubczak, P.; Abrahamian, J. F.; Faheem, S. A.; Willis, R. R., Virtual High Throughput Screening Confirmed Experimentally: Porous Coordination Polymer Hydration. *Journal of the American Chemical Society* **2009,** *131* (43), 15834-15842.

152. Feng, D.; Wang, K.; Wei, Z.; Chen, Y.-P.; Simon, C. M.; Arvapally, R. K.; Martin, R. L.; Bosch, M.; Liu, T.-F.; Fordham, S.; Yuan, D.; Omary, M. A.; Haranczyk, M.; Smit, B.; Zhou, H.-C., Kinetically tuned dimensional augmentation as a versatile synthetic route towards robust metal–organic frameworks. *Nature Communications* **2014,** *5* (1), 5723.

153. Ikealumba, W. C.; Wu, H., Some Recent Advances in Liquefied Natural Gas (LNG) Production, Spill, Dispersion, and Safety. *Energy & Fuels* **2014,** *28* (6), 3556-3586.

154. Xia; Ma; Guo; Hua, C., Determination and Study of the Solubility of Methane in Mixtures of Methanol plus Various Hydrocarbons at High Pressures. *Journal of Chemical & Engineering Data* **2006,** *51* (3), 1035-1038.

155. Jiang, J.; Furukawa, H.; Zhang, Y.-B.; Yaghi, O. M., High Methane Storage Working Capacity in Metal–Organic Frameworks with Acrylate Links. *Journal of the American Chemical Society* **2016,** *138* (32), 10244-10251.

156. Liang, C.-C.; Shi, Z.-L.; He, C.-T.; Tan, J.; Zhou, H.-D.; Zhou, H.-L.; Lee, Y.; Zhang, Y.-B., Engineering of Pore Geometry for Ultrahigh Capacity Methane Storage in Mesoporous Metal–Organic Frameworks. *Journal of the American Chemical Society* **2017,** *139* (38), 13300-13303.

157. Karaipekli, A.; Sarı, A., Capric–myristic acid/expanded perlite composite as form-stable phase change material for latent heat thermal energy storage. *Renewable Energy* **2008,** *33* (12), 2599-2605.

158. Yuan, S.; Sun, X.; Pang, J.; Lollar, C.; Qin, J.-S.; Perry, Z.; Joseph, E.; Wang, X.; Fang, Y.; Bosch, M.; Sun, D.; Liu, D.; Zhou, H.-C., PCN-250 under Pressure: Sequential Phase Transformation and the Implications for MOF Densification. *Joule* **2017,** *1* (4), 806-815.

159. Kirchon, A.; Day, G. S.; Fang, Y.; Banerjee, S.; Ozdemir, O. K.; Zhou, H.-C., Suspension Processing of Microporous Metal-Organic Frameworks: A Scalable Route to High-Quality Adsorbents. *iScience* **2018,** *5*, 30-37.

160. Vellingiri, K.; Szulejko, J. E.; Kumar, P.; Kwon, E. E.; Kim, K.-H.; Deep, A.; Boukhvalov, D. W.; Brown, R. J. C., Metal organic frameworks as sorption media for volatile and semi-volatile organic compounds at ambient conditions. *Scientific Reports* **2016,** *6* (1), 27813.

161. Vlasova, E. A.; Yakimov, S. A.; Naidenko, E. V.; Kudrik, E. V.; Makarov, S. V., Application of metal–organic frameworks for purification of vegetable oils. *Food Chemistry* **2016,** *190*, 103-109.

162. Kordas, A.; Magoulas, K.; Stamataki, S.; Tassios, D., Methane□hydrocarbon interaction parameters correlation for the Peng-Robinson and the t-mPR equation of state. *Fluid Phase Equilibria* **1995,** *112* (1), 33-44.

163. Choi, K. M.; Jeon, H. J.; Kang, J. K.; Yaghi, O. M., Heterogeneity within Order in Crystals of a Porous Metal–Organic Framework. *Journal of the American Chemical Society* **2011,** *133* (31), 11920-11923.

164. Wang, Z.; Hu, S.; Yang, J.; Liang, A.; Li, Y.; Zhuang, Q.; Gu, J., Nanoscale Zr-Based MOFs with Tailorable Size and Introduced Mesopore for Protein Delivery. *Adv. Funct. Mater* **2018,** *28* (16), 1707356.

165. Cai, G.; Jiang, H.-L., A Modulator-Induced Defect-Formation Strategy to Hierarchically Porous Metal–Organic Frameworks with High Stability. *Angewandte Chemie International Edition* **2017,** *56* (2), 563-567.

166. Liu, W.; Huang, J.; Yang, Q.; Wang, S.; Sun, X.; Zhang, W.; Liu, J.; Huo, F., Multi-shelled Hollow Metal–Organic Frameworks. *Angewandte Chemie International Edition* **2017,** *56* (20), 5512-5516.

167. Avci, C.; Ariñez-Soriano, J.; Carné-Sánchez, A.; Guillerm, V.; Carbonell, C.; Imaz, I.; Maspoch, D., Post-Synthetic Anisotropic Wet-Chemical Etching of Colloidal Sodalite ZIF Crystals. *Angewandte Chemie International Edition* **2015,** *54* (48), 14417-14421.

168. He, S.; Chen, Y.; Zhang, Z.; Ni, B.; He, W.; Wang, X., Competitive coordination strategy for the synthesis of hierarchical-pore metal–organic framework nanostructures. *Chemical Science* **2016,** *7* (12), 7101-7105.

169. Koo, J.; Hwang, I.-C.; Yu, X.; Saha, S.; Kim, Y.; Kim, K., Hollowing out MOFs: hierarchical micro- and mesoporous MOFs with tailorable porosity via selective acid etching. *Chemical Science* **2017,** *8* (10), 6799-6803.

170. Zhou, H.-C.; Long, J. R.; Yaghi, O. M .Introduction to Metal–Organic Frameworks. *Chemical Reviews* **2012,** *112* (2), 673-674.

171. Schoedel, A.; Ji, Z.; Yaghi, O. M., The role of metal–organic frameworks in a carbon-neutral energy cycle. *Nature Energy* **2016,** *1* (4), 16034.

172. Ma, L.; Falkowski, J. M.; Abney, C.; Lin, W., A series of isoreticular chiral metal–organic frameworks as a tunable platform for asymmetric catalysis. *Nature Chemistry* **2010,** *2* (10), 838-846.

173. Eddaoudi, M.; Kim, J.; Rosi, N.; Vodak, D.; Wachter, J.; O'Keeffe, M.; Yaghi, O. M., Systematic design of pore size and functionality in isoreticular MOFs and their application in methane storage. *Science* **2002,** *295* (5554), 469-72.

174. Szilágyi, P. Á.; Serra-Crespo, P.; Gascon, J.; Geerlings, H.; Dam, B., The Impact of Post-Synthetic Linker Functionalization of MOFs on Methane Storage: The Role of Defects. *Front. Energy Res.,* **2016,** *4* (9).

175. Fang, Y.; Banerjee, S.; Joseph, E. A.; Day, G. S.; Bosch, M.; Li, J.; Wang, Q.; Drake, H.; Ozdemir, O. K.; Ornstein, J. M.; Wang, Y.; Lu, T.-B.; Zhou, H.-C., Incorporating Heavy Alkanes in Metal–Organic Frameworks for Optimizing Adsorbed Natural Gas Capacity. *Chemistry – A European Journal* **2018,** *24* (64), 16977-16982.

176. Park, J.; Wang, Z. U.; Sun, L.-B.; Chen, Y.-P.; Zhou, H.-C., Introduction of Functionalized Mesopores to Metal–Organic Frameworks via Metal–Ligand–Fragment Coassembly. *Journal of the American Chemical Society* **2012,** *134* (49), 20110-20116.

177. Deng, H.; Doonan, C. J.; Furukawa, H.; Ferreira, R. B.; Towne, J.; Knobler, C. B.; Wang, B.; Yaghi, O. M., Multiple Functional Groups of Varying Ratios in Metal-Organic Frameworks. *Science* **2010,** *327* (5967), 846-850.

178. Koh, K.; Wong-Foy, A. G.; Matzger, A. J., A Porous Coordination Copolymer with over 5000 m2/g BET Surface Area. *Journal of the American Chemical Society* **2009,** *131* (12), 4184-4185.

179. Koh, K.; Wong-Foy, A. G.; Matzger, A. J., Coordination Copolymerization Mediated by Zn4O(CO2R)6 Metal Clusters: a Balancing Act between Statistics and Geometry. *Journal of the American Chemical Society* **2010,** *132* (42), 15005-15010.

180. Xuan, W.; Zhu, C.; Liu, Y.; Cui, Y., Mesoporous metal–organic framework materials. *Chemical Society reviews* **2012,** *41* (5), 1677-1695.

181. Zhou, H. C.; Yuan, D.; Zhao, D.; Timmons, D.; Zhou, H.-C., A stepwise transition from microporosity to mesoporosity in metal–organic frameworks by thermal treatment. *Chemical science* **2011,** *2* (1), 103-106.

182. Sun, L.-B.; Li, J.-R.; Park, J.; Zhou, H.-C., Cooperative Template-Directed Assembly of Mesoporous Metal–Organic Frameworks. *Journal of the American Chemical Society* **2012,** *134* (1), 126-129.

183. Reboul, J.; Furukawa, S.; Horike, N.; Tsotsalas, M.; Hirai, K.; Uehara, H.; Kondo, M.; Louvain, N.; Sakata, O.; Kitagawa, S., Mesoscopic architectures of porous coordination polymers fabricated by pseudomorphic replication. *Nature Materials* **2012,** *11* (8), 717-723.

184. Michels, N. L.; Mitchell, S.; Michels, N.-L.; Kunze, K.; Pérez Ramírez, J., Visualization of hierarchically structured zeolite bodies from macro to nano length scales. *Nature Chemistry* **2012,** *4* (10), 825-831.

185. Wang, C.; Zhang, Z.; Yue, T.; Sun, Y.; Wang, L.; Wang, W.; Zhang, Y.; Liu, C., "Bottom-Up" Embedding of the Jørgensen-Hayashi Catalyst into a Chiral Porous Polymer for Highly Efficient Heterogeneous Asymmetric Organocatalysis. *Chemistry - A European Journal* **2012,** *18* (22), 6718-6723.

186. Bunck, D.; Dichtel, W., Internal Functionalization of Three-Dimensional Covalent Organic Frameworks. *Angewandte Chemie International Edition* **2012,** *51* (8), 1885-1889.

187. Jasuja, H.; Zang, J.; Sholl, D. S.; Walton, K. S., Rational Tuning of Water Vapor and CO2 Adsorption in Highly Stable Zr-Based MOFs. *The Journal of Physical Chemistry C* **2012,** *116* (44), 23526-23532.

188. Drake, H. F.; Day, G. S.; Vali, S. W.; Xiao, Z.; Banerjee, S.; Li, J.; Joseph, E. A.; Kuszynski, J. E.; Perry, Z. T.; Kirchon, A.; Ozdemir, O. K.; Lindahl, P. A.; Zhou, H.-C., The thermally induced decarboxylation mechanism of a mixed-oxidation state carboxylate-based iron metal–organic framework. *Chemical Communications* **2019,** *55* (85), 12769-12772.

189. Wang, X.; Design and Synthesis Of Metal-Organic Frameworks for Sustainbale Energy-Related Applications. Ph.D Dissertation, Texas A&M University, College Sation, TX, 2016.

190. Choma, J.; Jaroniec, M.; Burakiewicz Mortka, W.; Kloske, M., Critical appraisal of classical methods for determination of mesopore size distributions of MCM-41 materials. *Applied surface science* **2002,** *196* (1-4), 216-223.

191. Jaroniec, M.; Solovyov, L., Improvement of the Kruk−Jaroniec−Sayari Method for Pore Size Analysis of Ordered Silicas with Cylindrical Mesopores. *Langmuir* **2006,** *22* (16), 6757-6760.

192. Dimick, S. M.; Powell, S. C.; McMahon, S. A.; Moothoo, D. N.; Naismith, J. H.; Toone, E. J., On the Meaning of Affinity: Cluster Glycoside Effects and Concanavalin A. *Journal of the American Chemical Society* **1999,** *121* (44), 10286-10296.

193. Park, T. H.; Wong-Foy, A. G.; Park, T.-H.; Hickman, A.; Koh, K.; Martin, S.; Wong Foy, A.; Sanford, M.; Matzger, A., Highly Dispersed Palladium(II) in a Defective Metal–Organic Framework: Application to C–H Activation and Functionalization. *Journal of the American Chemical Society* **2011,** *133* (50), 20138-20141.

194. Choi, K.; Jeon, H.; Kang, J.; Yaghi, O., Heterogeneity within Order in Crystals of a Porous Metal–Organic Framework. *Journal of the American Chemical Society* **2011,** *133* (31), 11920-11923.

195. Hendon, C. H.; Rieth, A. J.; Korzyński, M. D.; Dincă, M., Grand Challenges and Future Opportunities for Metal-Organic Frameworks. *ACS central science* **2017,** *3* (6), 554-563.

196. Fukushima, T.; Horike, S.; Kobayashi, H.; Tsujimoto, M.; Isoda, S.; Foo, M.; Kubota, Y.; Takata, M.; Kitagawa, S., Modular Design of Domain Assembly in Porous

Coordination Polymer Crystals via Reactivity-Directed Crystallization Process. *Journal of the American Chemical Society* **2012,** *134* (32), 13341-13347.

197. Cychosz, K. A.; Thommes, M., Progress in the Physisorption Characterization of Nanoporous Gas Storage Materials. *Engineering* **2018,** *4* (4), 559-566.

198. Diring, S. p.; Furukawa, S.; Takashima, Y.; Tsuruoka, T.; Kitagawa, S., Controlled Multiscale Synthesis of Porous Coordination Polymer in Nano/Micro Regimes. *Chemistry of Materials* **2010,** *22* (16), 4531-4538.

199. Tsuruoka, T.; Furukawa, S.; Takashima, Y.; Yoshida, K.; Isoda, S.; Kitagawa, S., Nanoporous Nanorods Fabricated by Coordination Modulation and Oriented Attachment Growth. *Angewandte Chemie International Edition* **2009,** *48* (26), 4739-4743.

200. Duong, T. D.; Sapchenko, S. A.; da Silva, I.; Godfrey, H. G. W.; Cheng, Y.; Daemen, L. L.; Manuel, P.; Ramirez-Cuesta, A. J.; Yang, S.; Schröder, M., Optimal Binding of Acetylene to a Nitro-Decorated Metal-Organic Framework. *Journal of the American Chemical Society* **2018,** *140* (47), 16006-16009.

201. Liu, M.; Liao, W.; Hu, C.; Du, S.; Zhang, H., Calixarene-Based Nanoscale Coordination Cages. **2012,** *51* (7), 1585-1588.

202. Dai, F.-R.; Wang, Z., Modular Assembly of Metal–Organic Supercontainers Incorporating Sulfonylcalixarenes. *Journal of the American Chemical Society* **2012,** *134* (19), 8002-8005.

203. Durot, S.; Taesch, J.; Heitz, V., Multiporphyrinic Cages: Architectures and Functions. *Chemical Reviews* **2014,** *114* (17), 8542-8578.

204. Zhang, D.; Martinez, A.; Dutasta, J.-P., Emergence of Hemicryptophanes: From Synthesis to Applications for Recognition, Molecular Machines, and Supramolecular Catalysis. *Chemical Reviews* **2017,** *117* (6), 4900-4942.

205. Zhang, D.; Martinez, A.; Dutasta, J. P., Emergence of Hemicryptophanes: From Synthesis to Applications for Recognition, Molecular Machines, and Supramolecular Catalysis. *Chem Rev* **2017,** *117* (6), 4900-4942.

206. Brown, C. J.; Toste, F. D.; Bergman, R. G.; Raymond, K. N., Supramolecular Catalysis in Metal–Ligand Cluster Hosts. *Chemical Reviews* **2015,** *115* (9), 3012-3035.

207. Chakrabarty, R.; Mukherjee, P. S.; Stang, P. J., Supramolecular Coordination: Self-Assembly of Finite Two- and Three-Dimensional Ensembles. *Chemical Reviews* **2011,** *111* (11), 6810-6918.

208. Wang, W.; Wang, Y.-X.; Yang, H.-B., Supramolecular transformations within discrete coordination-driven supramolecular architectures. *Chemical Society Reviews* **2016,** *45* (9), 2656-2693.

209. Dai, F.-R.; Qiao, Y.; Wang, Z., Designing structurally tunable and functionally versatile synthetic supercontainers. *Inorganic Chemistry Frontiers* **2016,** *3* (2), 243-249.

210. Qiao, Y.; Zhang, L.; Li, J.; Lin, W.; Wang, Z., Switching on Supramolecular Catalysis via Cavity Mediation and Electrostatic Regulation. **2016,** *55* (41), 12778-12782.

211. Chen, G. J.; Chen, C. Q.; Li, X. T.; Ma, H. C.; Dong, Y. B., Cu(3)L(2) metal-organic cages for A(3)-coupling reactions: reversible coordination interaction triggered homogeneous catalysis and heterogeneous recovery. *Chemical communications (Cambridge, England)* **2018,** *54* (82), 11550-11553.

212. Lu, W.; Yuan, D.; Yakovenko, A.; Zhou, H.-C., Surface functionalization of metal–organic polyhedron for homogeneous cyclopropanation catalysis. *Chemical Communications* **2011,** *47* (17), 4968-4970.

213. Gadzikwa, T.; Bellini, R.; Dekker, H. L.; Reek, J. N. H., Self-Assembly of a Confined Rhodium Catalyst for Asymmetric Hydroformylation of Unfunctionalized Internal Alkenes. *Journal of the American Chemical Society* **2012,** *134* (6), 2860-2863.

214. Mollick, S.; Fajal, S.; Mukherjee, S.; Ghosh, S. K., Stabilizing Metal–Organic Polyhedra (MOP): Issues and Strategies. *Chemistry – An Asian Journal* **2019,** *14* (18), 3096-3108.

215. Zhao, M.; Yuan, K.; Wang, Y.; Li, G.; Guo, J.; Gu, L.; Hu, W.; Zhao, H.; Tang, Z., Metal–organic frameworks as selectivity regulators for hydrogenation reactions. *Nature* **2016,** *539* (7627), 76-80.

216. Chughtai, A. H.; Ahmad, N.; Younus, H. A.; Laypkov, A.; Verpoort, F., Metal–organic frameworks: versatile heterogeneous catalysts for efficient catalytic organic transformations. *Chemical Society Reviews* **2015,** *44* (19), 6804-6849.

217. Navlani-García, M.; Martis, M.; Lozano-Castelló, D.; Cazorla-Amorós, D.; Mori, K.; Yamashita, H., Investigation of Pd nanoparticles supported on zeolites for hydrogen production from formic acid dehydrogenation. *Catalysis Science & Technology* **2015,** *5* (1), 364-371.

218. Wang, L.; Zhang, J.; Yi, X.; Zheng, A.; Deng, F.; Chen, C.; Ji, Y.; Liu, F.; Meng, X.; Xiao, F.-S., Mesoporous ZSM-5 Zeolite-Supported Ru Nanoparticles as Highly

Efficient Catalysts for Upgrading Phenolic Biomolecules. *ACS Catalysis* **2015,** *5* (5), 2727-2734.

219. Mahyari, M.; Shaabani, A., Nickel nanoparticles immobilized on three-dimensional nitrogen-doped graphene as a superb catalyst for the generation of hydrogen from the hydrolysis of ammonia borane. *Journal of Materials Chemistry A* **2014,** *2* (39), 16652-16659.

220. Wang, H.; Zhao, Y.; Cheng, F.; Tao, Z.; Chen, J., Cobalt nanoparticles embedded in porous N-doped carbon as long-life catalysts for hydrolysis of ammonia borane. *Catalysis Science & Technology* **2016,** *6* (10), 3443-3448.

221. Yang, L.; Cao, N.; Du, C.; Dai, H.; Hu, K.; Luo, W.; Cheng, G., Graphene supported cobalt(0) nanoparticles for hydrolysis of ammonia borane. *Materials Letters* **2014,** *115*, 113-116.

222. Sun, J.-K.; Zhan, W.-W.; Akita, T.; Xu, Q., Toward Homogenization of Heterogeneous Metal Nanoparticle Catalysts with Enhanced Catalytic Performance: Soluble Porous Organic Cage as a Stabilizer and Homogenizer. *Journal of the American Chemical Society* **2015,** *137* (22), 7063-7066.

223. Suzuki, K.; Takao, K.; Sato, S.; Fujita, M., The Precise Synthesis and Growth of Core–Shell Nanoparticles within a Self-Assembled Spherical Template. *Angew Chem Int Ed*. **2011,** *50* (21), 4858-4861.

224. Olenyuk, B.; Whiteford, J. A.; Fechtenkötter, A.; Stang, P. J., Self-assembly of nanoscale cuboctahedra by coordination chemistry. *Nature* **1999,** *398* (6730), 796-799.

225. Umegaki, T.; Xu, Q.; Kojima, Y., Porous Materials for Hydrolytic Dehydrogenation of Ammonia Borane. *Materials (Basel, Switzerland)* **2015,** *8* (7), 4512-4534.

226. Zhan, W.-W.; Zhu, Q.-L.; Xu, Q., Dehydrogenation of Ammonia Borane by Metal Nanoparticle Catalysts. *ACS Catalysis* **2016,** *6* (10), 6892-6905.

227. Du, S.; Hu, C.; Xiao, J.-C.; Tan, H.; Liao, W., A giant coordination cage based on sulfonylcalix[4]arenes. *Chemical Communications* **2012,** *48* (73), 9177-9179.

228. Pasquale, S.; Sattin, S.; Escudero-Adán, E. C.; Martínez-Belmonte, M.; de Mendoza, J., Giant regular polyhedra from calixarene carboxylates and uranyl. *Nature Communications* **2012,** *3* (1), 785.

229. Liu, Z.; Lv, L.; He, Y.; Feng, Y., An anionic metal–organic framework constructed from a triazole-functionalized diisophthalate featuring hierarchical cages for selective adsorptive C2H2/CH4 and CO2/CH4 separation. *CrystEngComm* **2017,** *19* (20), 2795-2801.

230. Wang, H.; Qiu, Z.; Liu, H.; Jayawardhana, A. M. D. S.; Yue, Z.; Daghlas, H.; Bowers, D. J.; Datta, B.; Zheng, Y.-R., Nanoparticles of Metal-Organic Cages Overcoming Drug Resistance in Ovarian Cancer. Front. Chem., **2019,** *7* (39).

231. Fang, Y.; Xiao, Z.; Li, J.; Lollar, C.; Liu, L.; Lian, X.; Yuan, S.; Banerjee, S.; Zhang, P.; Zhou, H.-C., Formation of a Highly Reactive Cobalt Nanocluster Crystal within a Highly Negatively Charged Porous Coordination Cage. *Angew Chem Int Ed* **2018,** *57* (19), 5283-5287.

232. Shumba, M.; Nyokong, T., Electrode modification using nanocomposites of boron or nitrogen doped graphene oxide and cobalt (II) tetra aminophenoxy phthalocyanine nanoparticles. *Electrochimica Acta* **2016,** *196*, 457-469.

233. Nam, K. M.; Shim, J. H.; Ki, H.; Choi, S.-I.; Lee, G.; Jang, J. K.; Jo, Y.; Jung, M.-H.; Song, H.; Park, J. T., Single-Crystalline Hollow Face-Centered-Cubic Cobalt Nanoparticles from Solid Face-Centered-Cubic Cobalt Oxide Nanoparticles. *Angew Chem Int Ed* **2008,** *47* (49), 9504-9508.

234. Kitakami, O.; Sato, H.; Shimada, Y.; Sato, F.; Tanaka, M., Size effect on the crystal phase of cobalt fine particles. *Physical Review B* **1997,** *56* (21), 13849-13854.

235. Dinega, D. P.; Bawendi, M. G., A Solution-Phase Chemical Approach to a New Crystal Structure of Cobalt. *Angew Chem Int Ed* **1999,** *38* (12), 1788-1791.

236. Fang, Y.; Li, J.; Togo, T.; Jin, F.; Xiao, Z.; Liu, L.; Drake, H.; Lian, X.; Zhou, H.-C., Ultra-Small Face-Centered-Cubic Ru Nanoparticles Confined within a Porous Coordination Cage for Dehydrogenation. *Chem* **2018,** *4* (3), 555-563.

237. Ahmed, A.; Seth, S.; Purewal, J.; Wong-Foy, A. G.; Veenstra, M.; Matzger, A. J.; Siegel, D. J., Exceptional hydrogen storage achieved by screening nearly half a million metal-organic frameworks. *Nature Communications* **2019,** *10* (1), 1568.

238. Program, U. S. D. o. E. H. *Hydrogen & Our Energy Future*; Annual Report, Oak Ridge National Laboratory, Oak Ridge, TN,2012

239. Pareek, K.; Rohan, R.; Chen, Z.; Zhao, D.; Cheng, H., Ambient temperature hydrogen storage in porous materials with exposed metal sites. *International Journal of Hydrogen Energy* **2017,** *42* (10), 6801-6809.

240. Staubitz, A.; Robertson, A. P. M.; Manners, I., Ammonia-Borane and Related Compounds as Dihydrogen Sources. *Chemical Reviews* **2010,** *110* (7), 4079-4124.

241. Navlani-García, M.; Mori, K.; Kuwahara, Y.; Yamashita, H., Recent strategies targeting efficient hydrogen production from chemical hydrogen storage materials over carbon-supported catalysts. *NPG Asia Materials* **2018,** *10* (4), 277-292.

242. Niu, Z.; Li, Y., Removal and Utilization of Capping Agents in Nanocatalysis. *Chemistry of Materials* **2014,** *26* (1), 72-83.

243. Chen, Y.-Z.; Zhou, Y.-X.; Wang, H.; Lu, J.; Uchida, T.; Xu, Q.; Yu, S.-H.; Jiang, H.-L., Multifunctional PdAg@MIL-101 for One-Pot Cascade Reactions: Combination of Host–Guest Cooperation and Bimetallic Synergy in Catalysis. *ACS Catalysis* **2015,** *5* (4), 2062-2069.

244. Iki, N.; Horiuchi, T.; Oka, H.; Koyama, K.; Morohashi, N.; Kabuto, C.; Miyano, S., Energy transfer luminescence of Tb3+ ion complexed with calix[4]arenetetrasulfonate and the thia and sulfonyl analogue. The effect of bridging groups. *Journal of the Chemical Society, Perkin Transactions 2* **2001,** (11), 2219-2225.

245. Santos, D. M. F.; Sequeira, C. A. C.; Figueiredo, J. L., Hydrogen production by alkaline water electrolysis *Química Nova*. **2013,** *36*, 1176-1193.